MAGNETIC NANOPARTICLES FOR SELECTIVE MAGNETIC SEPARATION IN BIOTECHNOLOGY

Peter Dušak

Doctoral Dissertation
Jožef Stefan International Postgraduate School
Ljubljana, Slovenia, February 2015

Evaluation Board:

Assist. Prof. Dr. Darja Lisjak, Chairman, Jožef Stefan Institute, Ljubljana, Slovenia

Assist. Prof. Dr. Alenka Mertelj, Member, Jožef Stefan Institute, Ljubljana, Slovenia

Prof. Dr. Josep López Santín, Member, Escola d'Enginyeria, Universitat Autònoma de Barcelona, Barcelona, Spain

MEDNARODNA PODIPLOMSKA ŠOLA JOŽEFA STEFANA
JOŽEF STEFAN INTERNATIONAL POSTGRADUATE SCHOOL

Peter Dušak

MAGNETIC NANOPARTICLES FOR SELECTIVE MAGNETIC SEPARATION IN BIOTECHNOLOGY

Doctoral Dissertation

MAGNETNI NANODELCI ZA SELEKTIVNO SEPARACIJO V BIOTEHNOLOGIJI

Doktorska disertacija

Supervisor: Prof. Dr. Darko Makovec

Co-Supervisor: Prof. Dr. Marin Berovič

Ljubljana, Slovenia, February 2015

Index

Abstract

A separation in biotechnology can be performed by magnetic separation, where magnetic carriers are dispersed into reaction mixture containing specific targets. A review of magnetic carriers for magnetic separation in biotechnology that are in use today shows that new methods for their synthesis are required. Nanoclusters of controlled size composed of superparamagnetic nanoparticles can be optimal solution for the magnetic carriers. They can be synthesized by the assembly of the nanoparticles in an aqueous suspension. Different interactions between the nanoparticles with different surface properties in the suspension can be applied for their heteroaggregation and controlled by engineering the surface properties of the nanoparticles. Up to now, mainly the heteroaggregation of larger micron- or submicron-sized particles has been studied, but no direct comparison between the heteroaggregation controlled by the two types of interactions, i.e., electrostatic or chemical, in the same system of the two types of the functionalized-nanoparticles has been reported.

The present work is a study of the two types of interactions in the same system of the two types of functionalized-nanoparticles. The interactions were studied: (i.) to develop a method for the controlled synthesis of magnetic carriers based on heteroaggregation of the nanoparticles in the aqueous suspensions and (ii.) to control bonding of magnetic nanoparticles onto larger targets, e.g., bacteria, in the process of their magnetic separation. The work is thematically divided into two parts. The first part was devoted to the synthesis of nanoclusters using controlled heteroaggregation of superparamagnetic iron-oxide nanoparticles in the aqueous suspensions, while the second part describes a possible application of the magnetic separation in biotechnology.

The heteroaggregation of nanoparticles in a suspension was studied on a model system composed of superparamagnetic carboxyl-functionalized silica-coated maghemite nanoparticles (cMNPs) (24 nm in size) and larger, amino-functionalized, silica nanoparticles (aSNPs) (92 nm). The heteroaggregates were formed with electrostatic attractions between the nanoparticles displaying an opposite electric surface charge, or with chemical interactions originating from covalent bonding between the molecules at their surfaces. The suspensions were characterized with measurements of the zeta-potential and hydrodynamic particle size using dynamic light scattering (DLS). The heteroaggregates were analysed by transmission (TEM) and scanning (SEM) electron microscopy. The kinetics of the heteroaggregation was followed by continuous monitoring of the changes in the average hydrodynamic size by DLS. The results show that covalent bonding is much more effective than attractive electrostatic interactions in terms of a much greater and more uniform coverage of the larger central aSNP by the smaller cMNPs in the outer layer.

A new method was developed for magnetic separation of lactic acid bacteria (LAB) *O. beni* at certain stage of malolactic fermentation (MLF) of wine. The method includes preparation of so called "magneto-responsive" bacteria by bonding of the amino-functionalized silica-coated maghemite nanoparticles (aMNPs) onto bacteria cell membranes in the suspension by applying the electrostatic interactions. The magneto-responsive bacteria were applied in the MLF and separated in the certain stage of the process from fermentation media using the high gradient magnetic separation (HGMS). The

adsorption of aMNPs onto the surface of *O. oeni* was analysed by TEM and SEM electron microscopy. The metabolism of so-prepared bacteria was followed by conversion of L-malic into L-lactic acid by enzymatic tests. Efficiency of the HGMS of the magneto-responsive bacteria from fermentation media was estimated using flow cytometry analysis. The aMNPs were successfully attached to the surface of LAB and did not have an influence on LAB metabolism. By using HGMS, the LAB with the attached magnetic nanoparticles were efficiently removed from the fermentation media resulted in complete stop of the fermentation process.

Povzetek

Eden izmed načinov ločevanja v biotehnologiji je magnetna separacija. Pri magnetni separaciji dispergiramo v tekočo mešanico produktov in neželenih primesi magnetne nosilce, na katere se vežejo tarčne molekule ali tarčne celice. Glede na današnji razvoj biotehnologije in potrebe po ločevanju v biotehnologiji se pojavljajo potrebe po novih sinteznih metodah za pripravo magnetnih nosilcev, ki bi se lahko uporabili v magnetni separaciji. Superparamagnetni nanoskupki določene velikosti bi bili zaradi visoke specifične površine in učinkovite separacije s pomočjo visokega gradienta magnetnega polja (HGMS) lahko idealna rešitev za magnetne nosilce uporabne v magnetni separaciji. Sinteza takih nanoskupkov s heteroaglomeracijo dveh vrst nanodelcev z različnimi površinskimi lastnostmi v vodnih suspenzijah je možna ob dobrem poznavanju interakcij med nanodelci. Do sedaj so bile študije heteroagregacije narejene večinoma na primeru mikronskih in submikronskih delcev z uporabo enega tipa interakcij, t.j. z elektrostatskimi ali kemijskimi interakcijami, medtem ko direktna primerjava dveh različnih interakcij v istem sistemu z dvema različnima tipoma funkcionaliziranih nanodelcev še ni bila opisana.

Predstavljeno doktorsko delo naslavlja dva aspekta aktualne problematike magnetne separacije, in sicer sintezo magnetnih nosilcev s heteroaglomeracijo nanodelcev v vodnih suspenzijah v superparamagnetne nanoskupke in pripravo magnetno odzivnih bakterij z vezavo superparamagnetnih nanodelcev na površino bakterij. Doktorsko delo je sestavljeno iz dveh delov. Prvi del je namenjen sintezi nanoskupkov s kontrolirano heteroagregacijo superparamagnetnih delcev železovega oksida v vodni suspenziji. Drugi del doktorske disertacije pa opisuje možnost uporabe magnetnih nanodelcev za magnetno separacijo v biotehnologiji.

Heteroagregacijo nanodelcev v vodnih suspenzijah sem preučeval na modelnem sistemu. Modelni sistem sta sestavljala dva tipa nanodelcev različnih velikosti; manjši nanodelci maghemita prevlečenimi s tanko plastjo amorfnega silicijevega oksida (velikost okoli 24 nm), funkcionalizirani s karboksilnimi skupinami (cMNPs) in večji nanodelci amorfnega silicijevega oksida (velikost okoli 100 nm) funkcionalizirani z amino skupinami. Različno funkcionalizirani nanodelce sem spajal v heteroagregate elektrostatsko, t.j. pri pH vrednosti, kjer je naboj na površini obeh tipov nanodelcev nasproten in se zato heteroaglomerirajo zaradi elektrostatskih privlačnih sil, ali kemijsko, s tvorbo kovalentne vezi med aktiviranimi karboksilnimi skupinami in amino skupinami funkcionalizacijskih molekul na površini obeh tipov nanodelcev. Suspenzije funkcionaliziranih nanodelcev sem karakteriziral z meritvami zeta potenciala in hidrodinamske velikosti z dinamičnim sipanjem svetlobe (DLS). Obliko in velikost nastalih nanoskupkov sem določil s presevno (TEM) in z vrstično elektronsko mikroskopijo (SEM). Kinetiko nastajanja skupkov modelnih nanodelcev sem meril kot spremembe povprečne velikosti normaliziranega hidrodinamskega premera s sprotnimi meritvami DLS. Rezultati so pokazali, da je pokritost večjih centralnih aSNPs z manjšimi cMNPs boljša in bolj enakomerna z uporabo kovalentne vezave kot v primeru elektrostatske vezave.

V okviru doktorata sem razvil novo metodo za magnetno separacijo mlečnokislinskih

bakterij (LAB) *O. oeni* v določeni stopnji mlečnokislinske fermentacije (MLF) v vinu. Metoda vključuje pripravo »magnetno odzivnih« bakterij z elektrostatsko vezavo nanodelcev maghemita prevlečenih s tanko plastjo amorfnega silicijevega oksida (velikost okoli 24 nm) in funkcionaliziranih z amino skupinami (aMNPs) na steno bakterijskih celic. Uporaba magnetno odzivnih bakterij v MLF omogoča njihovo magnetno separacijo iz fermentacijskega medija z uporabo HGMS. Bakterije z vezanimi nanodelci na površini sem karakteriziral s TEM in SEM analizo. Metabolizem tako pripravljenih bakterij sem zasledoval s pretvorbo L-jabolčne v L-mlečno kislino z encimsko analizo. Uspešnost HGMS je bila ovrednotena z metodami pretočne citometrije. Magnetni nanodelci so se uspešno vezali na površino LAB in niso imeli vplivan na njihov metabolizem. Z uporabo HGMS sem uspel LAB z vezanimi aMNPs uspešno odstraniti iz fermentacijskega medija v določeni stopnji MLF in s tem prekiniti proces fermentacije.

Abbreviations

A	=	Hamaker constant
a	=	particle radius
a-iNANO	=	amino-functionalized superparamagnetic iNANOvative^{TM}| silica nanoparticle clusters
aSNP	=	amino-functionalized silica nanoparticle
CFU	=	colony-forming unit
cMNP	=	superparamagnetic carboxyl-functionalized, silica coated maghemite nanoparticle
d	=	particle diameter
DLS	=	dynamic light scattering
DNA	=	deoxyribonucleic acid
EC	=	Enzyme Commission number
EDXS	=	energy-dispersive X-ray spectroscopy
F_d	=	drag force
FDA	=	Food and Drug Administration
F_m	=	magnetic force
grad H	=	gradient of the magnetic field strength
H	=	external magnetic field strength
h	=	minimum separation between the particle surfaces
HGMS	=	High Gradient Magnetic Separation
iNANO	=	superparamagnetic iNANOvative^{TM}| silica nanoparticle clusters
LAB	=	lactic acid bacteria
L-LDH	=	L-lactate dehydrogenase
L-MDH	=	L-malate dehydrogenase
M	=	magnetization
ME	=	malic enzyme
min	=	minutes
MLE	=	malolactic enzyme
MLF	=	malolactic fermentation
MNP	=	silica-coated maghemite nanoparticle
MNP-PEG	=	carboxyl-(polyethylene glycol)n-amine functionalized cMNP
M_P	=	particle magnetization
mRNA	=	messenger ribonucleic acid
NAD^+	=	nicotinamide adenine dinucleotide
NADP	=	nicotinamide adenine dinucleotide phosphate
OADC	=	oxaloacetate decarboxylase
R_m	=	radius of the magnetic particle
SEM	=	scanning electron microscopy
SNP	=	silica nanoparticle
TEM	=	transmission electron microscopy
V_A	=	van der Waals attractive forces

V_{elect}	=	potential energy resulting from electrostatic interactions
V_P	=	particle volume
V_R	=	electrical double layer repulsive forces
VSM	=	vibrating sample magnetometer
V_{steric}	=	potential energy resulting from steric interactions
$V_{structural}$	=	potential energy resulting from the presence of non-adsorbed species in solution
V_{vdW}	=	potential energy due to van der Waals interactions
WSC	=	WineScan™
μ_0	=	permeability constant of the vacuum
ϵ	=	solvent permittivity
ζ	=	zeta-potential
η	=	viscosity
κ	=	inverse Debye length
ν	=	velocity
ψ_s	=	surface electric potential

1 Introduction

In Introduction some basics as well as current status of the topics relevant to this thesis are presented. The Introduction is divided into materials part and biotechnology part. First, I begin with the description of magnetic separation, which could be used as an alternative solution for separation, purification and concentration of specific biological molecules from mixtures in the liquid media. The description of the magnetic separation is followed by description of magnetic nanoparticles as magnetic carriers for selective magnetic separation, which is the main topic of this work. I continue with the topics of colloidal suspensions and interactions between the nanoparticles in the colloidal suspensions.

In the second part of this chapter I address the malolactic fermentation as an example for the application where magnetic nanoparticles can be applied in biotechnology.

1.1 Magnetic separation

At the end of bioprocess, there is a need for separation, purification and concentration of products or specific targets, e.g., biomolecules, including specific proteins such as enzymes, or cells and microorganisms, from a liquid mixture. Products are usually difficult to separate. Moreover, the isolation, separation and purification of raw samples is also imperative prior to the analysis of specific targets [1]. Commonly used sample preparation techniques for biological analysis include various extraction techniques [2], e.g., electrophoresis [3-5], ultrafiltration [6,7], precipitation [8,9], etc. Although electrophoresis is low cost and simple to manipulate, it usually takes relatively long time and has low efficiency [10]. Ultrafiltration has high separation efficiency, but the membrane of ultrafiltration may exhibit adsorption toward biological macromolecules [6]. Precipitation is easy to operate, however, it may lead to the inactivation of biological macromolecules. Among these techniques, solid-phase extraction is one of the most important and powerful techniques because of its outstanding selectivity and recovery [11]. Although traditional solid-phase extraction techniques where the adsorbents are packed into columns have been applied in many successful cases, it is not suitable for coping with samples containing suspended solid or fouling components. Batch separation technique, during which the adsorbents are incubated directly with the samples, can solve the above problems. Many new materials such as nano-materials and mesoporous materials have been employed in this mode [12,13]. However, when using these materials as affinity adsorbents for the enrichment of specific targets, nonreversible adsorption and high-speed centrifugation are often unavoidable, which may result in sample loss and co-precipitation of unwanted components, i.e., contaminants [14]. The application using these advanced materials as adsorbents is restricted to a great extent. For biological analysis, a rapid, convenient, gentle and efficient sample preparation is needed. With the use of magnetic materials, magnetic separation techniques have shown their usefulness.

The magnetic separation was first described by William Fullaton in 1792 when he used a magnet to separate iron minerals [15,16]. Magnetic separation techniques are used in several different areas ranging from steel production to biotechnology, since they are rapid, cost effective and highly efficient [17]. Magnetic separation is usually gentle and

non-destructive to biological analytes such as proteins or peptides, and even large protein complexes, which tend to be broken up in process of traditional column chromatography, may remain active. Target analytes captured by magnetic materials can be easily and selectively removed from the reaction mixture, like fermentation broth, cell disruptates, blood or plasma, or from water of different sources. With the exception of wastewater treatment, they are employed mostly only on laboratory scale [18]. The removal of the magnetic carriers, i.e., small particles of a magnetic material, from a reaction mixture using an external magnetic field is much more selective and effective than centrifugation or filtration [19-21]. All steps of the magnetic separation can be done in a single vessel. Beside magnetic carriers and magnetic separator, no special equipment is needed for magnetic separation process. This all lowers the costs of magnetic separation compared to the before-mentioned separation techniques.

1.1.1 Magnetic separation in biotechnology

Magnetic separation is a technique where magnetic carriers are dispersed into a reaction mixture containing specific targets [22,23]. After binding specific targets with magnetic carriers, the conjugates are separated with an external magnetic field [22,24,25]. In general, the magnetic separation can be performed by two different methods, i.e., direct or indirect [26,27]. The direct method, is achieved by an appropriate affinity ligand coupled to magnetic carriers with an affinity towards a specific target. Magnetic carriers coated with an affinity ligand are than directly applied to the liquid mixture. During the incubation the specific targets are bound to magnetic carriers and stable magnetic complexes are formed (Figure 1a). They can be then recovered using an external magnetic field. By the indirect method, a free affinity ligand, e.g., appropriate antibodies, are firstly added to the liquid mixture with the specific targets. If possible the excess unbound affinity ligands are removed after the incubation and the resulting labelled complex is then captured by appropriate affinity magnetic carriers (Figure 1b).

Besides mentioned methods, magnetic separation can be either positive or negative [17,26] or on industrial scale magnetically stabilized fluidized beds and biocompatible two phase systems [27].

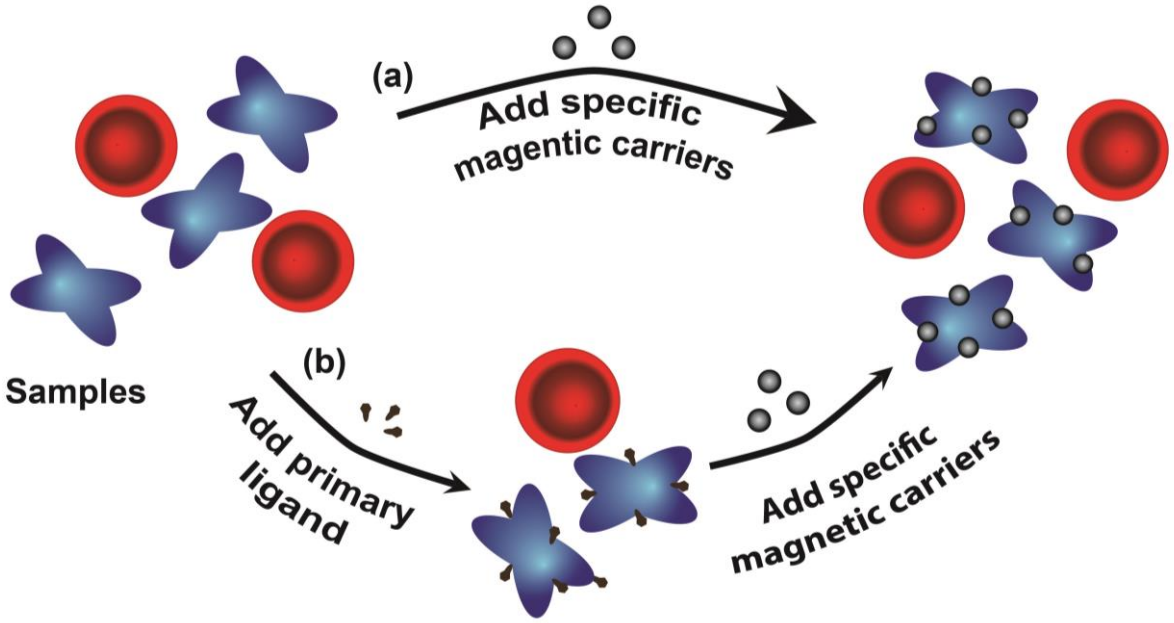

Figure 1: *Different methods of magnetic separation.* (a) Direct and (b) indirect method of magnetic separation. Modified from [27].

For magnetic separation, a variety of magnetic separators are available on the market [17]. There are two basic types of magnetic separator: batch and flow trough.

1.1.2 Batch magnetic separator

Batch magnetic separators are often used for separation on fixed volumes of reaction mixtures with the aim of removing targeted components. Magnetic separator design can be as simple as the application and removal of a permanent magnet to the wall of a test tube to cause aggregation, followed by removal of the supernatant (Figure 2a). The process is not quick, because it is limited by slow accumulation rates. The isolation of nucleic acids is mostly performed in the batch mode using commercially available lab-scale magnetic separators (particle concentrators) [17].

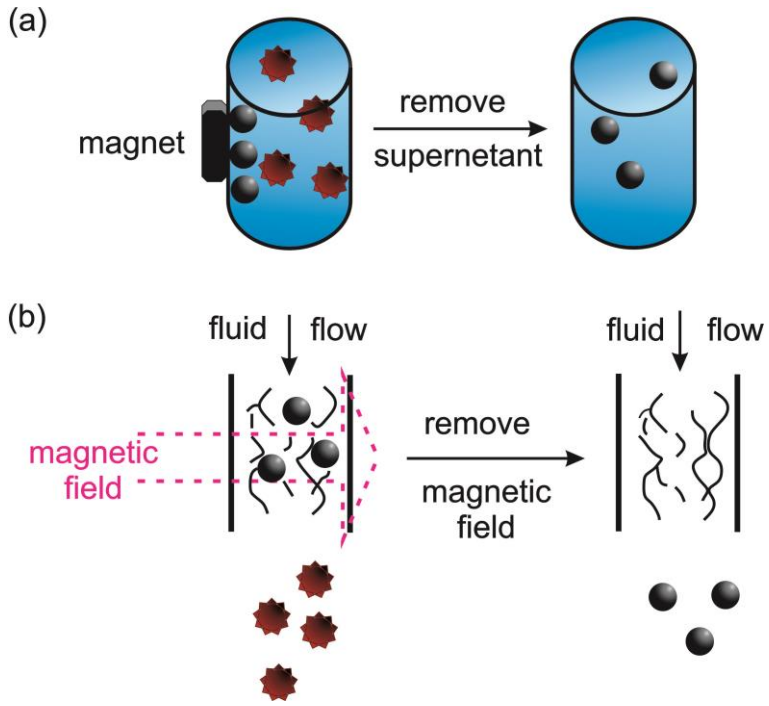

Figure 2: *Basic types of magnetic separator*. (a) The standard methods of magnetic separation: a magnet is attached to the container wall of a suspension of magnetically tagged (black spheres) and unwanted (red stars) biomaterials. The tagged particles are gathered by the magnet, and the unwanted supernatant solution is removed. (b) The principle of flow through magnetic separator. A solution containing tagged and unwanted biomaterials flows continuously through a region of strong magnetic field gradient, often provided by packing the column with steel wool, which captures the tagged particles. Thereafter the tagged particles are recovered by removing the field and flushing through with water. Modified from [25].

1.1.3 Flow- through magnetic separator

It is preferable to increase the separator efficiency by producing regions of high magnetic field gradient to capture the magnetic particles as they float or flow by in their carrier medium. A typical way to achieve this is to loosely pack a flow column with a magnetizable matrix of wire (e.g. steel wool) or beads (e.g., 0.3 mm iron spheres) [28] and then to pump the magnetically tagged fluid through the column while a field is applied (Figure 2b). This method is faster than the batch magnetic separation [25]. Problems can arise due to the settling and adsorption of magnetically tagged material on the matrix.

An alternative, rapid throughput method which does not involve any obstructions being placed in the column is the use of specifically designed field gradient systems, such as the quadrupolar magnetic separator [25]. In this type of magnetic separator four magnetic ‘‘poles’’ focus the magnetic field around a central, cylindrical area. The quadrupole separator splits an inlet, magnetically labelled, cell stream into two outlets one of which contains mainly the magnetically labelled cells [25].

1.1.3.1 High-gradient magnetic separation (HGMS)

When small or low magnetisable particles are used they have to be captured resorting to high gradient magnetic separators (HGMS). The HGMS consists of small columns filled with a magnetisable ferrous matrix (e.g., steel wool) to which a large external static field (~1 T), provided by an electromagnet or a strong permanent magnet, is applied (Figure 3).

The resulting magnetic gradients are as high as 10^4 T/m generating forces large enough to capture even weakly magnetic particles in a flow stream [29-31]. Typically, HGMS has been used to separate micron-scale aggregates [32], consisting of magnetic nanoparticles, or encapsulated magnetic nanoparticles into larger polymer beads [29,33]. The HGMS techniques have become commonplace in biotechnology where they are used for protein purification [34-37] or separation of cells [23,38,39]. Besides biotechnology HGMS were applied to treat water polluted with heavy metal ions, organic substances or microorganisms, treat water from conventional and nuclear power plants, treat urban waste water, etc. [24,40,41].

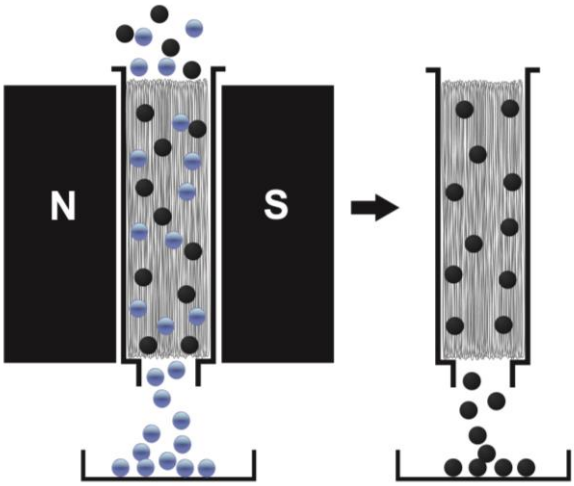

Figure 3: *A scheme of HGMS separator.* The sample (black spheres-magnetic material, blue spheres-nonmagnetic material) flows through column filled with a magnetisable ferrous matrix (grey lines) to which large external magnetic field is applied (left). Eluting the magnetic material from the column after the magnetic separation is finished (right). Modified from [42].

1.1.3.1.1 Forces acting on the magnetic particle in magnetic separator

All types of magnetic separators are based on the property of magnetic field to exert a force on a matter. The collection of magnetic particles depends strongly on the creation of magnetic field gradients, as well as on the particle size and magnetic properties, as shown by the Equation 1 for the magnetic force, F_m, acting on the magnetic particle in the magnetic field gradient [29,31]:

$$F_m = \mu_0 V_P M_P \, \mathrm{grad}H \qquad (1)$$

The variables that can be changed in Equation 1 and have the effect on the F_m are: the particle volume (V_P), particle magnetization (M_P) and the gradient of the magnetic field strength at the position of the particle (grad H). The constant in the Equation 1 is the permeability constant of the vacuum (μ_0) [22]. The magnetic force can be increased with increase of magnetization or by changing the particle volume. For example, if we would like to double magnetic force by the change of particle volume, we need to increase particle diameter (d) for $\sqrt[3]{2}$, as the change of volume is proportional to a cubic diameter ($V_P \propto d^3$).

In order to determine the F_m, one needs to know the field distribution and the magnetic response (i.e., M-H curves) of the particle. Magnetic responses associated with different classes of magnetic material will be discussed in section devoted to superparamagnetism (1.1.4.2 Superparamagnetism). For applications using F_m, two types of magnetic field are

available: a homogeneous magnetic field (e.g., in HGMS separator) and an inhomogeneous magnetic field (e.g., achieved by using an external permanent magnet). In homogeneous magnetic field, there is no gradient in the magnetic field because the magnetic flux density is constant over a distance. In HGMS, ferromagnetic materials are used to concentrate the external magnetic field so that the magnetic field gradient is larger and the magnetic force becomes stronger. In contrast, in the inhomogeneous magnetic field exists a gradient in the magnetic flux density [43].

For successful collection of magnetic particles by HGMS, the magnetic force attracting particles toward the wires (e.g., steel wool) must dominate the hydrodynamic drag force (F_d) acting on the magnetic particle as the particle suspension flows through the separator (Equation 2) [44,45].

$$F_d = 6\pi\eta R_m \Delta v \tag{2}$$

The influence on the drag force has the viscosity (η) of the medium (e.g., water), the radius of the magnetic particle (R_m), and the difference in velocities (Δv).

1.1.4 Magnetic carriers

The use of magnetic nanoparticles dispersed in liquid media is normally based on the ability to manipulate them with an external magnetic field. Such magnetic nanoparticles have attracted a lot of attention in biomedicine, for example, in drug delivery or in the detection and targeting of specific (bio)molecules or cells [25,46-49]. They can also be used in technologies related to magnetic separation, particularly in environmental engineering [50,51], in chemical engineering [52,53], or in bioseparation processes [54-56].

1.1.4.1 Magnetic material for magnetic carriers

As the magnetic material for the carriers, simple magnetic iron-oxides like maghemite (γ-Fe_2O_3) or magnetite (Fe_3O_4) are normally used in magnetic separation [18,57-60], because of their low cost and relatively simple synthesis. Several other ferrites containing Co, Cu, Ni and Mn exhibit higher magnetization and could be used in separation applications, but unlike the before-mentioned iron oxides are not biocompatible [38]. In contrast, the nanoparticles of iron oxide are considered to be nontoxic and were approved by the U.S. Food and Drug Administration (FDA) for *in vivo* medical applications [59].

1.1.4.1.1 Surface modification of magnetic nanoparticles

1.1.4.1.1.1 Coatings of magnetic nanoparticles

Due to the large nanoparticles' surface area, bare magnetic nanoparticles show strong tendency to form agglomerates. To avoid agglomeration, a suitable coating (Figure 4b) should be provided onto the iron oxide magnetic nanoparticles in order to achieve magnetic nanoparticles that have high chemical and colloidal stability as well as to reduce metal leaching and related toxicity (e.g., divalent Co, Ni, Mn) without deterioration of their magnetic properties [58,61-63]. It is known that during the co-precipitation of iron oxides surface hydroxyl groups are formed (Fe-OH) [64,65]. These groups are responsible for the amphoteric nature of iron oxides leading to positive ($Fe\text{-}OH_2^+$) or negatively ($Fe\text{-}O^-$) charged surfaces depending on the pH and ionic strength [65]. Due to this behaviour, colloidal stability by electrostatic repulsion is only achieved at extreme pH values and low ionic strengths and therefore do not provide adequate stability for most applications. To provide colloidal stability of their suspensions the magnetic nanoparticles

are generally coated with polymers [66], surfactants [67,68], inorganic materials [69] or low molecular weight chelating agents [70,71].
From inorganic materials, silica is the most commonly used for the coating of the magnetic nanoparticles. It generally allows the encapsulation of the magnetic cores while increasing the colloidal stability through electrostatic repulsion (silica is negatively charged at pH > 2 [72]). Furthermore, functionalization of the surface is easily achieved by using silane coupling agents [73,74].

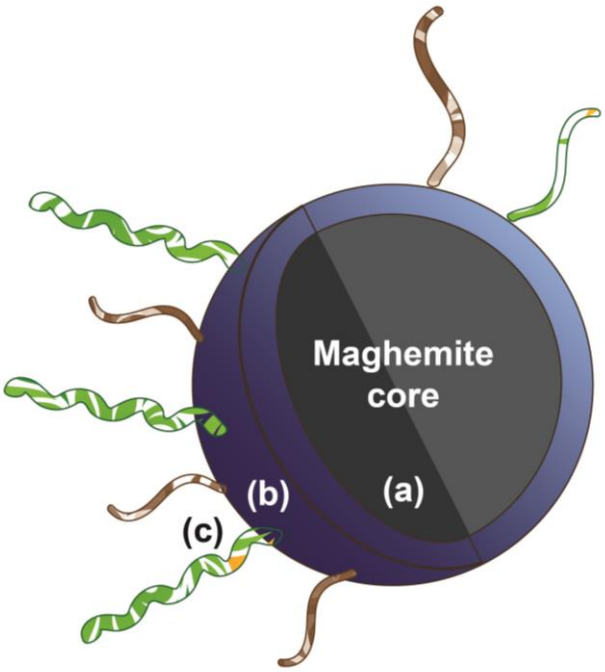

Figure 4: *Illustration of magnetic carrier.* Parts of magnetic carrier: magnetic core (a), coating of the core (b), functional groups on the carriers' surface (c).

1.1.4.1.1.2 Functionalization of magnetic nanoparticles

Functionalization means to provide specific functional groups at the magnetic nanoparticles surfaces for further bonding of different molecules to their surfaces. For example, silica coated magnetic nanoparticles can be functionalized by using silane coupling agents having amine, carboxyl, aldehyde, epoxy, vinyl groups, etc. (Figure 4c) [14]. For magnetic separation of specific targets, it might be desired to have a strong covalent binding between the nanoparticle surface and specific targets. This is achievable through coupling reaction between specific groups (e.g., -COOH, $-NH_2$, $-CONH_2$, -OH groups) on the surface of magnetic nanoparticles and $-NH_2$ or -SH groups on the specific targets in the presence of a coupling reagent (e.g., glutaraldehyde, carbodiimide, etc.) [75]. As a coupling reagent crosslinking reagents (or crosslinkers) can be used. These crosslinkers are chemical reagents used to bind molecules together with a covalent bond and are applied in protein-crosslinking applications, e.g., in the immobilization of proteins on solid supports for affinity purification [76,77]. For biological applications various biological molecules such as proteins [78,79], monoclonal antibodies [80], metal ligands [81], oligonucleotides [82,83], streptavidin [63,84], biotin and histidine [78,85] may be bound onto the functionalized magnetic nanoparticles by chemically coupling via amide or ester bonds.

When dispersing magnetic particles in a liquid medium it is beneficial if they are small

enough to be in the superparamagnetic state.

1.1.4.2 Superparamagnetism

Superparamagnetism is a phenomenon related to ferro/ferrimagnetic particles when their size is reduced below a certain limit and thermal excitation induces rapid fluctuations, compared to the observation time, of the nanoparticles' magnetic moments. The superparamagnetic limit is at approximately 20 nm for soft magnetic materials [64,86]. At this point these superparamagnetic nanoparticles no longer exhibit any spontaneous magnetic moments and, in contrast to larger ferromagnetic particles, they do not agglomerate in suspensions due to magnetic dipole-dipole interactions.

Superparamagnetism can be viewed as the combination of paramagnetic and ferrimagnetic behaviour (Figure 5). Like paramagnets, superparamagnetic materials exhibit zero remanence, i.e., in the absence of an applied external magnetic field (H) their average magnetization (M) is zero. However, their magnetic susceptibility is much higher than paramagnets and like ferrimagnets they reach magnetic saturation but without exhibiting a magnetic hysteresis loop. Highly magnetisable particles respond quicker as they generate greater magnetic flux densities when submitted to an applied external magnetic field. Therefore, less intense fields can be used for an efficient separation process and better process dynamics are achievable [38].

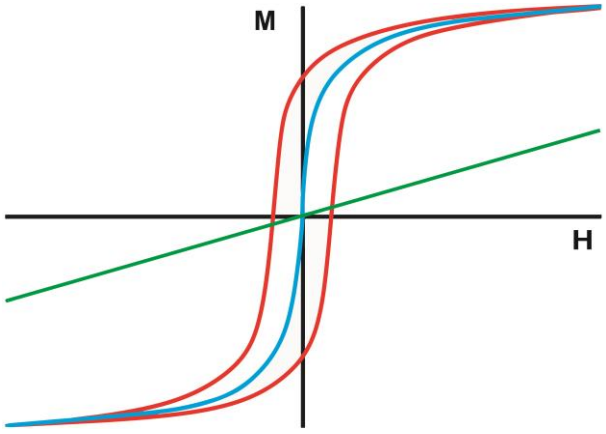

Figure 5: *Typical magnetization curves*. Magnetization (M) vs. magnetic field strength (H) curves are shown for paramagnetic (green), superparamagnetic (blue) and ferromagnetic (red) material.

1.1.4.3 Force acting on magnetic particle in a magnetic field gradient

However, the force acting on the magnetic particle in a magnetic field gradient is proportional to the particle's volume (Equation 1). It appears in practice, therefore, that individual superparamagnetic nanoparticles are just too small to be effectively separated [87]. The magnetic separation is much more effective if the superparamagnetic nanoparticles are assembled into nanoclusters, containing several superparamagnetic nanoparticles in a single nano-unit, but still retaining the relatively large surface area needed for bonding the targeted species [30]. For the magnetic separation of larger objects, such as cells and microorganisms, the individual superparamagnetic nanoparticles can be bonded onto their surfaces. Even if a relatively low surface concentration of the nanoparticles is bonded and the magnetization of the object is small, its magnetic moment in the magnetic field can be large enough for effective separation, because of its relatively large volume [88].

1.1.5 Colloidal suspensions

The term colloid originates from the Greek word »κολλα« meaning glue. In true (homogenous) solution, the solute is supposed to have lost its identity, e.g., it dissociates into its constituent ions, and apparently undergoes a charge in property. Colloidal particles retain their identity in a suspension. A colloidal suspension is considered a heterogeneous system [89,90]. The factors which contribute the most to the behaviour of colloidal system are particle size and shape, their surface properties, particle-particle and particle-solvent interactions. Moreover, in almost all colloidal systems, the contact area between particles and the dispersing medium is large, which is also one of the reasons why inter-particle forces play such an important role in the suspensions behaviour [90].

1.1.5.1 Origin of the surface charge

Most colloidal particles develop an electrostatic charge on their surface when they are immersed in polar medium, i.e., water. Direct evidence for the existence of charge on particles comes from the phenomenon of particle movement under an applied electric field (electrophoresis). Surfaces may become electrically charged by a variety of mechanisms [89,91]:

- Ionization of surface groups such as carboxyl and amino groups
- Differential dissolution of ions from surfaces of sparingly soluble crystals
- Isomorphic substitution
- Specific ion adsorption

The surface charge, more specifically charge density, plays an active role in colloidal stability. It is the surface charge density, which is responsible for the repulsive forces between charged, colloidal particles.

The liquid layer surrounding the particle, i.e., a double layer, exists of two parts; an inner region, called the Stern layer, where the ions are strongly bound and an outer, diffuse, region where they are less firmly attached (Figure 6). Within the diffuse layer there is a notional boundary inside which the ions and particles form a stable entity. When a particle moves (e.g. due to gravity), ions within the boundary move with it, but any ions beyond the boundary do not travel with the particle. This boundary is called the surface of hydrodynamic shear or slipping plane [89].

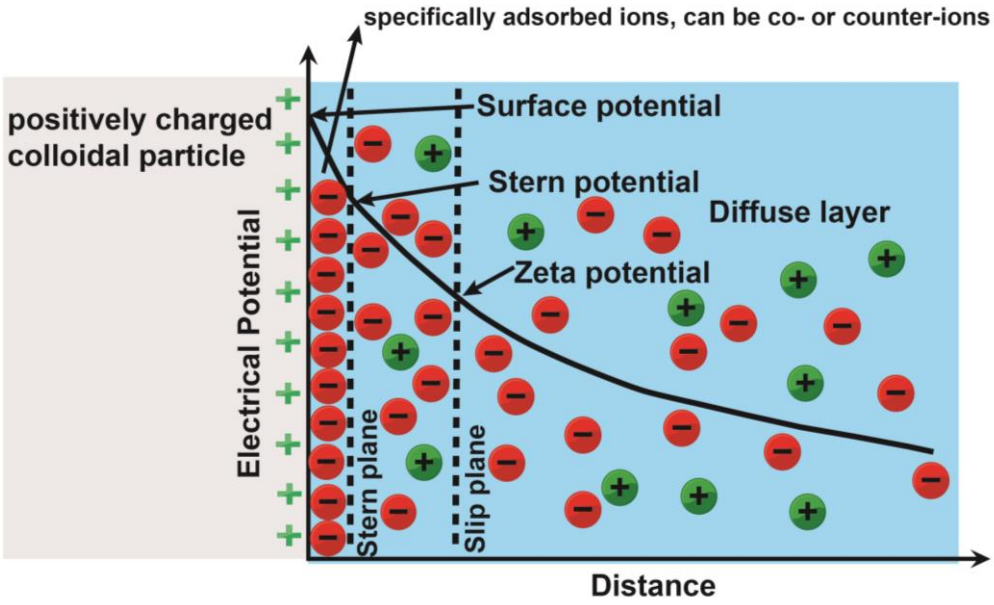

Figure 6: *Schematic presentation the electrical double layer*. The first layer adjacent to the charged surface is the Stern layer of specifically adsorbed ions, here the electrical potential falls linearly with distance. Next to the Stern layer is the diffuse layer, where the potential falls exponentially. The value of the electrical potential at the slip plane is the zeta-potential. Modified after [92,93].

1.1.5.1.1 Zeta-potential

Within the diffuse layer there is a notional boundary inside which the ions and particles form a stable entity. When a particle moves (e.g., due to gravity), ions within the boundary move. Those ions beyond the boundary stay with the bulk dispersant. Electrokinetic behaviour depends on the potential at the surface of shear between the charged surface and the electrolyte. The potential at this boundary is the zeta (ζ)-potential. The zeta-potential is the electrostatic potential at the surface of shear and not the potential at the surface of the particle. The exact location of the shear plane is unknown feature of the kinetic double layer. The magnitude of the zeta-potential gives an indication of the potential stability of the colloidal system. Zeta-potential can provide a measure of the net surface charge on the particle and potential distribution at the interface. If all the particles in suspension have a large negative or positive zeta potential then they will tend to repel each other and there will be no tendency for the particles to come together. In case when particles have low zeta-potential values, there will be no force to prevent the particles coming together and flocculating. However, if the particles have a density different form the dispersant, they will eventually sediment forming a close packed bed. Zeta potential serves as an important parameter in characterizing the electrostatic interaction between particles in dispersed systems and the properties of the dispersion [90,94].

Colloidal particles can be stabilized against coagulation (or flocculation) by electrostatic repulsion due to the presence of ions near their surfaces or by steric effects arising from organic molecules (often polymeric in nature) being attached to the surface particles [89]. The forces between the colloidal particles are important in connection to this work. Controlling the inter-particle forces enables us to control the aggregation behaviour of the nanoparticles in suspensions used to synthesis of heteroaggregates.

1.1.5.2 Inter-particle forces in suspensions

The forces that act between the particles have a great influence on many macroscopic properties of colloidal systems. Forces between particles could be separated in two groups: they could be either attractive or repulsive. The attraction/repulsion between two particles strongly depends on the nature of the particles and on the properties of the medium in which they are dispersed. The balance between attractive and repulsive forces determines the stability of a suspension. Van der Waals forces represent the attraction forces. The repulsion between the particles in a colloidal suspension could be obtained via electrostatic, steric, electrosteric or solvation (structural) forces [90,95,96]. Colloidal stability is governed by the total inter-particle potential energy, V_{total}, which can be expressed as:

$$V_{total} = V_{vdW} + V_{elect} + V_{steric} + V_{structural} \quad (3)$$

where V_{vdW} is the attractive potential energy due to van der Waals interactions between particles, V_{elect} the repulsive potential energy resulting from electrostatic interactions between like-charged particle surfaces, V_{steric} the repulsive potential energy resulting from steric interactions between particle surfaces coated with adsorbed polymeric species, and $V_{structural}$ is the potential energy resulting from the presence of non-adsorbed species in solution that may either increase or decrease suspension stability [96]. Non-adsorbing particles and/or molecules, which are smaller in comparison to the colloidal particles, or even solvent molecules, can cause structural forces. These are the so-called entropic depletion forces or solvation forces in the case of a solvent [97,98]. These forces can either promote stabilization or destabilization of the colloidal system [96]. The first two terms in Equation 3 are presented in the theory developed by Derjaguin and Landau and Verwey and Owerbeek (the DLVO theory), which predicts the stability of colloidal particles suspended in a polar liquids [96].

1.1.5.2.1 Van der Waals forces

Long-range forces resulting from van der Waals forces (vdW), also named London-van der Waals or dispersion forces, are ubiquitous and always attractive between like particles. V_{vdW} exhibits a power-law distance dependence whose strength depends on the dielectric properties of the interacting colloidal particles and intervening medium. For spherical particles of equal size, V_{vdW} is given by the Hamaker expression:

$$V_{vdW} = -\frac{A}{6}\left(\frac{2}{s^2-4} + \frac{2}{s^2} + \ln\frac{s^2-4}{s^2}\right) \quad (4)$$

where s is expressed as:

$$s = \frac{2\cdot a + h}{a} \quad (5)$$

and where h is the minimum separation between the particle surfaces, a the particle radius, and A the Hamaker constant. Long-range, attractive vdW forces between particles must be mitigated during colloidal processing to achieve the desired degree of suspension stability. To overcome the vdW attraction, there must be some type of the interparticle repulsion, such as electrostatic or steric forces [90,96].

1.1.5.2.2 Electrostatic forces

The stability of aqueous colloidal systems can be controlled by generating like-charges of

sufficient magnitude on the surfaces of suspended ceramic particles. The resulting repulsive V_{elect} exhibits an exponential distance dependence whose strength depends on the surface potential induced on the interacting colloidal particles and the dielectric properties of the intervening medium. Exact analytical expressions for the electrostatic potential energy cannot be given; therefore, analytical approximations or numerical solutions are used [96].

1.1.5.2.3 DLVO theory

The scientists Derjaguin, Verwey, Landau and Overbeek developed a theory (DLVO) in the 1940s which dealt with the stability of colloids in a suspension. DVLO theory suggests that the stability of a particle in a suspension dependents upon its total potential energy function V_{total} (Equation 6). The DVLO theory suggests that the stability of a colloidal system is determined by the sum, i.e., total potential energy function V_{total} (presented with blue line on Figure 7), of attractive van der Waals attractive (V_A) and electrical double layer repulsive (V_R) forces that exist between particles as they approach each other due to the Brownian motion they are undergoing.

$$V_{total} = V_A + V_R \tag{6}$$

If the particles are in close enough proximity, the London- van der Waal's attractive force will tend to pull the particle together (Equation 4). Bringing two particles together the electric field will overlap and this could cause the particle to repel each other. This is known as electrical double layer repulsion. The repulsive potential V_R is a far more complex function (Equation 7):

$$V_R = 2\pi a \varepsilon \psi_S^2 \exp(-\kappa h) \tag{7}$$

where ϵ is the solvent permittivity, κ is inverse Debye length and ψ_s is the surface electric potential.

This theory proposes that an energy barrier resulting from the repulsive force prevents two particles approaching one another and adhering together. But if the particles collide with sufficient energy to overcome that barrier, the attractive force will pull them into contact where they adhere strongly and irreversibly together. Therefore if the particles have a sufficiently high repulsion, the dispersion will resist flocculation and the colloidal system will be stable. However if a repulsion mechanism does not exist then flocculation or coagulation will eventually take place [99]. As the surface charge approaches zero the interaction curve approaches the pure van der Waals curve, and two surfaces now attract each other (Figure 7).

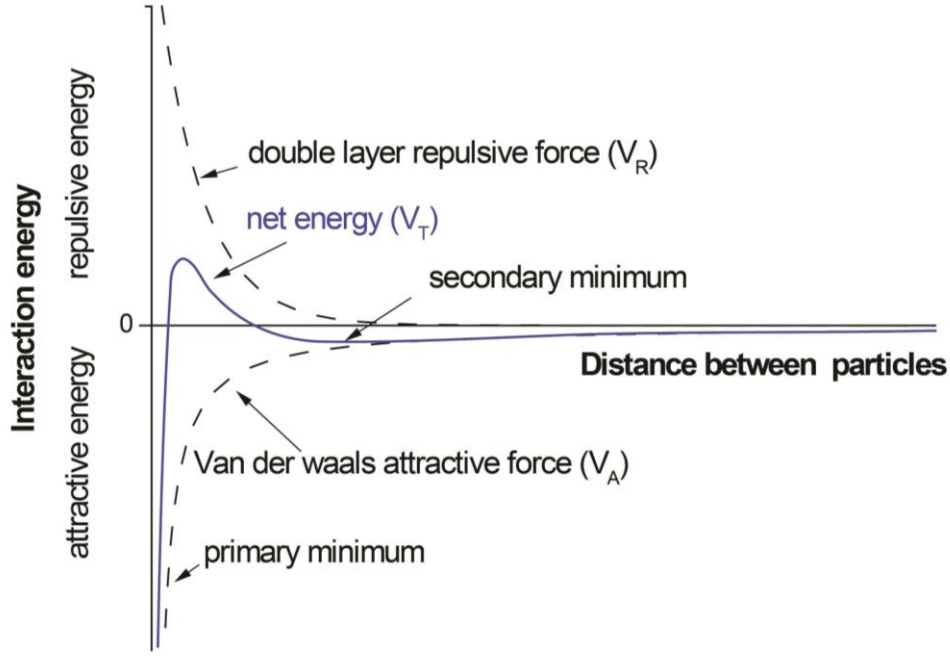

Figure 7: *The potential energy curves.* Diagram of interaction energy between two particles in polar media depending on the distance between two particles [89].

The main factor including two surfaces to come into contact is the lowering of their surface charge or potential, brought about by increased ion binding [95]. In Figure 8 curve V1 represent a well stabilized colloidal system with a repulsive energy maximum. This represents the energy barrier preventing or hindering the approach of two colloidal particles to contact. In contrast, curve V3 represents a case where repulsive barrier is absent, implying the unstable system. The colloidal particles will coagulate rapidly, as they will be attracted to a deep attractive energy minimum at contact. Curve V2 represent the transition between stability and coagulation at the primary minimum. The presence of a secondary minimum at relatively large interparticle distance is given by curve V2. If the secondary minimum is relatively deep, it should give rise to loose flocs. These weak flocs are sufficiently stable not to be broken up by Brownian motion, but may disperse under an externally applied force such as vigorous agitation. This type of coagulation can be easily redispersed by agitation [89].

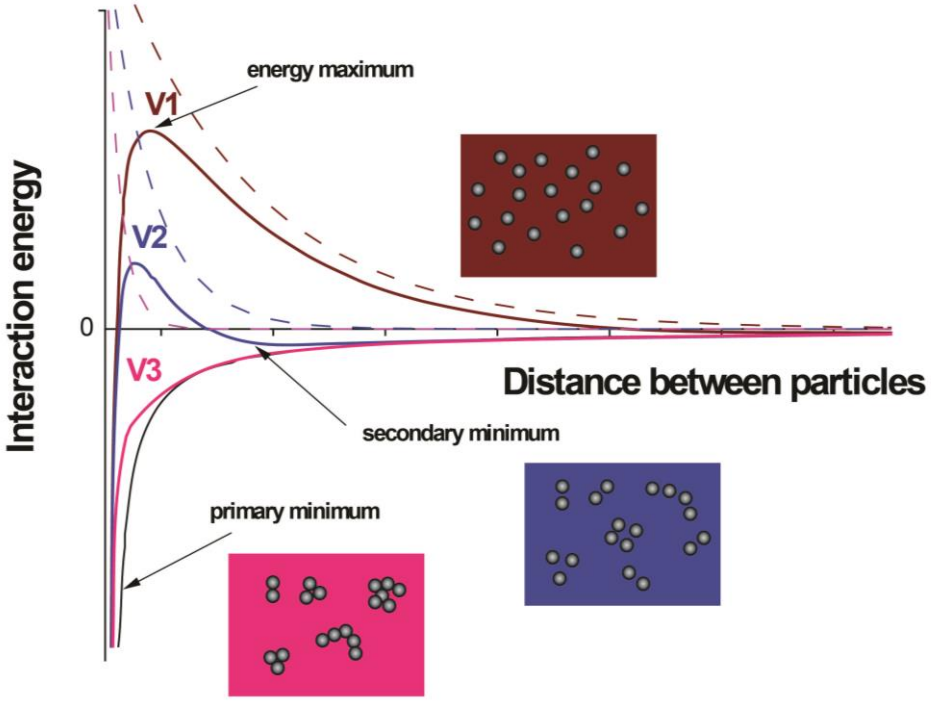

Figure 8: *Influence of the DLVO interaction on the colloidal stability.* Total energy curves (solid lines) obtained by the summation of an attractive potential curve (black solid line) with different repulsive potential curves (dashed line). The insets within the scheme presents the system corresponding to the potentials curves. From top to bottom V1, V2, V3. Modified from [89].

1.1.6 Heteroaggregates as magnetic carriers

Nowadays, micron-sized, superparamagnetic beads, i.e., spherical nanocomposite particles containing superparamagnetic nanoparticles dispersed in a solid matrix, usually a polymer, are the most frequently used materials as the magnetic carriers in bioseparation [12,27,59,68,79,100]. The superparamagnetic iron-oxide nanoparticles are usually synthesized within the pre-synthesized, micron-sized, porous polymer beads [45]. The nanosized superparamagnetic nanocomposite particles can also be synthesized by different synthesis processes, such as mini-emulsion polymerization [101], in-situ polymerization [102], polymer coating [87], and emulsion solvent evaporation [49]. The disadvantages of the composite carriers are in the low magnetization related to the dilution of magnetic properties with the non-magnetic matrix and the low specific surface.

As an alternative, the superparamagnetic nanoclusters can be synthesized by assembling individual superparamagnetic nanoparticles into nanoclusters in their aqueous suspension. The assembling can also be used to combine nanoparticles of different functional materials into multifunctional composite nanoparticles, for example, by combining magnetic nanoparticles with catalytic, photocatalytic, fluorescent, plasmonic, etc., nanoparticles [103-105]. Heteroaggregation, heteroassociation, heteroflocculation and heterocoagulation are some of the terms quoted in the scientific literature, which are used to describe mixed particulate systems. The heteroaggregation, i.e., the process of aggregation between nanoparticles of different types (composition, charge, or size), is generally used to describe permanent contact between particles and hence irreversibility. The simpler case of homoaggregation, where only one type of particle is present, is well studied and documented in the literature [106]. Two limiting regimes influencing the heteroaggregation kinetics have been observed in literature, i.e., diffusion-limited cluster aggregation and reaction-limited cluster aggregation [107]. In the diffusion-limited cluster

aggregation, in which every collision between particles results in the formation of a bond, whereas in the reaction-limited cluster aggregation, in which a large number of particle collisions are necessary before a stable bond is established. The cluster structure in both cases is fractal [108,109]. Generally, the diffusion-limited cluster aggregation results in the formation in the formation of dendrite-shaped aggregates [110,111], and the reaction-limited cluster aggregation leads to formation of compact aggregates [112]. However, when systems are composed of several species, the reaction kinetics are much more complex and no general kinetic theory is so far available [113,114]. Heteroaggregation has been shown to be important in many areas, such as waste-water treatment [41,115,116], catalytic materials [117], and in biotechnology, for example, in cell recovery [118-120].

When nanoparticles are suspended within a medium, random nanoparticle collisions are inevitable. As a result of these collisions, nanoparticles may rebound off one another, e.g., when they have the same surface charge, or aggregate, e.g., when they have opposite surface charge. The key to the synthesis of nanoclusters or composite nanoparticles is in controlling the interactions and parameters, e.g., relative nanoparticle size, number ratios, nanoparticle concentrations and ionic strength, between the nanoparticles in the suspension, which was the basis of my PhD. Understanding the interactions between the nanoparticles in the suspension is also of crucial importance for bonding a high surface concentration of superparamagnetic nanoparticles onto large targets, such as microorganisms, in the process of their magnetic separation.

1.1.6.1 Interactions between nanoparticles in a suspension

Generally, the interactions between nanoparticles in the suspension, which can be applied in controlled heteroaggregation of nanoparticles, can be divided into electrostatic attractions, acting between nanoparticles displaying opposite surface charges, and chemical interactions, originating from chemical reactions between different molecules at the nanoparticles' surfaces.

1.1.6.1.1 Heteroaggregates formed by electrostatic interactions

The electrostatic heteroaggregation is based on electrostatic interactions in the suspension [107]. Unlike van der Waals interactions, which are primarily attractive in nature, electrostatic interactions can be either attractive (between oppositely charged particles) or repulsive (between like-charged particles) and even directional (in the case of particles with asymmetric surface charge distributions) [121]. While van der Waals attractions will result in nonspecific spontaneous agglomeration, electrostatic forces can be applied to control the aggregation.

The heteroaggregates formed by electrostatic interactions between oppositely charged nanoparticles were synthesized by the attachment of smaller nanoparticles, e.g., gold or maghemite, to the functionalized surfaces of larger nanoparticles, e.g., silica or polystyrene [122-125]. Another possibility for synthesizing heteroaggregates by electrostatic interactions is by using layer-by-layer techniques, where a multilayer of smaller nanoparticles is attached onto larger templates [126-130].

1.1.6.1.2 Heteroaggregates formed by chemical interactions

Even better control over the process of heteroaggregation in suspensions can be achieved by using the chemically-directed assembly of nanoparticles in suspensions [82,131]. The nanoparticles will assemble into clusters as a result of chemical interactions originating from covalent bonding [132], hydrogen bonding [133,134], or donor-acceptor interactions [135]. To control the surface chemistry of the nanoparticles, they are usually

functionalized. For instance, heteroaggregates were formed by the hydrogen bonding between amino-functionalized gold nanoparticles and crown-ether decorated superparamagnetic iron-oxide nanoparticles [136] or by grafting gold nanoparticles onto thiol-functionalized magnetic nanoparticles [137]. Heteroaggregates were also formed by using the assembly of amino-functionalized magnetite nanoparticles and NiO nanoparticles [138]. Usually, the formation of heteroaggregates is studied using larger silica spheres, e.g., thiol- or amino functionalized, and smaller functionalized nanoparticles, such us palladium [139], or magnetite [140].

Specific biomolecular crosslinking interactions originating from DNA duplexes [141,142], biotin-avidin interactions [143], antigen-antibody recognition [144], or low-affinity immune-system carbohydrate-selectin interactions [131] can also be applied for improved selectivity of the interactions between nanoparticles.

In addition, the nanoparticles can be assembled into heteroaggregates by using crosslinker molecules [145,146] or click reaction, i.e., reaction between azide group and alkynyl group of particles [147]. Typical click reactions display several important criteria, such as high efficiency under mild conditions, minimal by-products, and limited side reactions. The most well-documented example is the copper (Cu) (I) catalyzed alkyne-azide cycloaddition to form 1, 2, 3 triazoles [148].

1.1.6.2 Parameters influencing on the structure of heteroaggregates

According to literature data, particle number ratios [113], relative particle sizes [132], particle concentrations [149] and ionic strength of the suspension [150] influence the process of heteroaggregation between oppositely charged particles in the aqueous suspensions.

1.1.6.2.1 Influence of a relative nanoparticle size and a nanoparticle number ratio on heteroaggregation in suspension

When nanoparticles were similar in size and equal in particle number ratio (Figure 9a), the dissimilar particles collide in a random manner and form irregular clusters of particles [150]. The larger the cluster the more likely they are to become visible precipitates. By keeping the relative nanoparticle size constant and changing the nanoparticle number ratios the formed structures of heteroaggregates can be controlled [151].

If there was a large difference in particle size and particle number ratio, the smaller particles (in excess) adsorbed onto the surface of the larger ones (Figure 9b) [113]. The structures of heteroaggregates can be controlled by controlling nanoparticle number ratios. By changing the nanoparticle number ratio from equal to large excess of smaller to larger particles Hiddessen et al., [131] synthesize heteroaggregates of different structures, for example, raspberry-like heteroaggregates or rings formed when smaller particles were in large excess and elongated chains, when the amount of nanoparticles was equal.

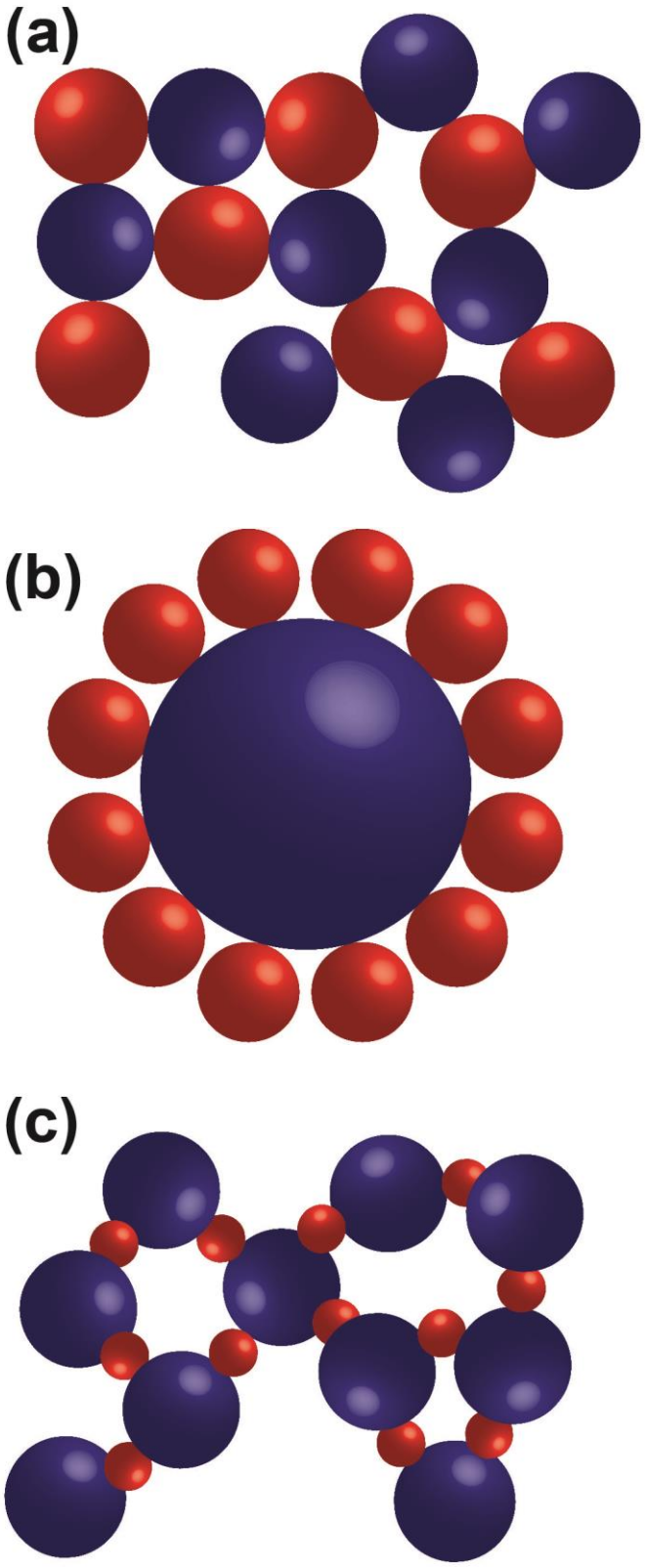

Figure 9: *A schematic representation of heteroaggregation of particles with different particle size and different particle number ratio.* Different particles of the same size with the same particle number ratio (a), forming irregular clusters of particles; different particles with a large size and particle number ratio (b), where the smaller particles are adsorbed onto the surface of larger particles; and different particles with a large size and smaller particle number ratio (c), where the smaller particles make “bridges” between larger particles.

1.1.6.2.2 Influence of pH on heteroaggregation in suspensions

Besides relative nanoparticle size and nanoparticle number ratio, a pH of the suspension has an important role on heteroaggregation. Heteroaggregation between oppositely functionalized nanoparticles in a suspension is usually the most effective at the pH value, where the opposite nanoparticles display the highest surface charge [51,132,152]. At that pH the like-particles repeal each other and dislike-particles attract each other. In contrast, no heteroaggregation was occurred at pH values, where the differently functionalized nanoparticles display same surface charge [153,154].

1.1.6.2.3 Influence of ionic strength on heteroaggregation in suspension

The ionic strength is another parameter that has an influence on the process of heteroaggregation. By controlling the added amount of salt different structures of heteroaggregates can be formed [150]. For example, at low salt concentration, where the long-range electrostatic interactions dominated, the open fractal heteroaggregates were synthesized [150,155]. However, at high salt concentration, where the short-range interactions are relevant, the heteroaggregates become very compact, with the aggregation kinetics being extremely fast [156].

1.1.6.3 Interactions between functionalized nanoparticles and microorganisms

The above mentioned interactions and parameters that influence the heteroaggregation between nanoparticles in the suspension are also important for the bonding of a high surface concentration of superparamagnetic nanoparticles onto microorganisms, which can be further separated from the suspension using magnetic separation.

For the separation of larger targets, e.g., yeast or bacteria, by magnetic separation a high surface concentration of attached magnetic nanoparticles could be achieved by electrostatic interactions between microorganisms (negatively charged) and oppositely (positively) charged magnetic nanoparticles [88,157]. Using the electrostatic interactions between functionalized nanoparticles and microorganisms, the surface coverage of microorganisms can be controlled by changing the concentration of functionalized nanoparticles and/or the incubation time. Singh et al., [158] found out that the higher concentration of functionalized magnetic nanoparticles and longer incubation time significantly increased the coverage of bacteria cells.

Biomolecular interactions between functionalized magnetic nanoparticles and microorganisms are another possibility to achieve even denser and more specific surface coverage of attached magnetic nanoparticles onto microorganisms compared to electrostatic interactions. For specific magnetic separation of larger biological targets, e.g., bacteria cells, with smaller magnetic nanoparticles by biomolecular interactions, magnetic nanoparticles are usually functionalized with antibodies against surface antigens of cells [159], proteins [160] or antibiotic [161-163]. In contrast to electrostatic interactions, where functionalized nanoparticles would attach onto every particle in the suspension with opposite surface charge, nanoparticles functionalized with biomolecules would attach to specific microorganism on the principle of key and lock model [162].

1.2 Malolactic fermentation

Winemaking normally involves two fermentation processes: an alcoholic fermentation and a malolactic fermentation (MLF). Yeasts conduct the alcoholic fermentation in wine, mainly converting sugars to ethanol and carbon dioxide. MLF is so-called secondary fermentation and generally occurs just after the alcoholic fermentation in winemaking, with a delay more or less long according to the wine-making conditions, bacteria

concentration and physical and chemical factors of the wine. This phase consists of an adaptation phase of the cells to stress factors of the wine. It starts as soon as the bacterial population reaches a concentration of 10^6 colony-forming units (CFU)/mL [164] and its duration is approximately 5 days to 3 weeks according to physical and chemical factors [165]. MLF is performed by the lactic acid bacteria (LAB), that converts the L-malic acid to L-lactic acid and carbon dioxide (Equation 8) [166] with the mass balance (Equation 8a)[167].

$$C_4H_6O_5 \rightarrow C_3H_6O_3 + CO_2 \quad (8)$$

$$1g \quad \rightarrow 0.67g \quad + 0.33g \quad (8a)$$

Basically, the two acidic groups of malate are replaced with only one acidic group present in lactate which results in a decrease in acidity of the wine. Different bacteria genera of LAB (*Lactobacillus*, *Pediococcus*, *Leuconostoc* and, principally, *Oenococcus*) have been reported to carry out MLF in wine produced worldwide (Table 1) [168-170]. Under certain conditions, the contributions made by MLF improve wine quality, but the same contributions may be considered highly undesirable under a different set of circumstances (see Table 2) as found in the cool- versus warm- viticultural regions. MLF in wine is desirable for three reasons: to decrease the acidity, to enhance the organoleptic characteristic and to increase the microbiological stability of wine [171]. MLF is encouraged in cool viticultural regions (e.g. northern Europe, New Zealand, Canada or northeast USA [172]) where grapes may have high levels of malic acid, in wine aging in oak barrels, when long-time maturation in bottles is part of the process (e.g. Champagne), or when a specific organoleptic profile is required, as in Chardonnay, Burgundy white wines and Bordeaux red wines [173].

Table 1: *List of the most widespread lactic acid bacteria species in grape must and wine [166].*

- Lactobacilli	- Facultative heterofermenters	- *Lactobacillus casei* - *Lactobacillus plantarum*
	- Strict heterofermenters	- *Lactobacillus brevis* - *Lactobacillus hilgardii*
- Cocci	- Homofermenters	- *Pediococcus damnosus* - *Pediococcus pentosaceus*
	- Heterofermenters	- *Leuconostoc oenos (Oenococcus oeni)* - *Leuconostoc mesenteroides* - *subsp. mesenteroides*

In some wines MLF is considered spoilage, especially in warm viticultural regions with grapes containing less malic acid. Uncontrolled or spontaneous MLF implies several risks, such as a considerable increase in volatile acidity, consumption of residual sugars and formation of undesirable metabolites, such as biogenic amines, that can affect human health and lead to low quality wines [174,175]. In addition to undesirable organoleptic changes, the colour of red wine may be reduced by as much as 30 % [176], and biogenic amines may be produced [177]. If MLF is not desired, the growth of LAB in wine must be suppressed by removing or inactivating the bacteria that are present. This can be achieved by employing antimicrobial compounds as wine preservatives and genetic modification of yeast strains to produce antimicrobial agents such as bacteriocins [173].

Table 2: *Influence of LAB's metabolism on wine sensory profile* [178].

Bacterial strain	Advantage	Risk
Selected ***O. oeni***	- Reduction of total acidity - Reduction of ketone and aldehyde compounds (reducing SO_2 requirement) - Partial microbial stability - Reduction of grassy and vegetative notes - Increase in front-pallet volume - More diacetyl level control - Dominance over wild bacteria	- Production of volatile acidity (especially under high pH conditions, in presence of residual sugars and after L-malic acid degradation) - Loss of colour - Production of ethyl carbamate
Spontaneous ***O. oeni***	- Reduction of total acidity - Reduction of ketone and aldehyde compounds (reducing SO_2 requirement) - Partial microbial stability - Reduction of grassy and vegetative notes - Increase in front-pallet volume	- Long lag phase involving an increase in the volatile acidity depending on the pH - Significant bacterial growth involving a high production of diacetyl - Production of spoilage aromas and flavours (mousy off flavour, sweat, sauerkraut) - Reduction of esters (fruity characters) - Loss of varietal aromas - Colour loss by direct action on polyphenols - Production of biogenic amines - Production of ethyl carbamate

1.2.1 Factors influencing the MLF

Wine is a complex environment (sugar, fatty acids, amino acids, organic acids, phenol components, ethanol, SO_2, pH). Its physical and chemical characteristics vary according to numerous conditions: vine variety, climatic conditions, and winemaking conditions. These physical and chemical characteristics do not correspond to the optimum conditions for growth of LAB and particularly *Oenococcus* oeni (*O. oeni*) and are, thus, stressful. Therefore, these parameters have a major impact on the progress of MLF. The factors influencing MLF can be divided into the following categories [165]:

– The chemical and physical composition of wine.

– The microbial interactions between the LAB and other wine microorganisms.

1.2.1.1 Influence of physical and chemical factors on MLF

1.2.1.1.1 Influence of temperature

Temperature has an important role in the final quality of wine [179]. It modifies growth speed of all microorganisms (yeasts and bacteria). Majority of LAB being mesophilic [180], its optimum growth is between 25 and 30°C in laboratory culture. In wine the

optimum temperature of growth is different from that obtained in a laboratory. The ideal temperature for growth of *O. oeni* in wine and consumption of L-malic acid is between 20 and 25°C, according to the strain studied [181]. This value is modified according to physical and chemical parameters and notably ethanol content. The higher the ethanol content, the more of the optimum growth temperature is decreased. The average temperature at which MLF is carried out in the cellars is between 18 and 22°C. These conditions are therefore favourable for the growth of *O. oeni*. However, in certain cases temperature is often less than 18°C, bacterial growth is then slower, enzymatic activities are reduced and MLF starts late. Low temperature has an impact on the molecule and notably on transcription, mRNA translation and DNA replication [180]. In fact, cold temperatures induce formation of secondary structures in the mRNA which slow down translation [182]. Temperature changes can equally induce negative DNA rolling and modify topoisomerase activities and DNA gyrase [183,184].

1.2.1.1.2 Influence of pH

pH is the factor which has most influence on development of LAB in wine. Most LAB are neutrophilic. Generally, the optimum pH growth of LAB is close to neutrality [185]. Some families of bacteria such as *Lactobacillus* and *Oenococcus* show more acidophilic behaviour. In terms of initiation and completion of MLF, wines of pH 3.3 and above generally exhibit few problems, whereas at lower pH, difficulties may be experienced [186]. *O. oeni* usually represents the dominant species in wine below pH 3.5. At higher pH *Lactobacillus* and *Pediococcus spp*. may survive and grow. The pH strongly affects malolactic activity of the cell [187]. Although sugar utilization and growth of *O. oeni* are inhibited by low pH [188], malolactic activity is the highest at pH 3.5 to 4.0.

1.2.1.1.3 Influence of ethanol content

Ethanol, produced by yeast during alcoholic fermentation, is considered as one of the main factors which inhibits growth of LAB in wine. The final ethanol content is very variable according to the wine 10-16 % (v/v). Different types of LAB are more or less tolerant to ethanol. *O. oeni* can tolerate content attaining 14 % (v/v) [181,189]. These values are however variable according to the strain studied [187]. Resistance to ethanol also varies according to other environmental conditions such as temperature and wine pH [181,189]. Cell tolerance to ethanol diminishes when environmental pH is low and temperature increases. Low concentrate in ethanol 3-5 % (v/v) can stimulate *O. oeni* growth [181,189]. Ethanol toxicity is generally attributed to the fact that this molecule inserts itself into the hydrophobic part of the membrane lipid double layer [190]. Destabilization of the membrane structure then occurs which later affects several cell processes such as DNA replication, enzymatic activities, metabolites transport and peptidoglycane synthesis [190,191].

1.2.1.1.4 Influence of sulphur dioxide

Sulphur dioxide (SO_2) is another factor which plays an essential role in the growth of *O. oeni* and on the realization of MLF [179]. This component, found in wine with variable concentrate according to the wine-making conditions, has two origins: an exogenous origin and an endogenous origin.

The exogenous SO_2 originates from sulphuring during wine-making. Sulphur dioxide is mainly used for its antioxidant effect and antimicrobial activity. It can be added to grape must when it is being put into the vat, to limit proliferation of LAB and thus avoiding interruption of alcoholic fermentation [192].

Endogenous SO_2 originates from yeast metabolism. During alcoholic fermentation, yeasts synthesize and naturally liberate molecular SO_2 in wine. The quantity varies

according to yeast strain and wine-making conditions [193,194].

1.2.1.2 Influence of microbial interactions between the LAB and other wine microorganisms

During the process of wine-making, there is large microbial diversity. *O. oeni* coexists with several other micro-organisms: LAB and essentially yeasts. This bacterium is in competition with the latter for usage of wine nutriments.

1.2.1.2.1 Interactions between yeasts and LAB

During alcoholic fermentation, yeasts multiply. Yeasts consume sugar and nitrogenous sources, including amino acids, more quickly than bacteria and liberate toxic metabolites (ethanol, fatty acids, SO_2) for the LAB that are also at the origin of regression of the bacterial population [193,195]. Yeasts can equally produce and liberate substances possessing a bacteriostatic or bactericidal effect which affects MLF [194,196]. At the end of alcoholic fermentation, yeast autolysis thus liberates growth factors (amino acids, vitamins, mannoproteins) for the LAB [195,197]. These molecules allow a quick growth of the bacteria and a decrease in the latency time between the two fermentations. Yeasts/bacteria interaction is complex, firstly opposing, then synergic, and is still relatively unknown [193].

1.2.1.2.2 Interactions between LAB

This phenomenon of competition also exists between different types of LAB. During the wine-making process, opposing effects between different bacterial types entitled *Pediococcus, Lactobacillus, Leuconostoc* and *Oenococcus* can be found [198]. These effects are probably due to liberation of components with antimicrobial property such as bacteriocines [199].

1.2.1.2.3 Bacteriophages

As for during the development process of dairy products, phage represents a threat for the MLF process. *O. oeni* strains can be infected by phage [200]. These phage attacks appear in wine together with a slowdown of MLF [187]. The phages, isolated from wine, are able to induce lytic and lysogene cycles in *O. oeni* [200,201]. Difficulties in MLF due to phage can therefore result in a need for more time, thus allowing for undesirable bacteria such as *Pediococcus* to develop.

1.2.2 Lactic acid bacteria

LAB are present in all grape musts and wines. Depending on the stage of the winemaking process, environmental conditions determine their ability to multiply. Their impact on wine quality depends not only on environmental factors acting at the cellular level but also on the selection of the best adapted species and strains of bacteria.

All the strains have a similar cellular organization, but their physiological differences account for their specific characteristics and varying impact on wine quality. They are classified according to their morphological, genetic, and biochemical traits [166].

1.2.2.1 Cell wall

The cell wall of Gram-positive bacteria, such as LAB, is essentially composed of a peptidoglycan (murein), a specific component found on the outer side of the cytoplasmic membrane of almost all bacteria (Figure A1, Appendix) [202]. The main structural features of peptidoglycan are linear glycan strands cross-linked by short peptides. The

glycan strands of the cell wall consist of the repeating disaccharide *N*-acetylmuramic acid and *N*-acetylglucosamine (Figure A2, Appendix). They alternate along the entire length of the chain, linked by β-type (1-4) glycosidic bonds that can be hydrolyzed by lysozyme or mutanolysine. A chain of four amino acids is linked to muramic acid; L-alanine, D-alanine and D-glutamic acid are in majority. A peptide bond links the tetrapeptide of another polysaccharidic chain to the third amino acid (Figure A2, Appendix). The peptidic chains vary depending on the species of the bacteria. The sequence of their amino acids can be used in taxonomy [166].

The cell walls of LAB, like those of nearly all Gram-positive bacteria, also contain ribitol phosphate or glycerol phosphate polymers called teichoic acids. Glycerol based teichoic acids contain a glycolipid by which they attach themselves to the external layer of the plasmic membrane. They pass through the peptidoglycan and are at the surface of the cell wall acting as the antigenic sites of bacteria. The proportion of peptidoglycans and teichoic acids varies depending on the species and also the phase of the cell development cycle. Teichoic acids can represent up to 50 % of the weight of the cell wall. The cell wall is rigid and gives the cell its form: round for cocci, elongated for bacilli. It permits the cell to resist very high internal osmotic pressures (up to 20 bars) [203]

There are more than 100 known surface proteins of Gram-positive bacteria [204]. Many of these proteins share some conserved features needed for cell wall anchoring [205].

Water, mineral ions, substrates and metabolic products diffuse freely across the cell wall. At this level, proteases also release amino acids from proteins and peptides which are used for cellular metabolism [166].

1.2.2.2 Multiplication of LAB

All bacteria multiply by binary division (Figure 10). A cell gives two completely identical daughter cells. Multiplication supposes, on the one hand, division of nuclear material, and on the other hand, synthesis for the construction of new cellular envelopes and cytoplasmic elements, in particular ribosomes and enzymes.

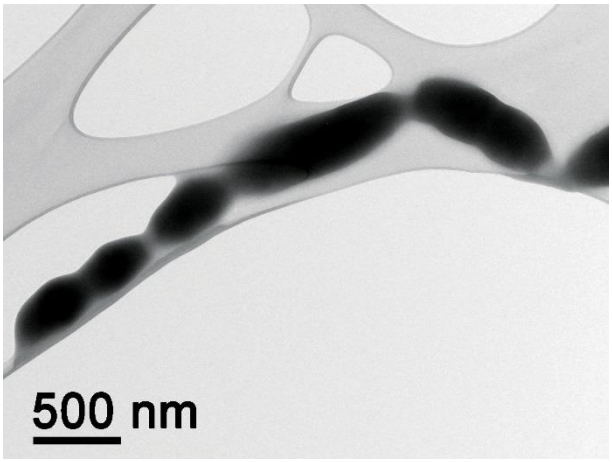

Figure 10: *Multiplication of O. oeni*. TEM image of binary division of *O. oeni*.

The replication occurs almost during the entire cellular cycle at the mesosomes. When it is finished, the scission of the cytoplasm begins. A septum is formed in the middle of the cell as a result of the synthesis of portions of the membrane and the cell wall. It separates the mother cell little by little into two daughter cells. The genetic material and the other cellular components are simultaneously distributed between them. Finally, when the septum is completely formed, the two daughter cells separate. Cell and nucleus

division are not synchronous; replication is quicker. Moreover, a replication cycle can start before cell division is completed. For this reason, bacteria cells in their active growth phase contain more than one chromosome per cell. During division, plasmids (much smaller than the chromosome) are not always correctly distributed between the cells after their replication, hence their instability over generations [166].

1.2.2.3 Taxonomy

The objective of taxonomy is to identify, describe and class microorganisms. Classification is made according to several hierarchical levels. For bacteria, the highest level corresponds with their classification among procaryotes. In a species of bacterium, strains grouped together share a number of identical characters. These characters radically differentiate them from other strains [166].

Phenotypes include morphological, physiological, biochemical and immunological characters as a whole and the composition of certain cellular components. A first level takes into account the percentage of guanine and cytosine bases in the DNA; the (G + C) % with respect to the total number. Two strains are not necessarily related because they have the same (G + C) %. In fact, the base composition does not give any indication of the DNA sequence. Among Gram-positives, LAB belong to the phylum *Clostridium*.

The *Clostridium* branch consists of three groups: the first includes the *Lactobacillus*, *Pediococcus*, *Leuconostoc*, *Oenococcus*, and *Weissella* genera; the second, *Streptococcus* and *Lactococcus*; and the third, *Carnobacterium*, *Vagococcus* and *Enterococcus* [166].

Dicks et al. [206] proposed a new species, *Oenococcus oeni*, for bacteria previously known as *Leuconostoc oenos*, currently the only species in the *Oenococcus* genus. This proposition was based on the phylogenetic distance of *O. oeni* with respect to other LAB.

1.2.2.3.1 Oenococcus oeni

O. oeni (formerly *Leuconostoc oenos*) [206] is the major bacterial species found in wines during MLF, and is well adapted to the low pH, high SO_2 and ethanol levels of concentration in wine [168]. Such harsh conditions result in very slow growth and poor cell density of biomass in wine. The slow growth and poor yields of the bacteria were frequently encountered when starter cultures were used to inoculate wine or cider, with MLF taking up to several weeks or even months for completion in such conditions. Even under more favourable conditions (optimal pH, appropriate sugar without ethanol) the specific growth rate of *O. oeni* is low; ranges of 0.01-0.04 h^{-1} on glucose and 0.06-0.10 h^{-1} on glucose/fructose mixture have been observed [207].
Description of *O. oeni* [166]:

- Non-mobile, non-sporulating, spherical or slightly elongated cells, assembled in pairs or small chains; diameter 0.5-0.7 μm, a length 0.7-1.2 μm.
- Facultative anaerobiosis.
- Chemo-organotroph: requires a rich medium and fermentable sugars.
- Optimum growth temperature 20-30°C.
- Metabolic products of glucose: CO_2, lactic acid and ethanol.
- Arginine is metabolized by certain strains of *O. oeni*, whereas other *Leuconostoc* species respond negatively to this test.

– (G + C) % from 38 to 44 %.

– No teichoic acid.

1.2.2.3.2 Metabolism of LAB

Metabolism represents the biochemical reactions of degradation and synthesis carried out by the bacteria cell during multiplication. LAB are chemotrophic: they find the energy required for their entire metabolism from the oxidation of chemical compounds [166]. Research in progress is showing that these bacteria can modify some of the components and sensory properties of wine, providing a new opportunity to alter the chemistry and possibly the aroma and flavour perception of wine (Figure 11) [208].

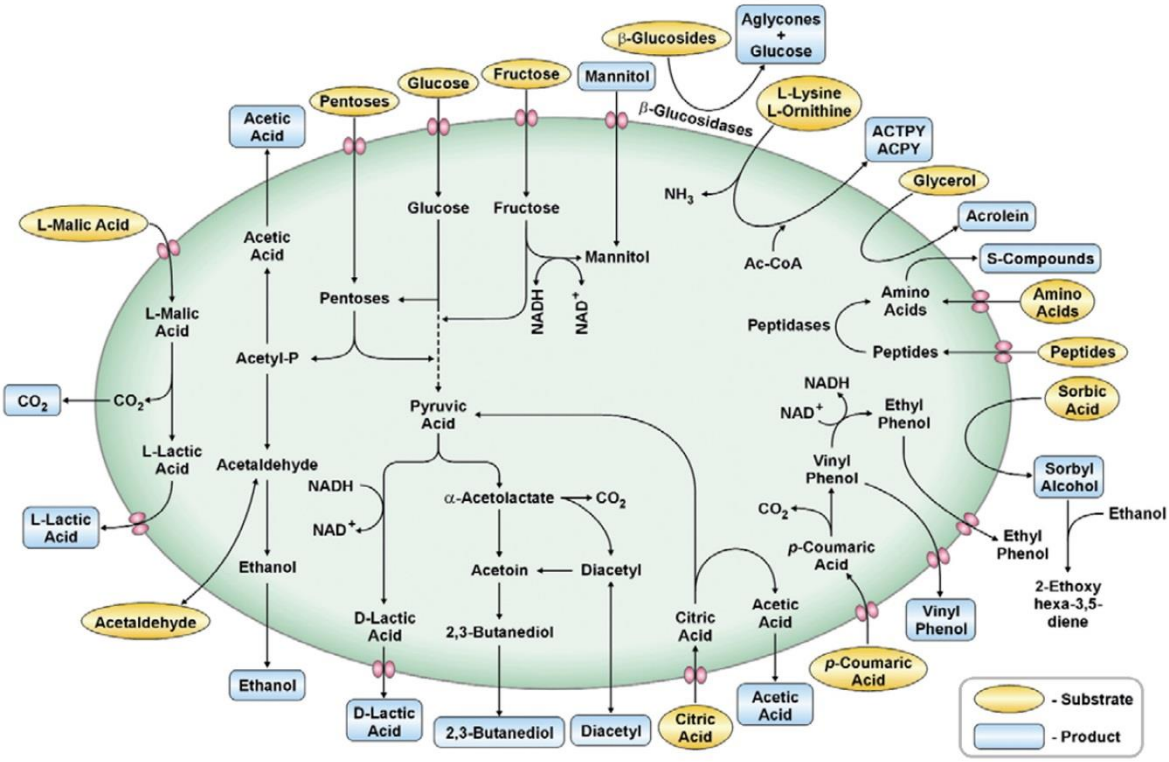

Figure 11: *A schematic representation of the biosynthesis and modulation of flavour-active compounds by malolactic bacteria* [208].

The metabolism of sugars and organic acids during MLF can be divided into three phases. During the growth phase (Phase I), sugar catabolism occurs with little production of acetic and lactic acid; minimal citric and malic acid are metabolised in this phase. As the bacterial cell numbers increase above $5 \cdot 10^6$ CFU/mL during Phase II, the catabolism of sugar ceases and malic acid metabolism proceeds accompanied by production of lactic acid; citric acid remains untouched at this stage, and there is no acetic acid produced during malic acid degradation. Phase III is characterized by the metabolism of citric acid accompanied by an increase in acetic acid. The increase of lactic acid content in the wine results in a softer mouth-feel and the acetic acid contributes to the volatile acidity of the wine (Figure 11) [208].

Generally, wine LAB are known to be particularly fastidious microorganisms with complex nutrient requirements. For a long time, the degradation of malic acid to lactic acid (Equation 8) was believed to be the source of energy for the growth of the malolactic

bacteria in wine. LAB cannot grow with L-malic acid as a unique carbon source, therefore these microorganisms need an additional energy source, such as residual fermentable sugars, i.e., glucose or fructose or amino acids such as arginine, to allow cell growth [171]. A source of carbon (derived from sugars), nitrogen (derived from free amino acids or short peptides), vitamins (nicotinamide (B_3), thiamine (B_1), biotin (B_7) and pantothenic acid (B_5)), mineral ions (Mn^{2+}, Mg^{2+}, K^+ and Na^+) and purine derivatives (guanine, adenine, xanthine and uracil) are all required for optimum growth [209].

1.2.2.3.2.1 Sugar metabolism

Better growth of *O. oeni* was obtained in the presence of sugar mixtures (glucose/fructose, glucose/sucrose and fructose/sucrose) compared with single sugars [188]. Bacteria using the heterofermentative pathway transform hexoses principally but not exclusively into lactate. The other molecules produced by this metabolism are essentially CO_2, acetate and ethanol; this is the pentose phosphate pathway (Figure A3, Appendix). Pyruvate is further reduced by a D-lactate dehydrogenase in D-lactate that is partly used for the peptidoglycan synthesis, thus reducing the quantity to be rejected by the cell and avoiding D-Ala synthesis [166,210]. *Oenococcus* ferments fructose to fructose-6-P, which then enters the pentose-P pathway and is converted to mannitol without the co-formation of sorbitol [211].

1.2.2.3.2.2 Amino acid metabolism

Oenococcus strains are fastidious organisms that require amino acids and vitamins in addition to a fermentable carbohydrate. Ritt et al. [212] demonstrated that that *O. oeni* was able to assimilate various oligopeptides to fulfil amino-acid requirements. Fourcassie et al. [213] demonstrated the absolute requirement for four amino acids (arginine, glutamic acid, tryptophan and isoleucine), while six others (valine, methionine, cysteine, leucine, aspartic acid and histidine) are required for optimum growth of *O. oeni*. A range of amino acids is found in wine [166,214]. Arginine, being one of the most important amino acids in grape must and wine, represents a potential source of energy and increases the viability of *O. oeni* [215]. In wine, heterofermentative LAB may degrade arginine during MLF via the arginine deiminase (ADI) pathway (Figure A4, Appendix), leading to the formation of ammonia, ornithine, citrulline, ATP and CO_2 [216]. *Oenococci* were able to degrade arginine at pH 3.9 and partially at pH 3.6, but not at pH 3.3 [217].

The growth of *O. oeni* was significantly enhanced in the presence of low sugar concentration with organic acids such as malate or citrate.

1.2.2.3.2.3 Organic acid metabolism

Citrate and malate are the two major organic acids metabolized by *Oenococcus*. Within bacteria, citric acid is split into an oxaloacetate molecule and an acetate molecule by the lyase (Figure A5, Appendix). Oxaloacetate is then decarboxylated into pyruvate. Pyruvate is the source of acetoin compounds: diacetyl, acetoin and 2,3-butanediol. The first is particularly important organoleptically. It is the very aromatic molecule that gives butter its smell [166].

LAB metabolise L-malate by one of three different enzymatic pathways (Figure A6, Appendix), converting it to L-lactate and CO_2 [166]. Some LAB, e.g., *O. oeni*, possess an active malolactic enzyme, which decarboxylates L-malate directly to L-lactate without free intermediates. Several studies have shown that L-malate stimulates the growth and biomass production of *O. oeni* [218-220]. *O. oeni* changes its metabolism, when pH drops below pH 3.5. Below pH 3.5, L-malate is metabolised at a high rate, whereas carbohydrate metabolism proceeds very slowly [173].

1.2.2.3.3 Malolactic enzyme

The decarboxylation of malic acid to lactic acid forms the basis of malolactic fermentation. In recent years it has become clear that the transformation of L-malic acid into L-lactic acid is not a true fermentation, but rather the enzymatic decarboxylation of malic acid, which could be catalysed by three possible pathways (Figure A6, Appendix). First observations indicated a two-step reaction of malic enzyme (ME, EC 1.1.1.38-oxaloacetate-decarboxylating, 1.1.1.39-decarboxylating and 1.1.1.40-oxaloacetate-decarboxylating using $NADP^+$) and L-lactate dehydrogenase (L-LDH, EC 1.1.1.27). Thereafter a three-step reaction including L-malate dehydrogenase (L-MDH, EC 1.1.1.37), oxaloacetate decarboxylase (OADC, EC 4.1.1.3) and L-LDH was also discussed or even a possible complex of two or three enzymes was presumed [221]. Caspritz and Radler [222] proved that the responsible enzyme, referred to as the malolactic enzyme (MLE, not EC classified), consists of two identical subunits and directly converts L-malic into L-lactic acid. The active form is composed of two or four identical subunits of 60-70 kDa and the protein is strongly homologous to malic enzymes from different organisms [173]. This reaction is performed in the presence of catalytic concentrations of nicotinamide adenine dinucleotide (NAD^+) and Mn^{2+} but the mechanism of the MLE remains unclear because no reduction of NAD^+ or detection of free reaction intermediates were reported [223]. Schumann at al. [221] prepared the recombinant MLE from *O. oeni* strain DSM 20255 that retained 95 % of its activity after 3 months at room temperature and 7 months at 4°C.

1.2.3 Control of MLF

The control of MLF may be governed in several ways. It can be promoted through: strain selection, starter culture development and improved reactivation, development of malolactic reactors with free or immobilized bacteria, or enzymes or the construction of recombinant wine yeast strains conducting concurrent alcoholic fermentation and MLF [173]. Controlled MLF by the use of selected immobilized LAB is desired for the following reasons [224]:

- Natural MLF takes a long time, and growth limitations of lactic acid microflora affect and depend on the physical-chemical properties and nutritional composition of wine, e.g., fatty acids and ethanol may inhibit LAB growth. Therefore, immobilization techniques aim to increase the tolerance of the MLF bacteria.

- The development of desired flavour by using selected cultures of bacteria.

- The acceleration of MLF by higher cell densities achieved by immobilization techniques.

- The feasibility of application and commercialization of the process by lyophilized and immobilized cultures.

- The reuse of cell for MLF and the application of continuous processes [225,226].

During recent years several technologies have been proposed to control MLF of wines by using LAB, principally *O. oeni* [225]. These alternative technologies usually involve the use of high densities of the bacteria cells, free or immobilized by adsorption onto or encapsulation into different matrices, such as calcium alginate [227,228] or pectate [229], κ-carrageenan [230-232], polyacrylamide [230], cellulose [233,234] and poly(vinyl alcohol) hydrogel [235]. Genisheva et al. [236] used natural residues, e.g., corn cobs,

grape skins and grape stems for support of *O. oeni* cells in MLF. As a support for immobilization have also been used chemically modified chitozan beads (CCB)-chitopearls [226]. The study of the literature has shown numerous studies for developing MLF using different types of bioreactors with free or immobilized LAB. However, direct enzymatic bioconversion has scarcely been studied and only one enzymatic reactor has been reported. The ME (EC 1.1.1.38) of the LAB enables direct conversion of L-malic acid into L-lactic acid and carbon dioxide [222,237].

However, the encapsulation method has mass transfer limitations for nutrients that lead to inactivation, or even death, of the cells in the centre. To control MLF, instead of entrapment or immobilizing bacteria cells onto different matrices, magnetic nanoparticles could be absorbed onto the LAB cells' surface, as in case of separation of magnetic responsive yeast from sparkling wine [88]. Magnetic responsive LAB could be separated from wine at the end or at a certain point of MLF using an external magnetic field and so end or preventing further spontaneous MLF. There are already reports of isolation of Gram-positive bacteria (as it is *O. oeni*) from aqueous solution by using vancomycin [161] or aminoglycoside antibiotic -modified magnetic nanoparticles [163].

2 Aims and Hypothesis

2.1 Aims

In recent years, the influence of biotechnology has increased. New ways of biosynthesis have been developed and are being further developed in biotechnology. At the end of biosynthesis or biotechnology process, there is a need for separation of products or specific targets from the liquid mixture. A possible way to separate targeted species from the liquid mixture is magnetic separation, where appropriate magnetic carriers are bonded with targeted species in the liquid mixture. After the attachment of the targeted species onto the magnetic carriers of they are separated from the liquid mixture using an external magnetic field. The removal of such magnetic carriers by using of the magnetic field is more selective, efficient, and often also much faster than centrifugation or filtration.

Magnetic nanoparticles are of great interest for use as magnetic carriers in the separation. Decreasing a size of the particles used in magnetic separations from micrometers to nanometers increases the available absorptive surface by 100 to 1000 times. It is also beneficial, if the magnetic particles are small enough to be in superparamagnetic state (below approximately 20 nm), because they do not agglomerate due to magnetic dipol-dipol interactions. However, decrease of the size of the magnetic carriers to nano size, required for superparamagnetism is not practical, because the magnetic force acting on a particle in a field gradient is proportional to the particle volume (Equation 1). If the particles are too small, e.g., superparamagnetic, the magnetic forces acting on them in a magnetic-field gradient will not be large enough for efficient separation. The only way for effectively increase of the magnetic force F_m acting on a magnetic particle in a stable suspension exposed to a magnetic field gradient, while maintaining the superparamagnetic state, is to increase the particle volume. Therefore, because of the size limitation intrinsic to superparamagnetism, the only possibility is to create an assembly of a large number of superparamagnetic nanoparticles, i.e., superparamagnetic nanocluster. The minimum size for such nanoclusters of superparamagnetic iron-oxide nanoparticles that can be effectively manipulated by a magnetic field gradient was estimated to be approximately 50 nm. The ideal superparamagnetic nanoclusters for applications related to magnetic manipulation should be of uniform size of approximately 60 nm; they should have a high, effective absorptive surface area; and they should contain a large fraction of the magnetic material.

The main purpose of this thesis was to obtain the additional knowledge of interactions between different types of nanoparticles in an aqueous suspension. The obtained knowledge is crucial for synthesis of magnetic carriers - superparamagnetic nanoclusters using of the assembly of superparamagnetic nanoparticles in the suspensions. The same approach can also be used in the synthesis of multifunctional nanocomposite particles, combining nanoparticles of different materials, e.g., superparamagnetic nanoparticles with nanoparticles with catalytic, fluorescent, or plasmonic properties. On the other hand, bonding between two different types of nanoparticles represents a model for bonding individual superparamagnetic nanoparticles onto larger objects, e.g., microorganisms, which is a crucial part in the process of their magnetic separation. Therefore, the first aim

to be reached in this PhD thesis was to synthesize magnetic carriers with heteroaggregation of superparamagnetic maghemite nanoparticles in an aqueous suspension into superparamagnetic nanoclusters. Such magnetic carriers would have a high, effective absorptive surface area and contain a large fraction of magnetic material.

The second goal of this thesis is related to the possible application of magnetic separation in biotechnology. The aim was to prepare "magneto-responsive" bacteria with attachment of functionalized superparamagnetic nanoparticles onto the surfaces of LAB (*O. oeni*). The magneto-responsive bacteria could be used for the control of MLF in wine. At the certain stage or at the end of MLF, magneto-responsive bacteria could be separated from wine by using an external magnetic field.

2.2 Hypothesis

For the use of magnetic nanoparticles as magnetic carriers, e.g., in biotechnology, biomedicine and environmental engineering, it is necessary to know and understand the interactions between nanoparticles in the suspension. The first part of this thesis was devoted to the hypothesis stating that appropriate magnetic carriers for magnetic separation or multifunctional composite nanoparticles, combining nanoparticles of different materials can be synthesized by the control of interactions between nanoparticles in the aqueous suspension by controlling the nanoparticles' surface properties.

The understanding of the interactions between nanoparticles and various other objects in liquid mixture, e.g., the interactions between magnetic carriers and targeted species, is crucial for their magnetic separation. So, my next hypothesis in this thesis was, that by the controlling of interactions between the magnetic nanoparticles and surface of larger objects, e.g., microorganisms, magnetic nanoparticles can be attached to their surfaces. Magnetically modified microorganisms can be than separated from the suspension in the process of magnetic separation.

On the other hand, the microorganisms, e.g., bacteria, with attachment magnetic nanoparticles onto the surfaces can be manipulated with an external magnetic field during their fermentation process. In the second part of this thesis I was following the hypothesis stating that the MLF in wine can be controlled by magnetic separation of magneto-responsive bacteria, prepared by the attachment of magnetic nanoparticles onto bacteria cells, in a certain stage of MLF.

3 Materials and methods

3.1 Controlled synthesis of heteroaggregates

3.1.1 Materials

Silica nanoparticles (SNPs) were synthesized using a modified Stöber process by Dr. Marjan Bele from the National Institute of Chemistry, Ljubljana, Slovenia [238]. For the amino-functionalization of the silica nanoparticles (aSNPs) and amino-functionalization of the superparamagnetic silica-coated maghemite nanoparticles (aMNPs) 3-(2-aminoethylamino)propylmethyldimethoxysilane (APMS) was grafted onto their surfaces, as described elsewhere [74].

Detailed information about the synthesis and functionalization of the superparamagnetic maghemite nanoparticles is given in Section A1.3 in Appendix. In brief, maghemite (γ-Fe_2O_3) nanoparticles were synthesized using co-precipitation from aqueous solutions and then the stable aqueous suspension of the nanoparticles was prepared using citric acid as the surfactant, as described elsewhere [70]. The nanoparticles in the stable suspension were coated with a thin layer of silica using the hydrolysis and polycondensation of tetraethoxysilane (TEOS) in the presence of an alkaline catalyst NH_4OH, as described in ref. [69]. The silica-coated maghemite nanoparticles (MNPs) were functionalized with grafting presynthesized carboxyl-terminated silane molecules onto their surfaces to get carboxyl-functionalized silica-coated maghemite nanoparticles (cMNPs) or by grafting APMS to get aMNPs, as described in ref. [74].

The controlled heteroaggregates of functionalized superparamagnetic nanoparticles and superparamagnetic clusters were synthesized by using amino-functionalized superparamagnetic iNANOvative^{TM}|silica nanoparticle clusters (a-iNANO) that were kindly provided by a Nanos Scientificae d.o.o. (Nanos Sci).

Other chemicals used for the synthesis of heteroaggregates were 1-ethyl-3-[3-dimethylaminopropyl]carbodiimide hydrochloride (EDC), *N*-hydroxysulfosuccinimide (Sulfo-NHS), carboxy-(polyethylene glycol)$_n$-amine ($CAPEG_n$) with 8 (CAPEG8) or 24 (CAPEG24) ethylene glycol units and were purchased from Thermo Scientific.

3.1.2 Controlled heteroaggregation of model nanoparticles in an aqueous suspension

3.1.2.1 Electrostatic heteroaggregation

For the electrostatic heteroaggregation the aqueous suspension of aSNPs at pH 5.5 was vigorously admixed into the suspension of cMNPs at pH 5.5 at room temperature. The cMNPs/aSNP number ratio R was kept constant at $R = 89$ or $R = 15$, whereas the concentration of cMNPs was changed (0.7 and 15 mg/mL).

3.1.2.2 Chemically-driven heteroaggregation

The chemical interactions between the two types of nanoparticles, aSNPs and cMNPs, were the result of direct covalent bonding between the activated carboxyl groups and the amino groups of the functionalized molecules at the nanoparticle surfaces or by using heterobifunctional crosslinkers. The carboxyl surface groups of cMNPs were activated using single-step EDC coupling protocol [76]. In brief, the pH of the suspensions containing cMNPs (15 mg/mL, 4 mL) was adjusted to 5.5 with HCl (0.01 mol/L). The calculated amount of 5-fold molar excess of EDC (19 mg) was admixed to the suspension of cMNPs. After 5 min of rigorously stirring the calculated amount of aSNPs suspension (11 mg/mL, 4 mL) was added and the pH was adjusted to 7.3 with HCl (0.01 mol/L). The reaction mixture was stirred at room temperature for 2 hours. The formation of a covalent bond between the aSNPs and the cMNPs was studied for two different concentrations of cMNPs (0.7 and 15 mg/mL) and cMNPs/aSNP number ratios of R = 89 or R = 15.

3.1.2.2.1 Heteroaggregation using heterobifunctional crosslinker

Apart from the direct bonding between the activated carboxyl groups and the amino groups of the functionalization molecules, the heterobifunctional crosslinker molecules were used for the nanoparticles' assembly. The crosslinkers were first bonded to the activated cMNPs and subsequently reacted with the aSNPs. As a heterobifunctional crosslinker, CAPEGn samples with two different molecular weights (CAPEG8, 442 g/mol and CAPEG24, 1146 g/mol) were used (see Figure A11 and Figure A12 in Appendix). First, EDC in a 5-fold molar excess (19 mg) was used to form active ester functionalities with carboxylate groups on the cMNPs (15 mg/mL, 4 mL). To increase the solubility and stability of the active intermediate Sulfo-NHS (22 mg) was added to the suspension of cMNPs [76]. The pH value of the reaction mixture was adjusted to 5.5 using the HCl (0.01 mol/L) and stirred for 20 min at room temperature. After that the activated cMNPs were washed with distilled water using centrifugation (15,600g, 5 min). Second, the prepared stock solution of CAPEGn dissolved in DMSO, with the concentration of CAPEG8 (67 mg/mL) or CAPEG24 (250 mg/mL), was added to the suspensions of the cMNPs with the activated carboxyl groups. The added amount of CAPEGn stock solution was calculated with respect to the number of carboxylate groups on the cMNPs in the molar ratio 1.5:1. Then the pH value of the reaction mixture was adjusted to 7 using NaOH (0.01 mol/L). Finally, the reaction mixture was stirred for 2 hours at room temperature. To remove any unbound CAPEGn, the nanoparticles were washed with distilled water using centrifugation (12,800g, 5 min). The CAPEGn functionalized cMNPs were labeled as MNP-PEG8, for CAPEG8, and MNP-PEG24, for CAPEG24. The aSNPs and MNP-PEG (MNP-PEG8 or MNP-PEG24) were chemically bonded at the higher concentration of MNP-PEG (15 mg/mL) and the MNP-PEG/aSNP number ratio of R = 89.

The pH of the suspensions containing MNP-PEG (15 mg/mL, 2 mL) was adjusted to 5.5 with HCl (0.01 mol/L). The calculated amount of 5-fold molar excess of EDC (9.5 mg) was admixed into the suspension of MNP-PEG. After 5 min of rigorously stirring, the calculated amount of aSNPs suspension (11 mg/mL, 2 mL) was added and the pH was adjusted to 7.3 with HCl (0.01 mol/L). The reaction mixture was stirred at room temperature for 2 h. The formed heteroaggregates were collected with a permanent magnet, washed with and dispersed into distilled water.

3.1.2.3 Controlled heteroaggregation of functionalized superparamagnetic nanoparticles and superparamagnetic clusters in an aqueous suspension

For the controlled heteroaggregation of functionalized superparamagnetic nanoparticles and superparamagnetic clusters, the aSNPs used in the model system were replaced with a-iNANO. The heteroaggregates were synthesized by chemical interactions between a-iNANO and cMNPs, which was the result of direct covalent bonding between the activated carboxyl groups and the amino groups of the functionalized molecules at the nanoparticle surfaces. The carboxyl surface groups of cMNPs were activated using single-step EDC coupling protocol [76]. Briefly, the pH of the suspensions containing cMNPs (1 mg/mL, 4 mL) was adjusted to 5.5 with HCl (0.01 mol/L). The calculated amount of 5-fold molar excess of EDC (1.5 mg) was admixed to the suspension of cMNPs. After 5 min of rigorous stirring the calculated amount of a-iNANO suspension (2 mg/mL, 3 mL) was added and the pH was adjusted to 7.5 with HCl (0.01 mol/L). The reaction mixture was stirred at room temperature for 2 hours. The heteroaggregation of the a-iNANO and the cMNPs was studied for two different cMNPs/a-iNANO number ratios, i.e, R = 100 or R = 20.

3.1.3 Controlled synthesis of superparamagnetic heteroaggregates

In order to assemble the two types of nanoparticles, i.e., aMNPs and cMNPs, into superparamagnetic heteroaggregates, the carboxyl groups on the surfaces of the cMNPs were activated using single-step EDC coupling protocol [76]. Briefly, the pH of the suspensions containing cMNPs (1 mg/mL, 100 mL) was adjusted to 5.5 with HCl (0.01 mol/L). The calculated amount of 5-fold molar excess of EDC (32 mg) was admixed to the suspension of cMNPs. After 5 min of rigorously stirring the calculated amount of aMNPs suspension (8 mg/mL, 2 mL) was added drop-wise to the suspension of the activated cMNPs and the pH was adjusted to 7.3 with HCl (0.01 mol/L). The reaction of the amide bonds' formation between the activated cMNPs and the aMNPs was carried out during vigorous stirring at room temperature for 3 hours. The formation of a covalent bond between the aMNPs surrounded by the cMNPs was achieved at cMNPs/aMNP number ratios of R = 6 (Figure 12). The formed heteroaggregates were collected with a permanent magnet (the magnetic field at the surface of the magnet was measured with a gaussmeter to be approximately 0.5 T), washed with and dispersed into distilled water.

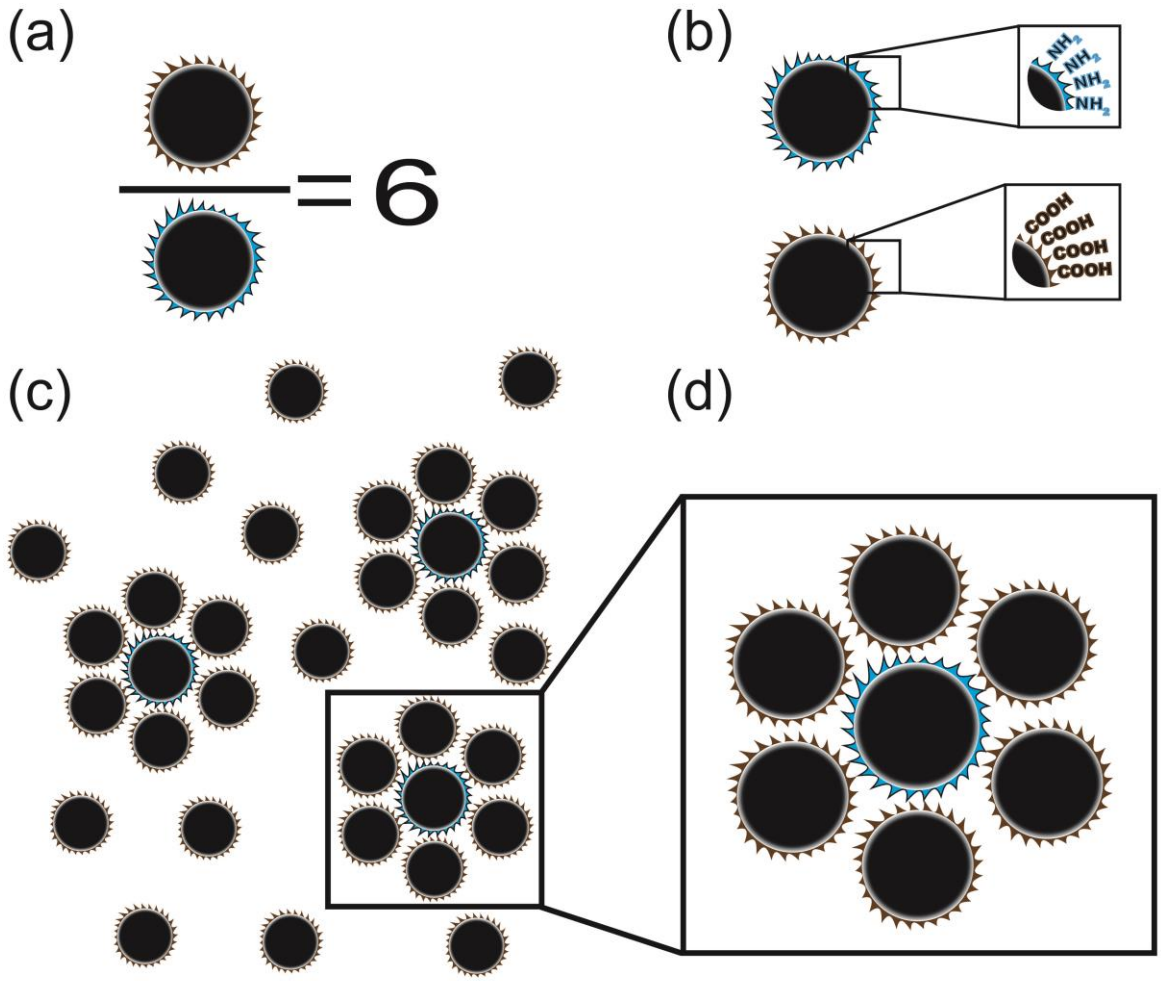

Figure 12: *Schematic presentation of superparamagnetic heteroaggregates synthesis.* (a) cMNPs/aMNP number ratios of R = 6, (b) functional groups of aMNPs or cMNPs, (c) attachment of cMNPs onto aSNPs in suspension at pH 7.3 and (d) magnification of formed superparamagnetic heteroaggregate.

3.1.4 Characterization

The use of the larger (90 nm in diameter size) amorphous SNPs and the smaller crystalline maghemite nanoparticles (11 nm) made the analysis of the formed heteroaggregates using transmission electron microscopy (TEM) relatively straightforward. For the TEM analysis the materials were deposited by drying the suspension on a copper-grid-supported transparent carbon foil. A field-emission electron-source TEM (JEOL 2010F) coupled with an energy-dispersive X-ray spectroscopy (EDXS) microanalysis system (LINK ISIS EDS 300) was operated at 200 kV. The nanoparticle size, expressed as an equivalent diameter, was estimated using visual measurements on at least 500 nanoparticles. The area of the nanoparticles was estimated from the TEM images using DigitalMicrograph™ Gatan Inc. software. The heteroaggregates were also observed with a scanning electron microscope (SEM). For the SEM analysis the materials were deposited by drying the suspension on a graphite specimen mount and observed without any additional conductive surface coating. The field-emission electron-source SEM (JEOL 7600F) was operated at 15 kV. The suspensions of the functionalized nanoparticles were monitored with electro-kinetic

measurements of the zeta (ζ)-potential with ZetaProbe Analyzer (Zeta PALS Zeta Potential Analyzer, Brookhaven Instruments Corporation). Ten measurements (10 cycles per measurement) were made for each suspension at a particular pH.

3.1.4.1 The kinetics of the heteroaggregation

The kinetics of the heteroaggregation between the cMNPs and aSNPs in the aqueous suspension was monitored using DLS analysis. The light source was a He-Ne laser with a wavelength of 632.8 nm. The intensity-correlation function was measured using an ALV-6010/160 correlator that enables measurements over a time range of 10^8-10^3 s. For each experiment, the nanoparticle suspensions were admixed into a disposable glass vial, and shaken to mix well before measuring the intensity of the auto-correlation function at a 135° scattering angle. The temperature in the scattering cell was maintained at 23°C. The mean diameter of the aggregates was continuously monitored in situ for approximately 3 hours. For the first 30 min, each data point was collected in 60 s intervals. Then, from 30 to 196 min, each data point was collected in 15 min intervals. The nanoparticle concentrations used in the experiment for cMNPs was 0.7 mg/mL and the cMNPs/aSNP number ratios R = 89 and R = 15. To relate the changes in the measured average hydrodynamic size with the heteroaggregates formation, the samples were extracted after different times of heteroaggregation and inspected using the TEM. The samples for the TEM characterization of the formed heteroaggregates were prepared by taking a sample of the suspension, where the heteroaggregates were formed at a higher cMNP concentration (15 mg/mL) and the nanoparticle number ratio R = 89, immediately diluted by 100-times in ethanol and deposited by drying on the TEM specimen support.

3.1.4.2 The effect of ionic strength on the zeta-potential of the suspensions and the kinetic of aggregation

The ζ-potential of nanoparicles suspensions were measured at a constant pH, i.e., for the cMNP and the aSNP at 5.5 and for the aMNP at 4, and different ionic strengths (0.1-1000 mM KCl). Ten measurements (10 cycles per measurement) were made for each suspension.

The effect of changed ionic strength (0.1-150 mM KCl) in the nanoparticle suspensions at pH 5.5 for cMNPs or aSNPs and pH 4 for aMNPs was investigated by measuring the dynamics of nanoparticle aggregation. For each experiment, the nanoparticle suspension was pipetted into a disposable glass vial, and shaken so as to mix well before measuring the intensity of the auto-correlation function at a 135° scattering angle. The temperature in the scattering cell was maintained at 23°C. The mean diameter of the aggregates was continuously monitored in situ for approximately 100 min. For the first 10 min, each data point was collected in 2 s intervals. From 10 to 100 min, each data point was collected in 20 s intervals. The particle concentrations used in the experiment were 0.7 mg/mL for the cMNPs, 0.5 mg/mL for the aSNPs and 0.15 mg/mL for the aMNPs.

3.2 Preparation of magneto-responsive bacteria for the magnetic separation in biotechnology

3.2.1 Bacterial cultures

Dry LAB strain *O. oeni* (UVAFERM BETA, MBR® process) used in the experiments were provided by Lallemand Inc. (Europa) and stored according to the manufacturer's

recommendations.

3.2.1.1 Reactivation of bacteria and inoculation

The bacteria package was removed from freezer 30 min before use. The reactivation of freeze-dried bacteria was conducted in accordance with supplier's recommendations. The mass of freeze-dried bacteria (e.g., 89.38 mg) was rehydrated in 20 times its weight (e.g., 1.788 mL) of distillated water at 20°C for a maximum 15 min. Calculated amount of bacteria suspension, that corresponded to 10^7 CFU/mL initial population of bacteria, was given into 1:1 % (v/v) mixture distillated water/ synthetic media or wine. So, activated bacteria were inoculated into synthetic media or wine.

3.2.1.2 Fermentation media

3.2.1.2.1 Synthetic media

MLF and HGMS were carried out in a synthetic media with the chemical composition shown in Table 3 (in g/L of distilled water), at pH 3.2:

Table 3: *The composition of the synthetic media.*

Component	[g/L]
Ethanol	81
Glycerol	5.2
Glucose	0.7
Fructose	0.9
Citric acid	0.5
Malic acid	2

As bioactivator, 0.3 g L^{-1} of Supravit (Esseco) was added to the initial substrate.

3.2.1.2.2 Wine

MLFs were also carried out in a wine mixture Chardonny and Pinot blanc (mixture for sparkling wine) after alcoholic fermentation. The wine samples were kindly provided by Ptujska klet. Before the start of MLF, the wine was not previously sulphurized or filtered. Initial total residual sugar content in wine before MLF was 1.5 g/L, 11 % (v/v) of ethanol, 3 g/L of L-malic acid, 0.21 g/L citric acid and < 0.1 g/L of L-lactic acid, with pH 3.07. As bioactivator, 0.3 g L^{-1} of Supravit (Esseco) and 0.2 g/L of Opti'malo plus (Danstar Ferment AG) was added to the initial substrate (contents of activator are listed in Section A1.5 in Appendix).

3.2.1.3 Sampling

Samples were taken at the beginning and at the end of malolactic fermentation. For WineScan (WSC) analysis samples were not filtered, wherase for enzymatic analysis of acids the samples were filtered through 0.2μm filter (regenerated cellulose, Chromafil).

3.2.1.4 Fermentation processes

A glass bioreactor (Figure 13) with the total volume of 0.5 L closed with fermentation bung was filled with fermentation media and inoculated with bacteria or magneto-responsive bacteria. The fermentation were carried out for 21 days, at 22°C without mixing in triplicates.

Figure 13: *Glass bioreactor.*

3.2.2 Preparation of magneto-responsive bacteria

Magneto-responsive bacteria were prepared by electrostatic adsorption of positively charged aMNPs onto *O. oeni* displaying negative surface charge. First, the prepared bacteria suspension was either washed 3 times with distillated water using Centrifuge 5430, Eppendorf (6900g, 2 min) or ultrafiltrated (Solvent resistant stirred cell, Millipore; ultrafiltration membrane 30 kDa; 2 bar of N_2 pressure; bacteria suspension (starting volume was 15 mL) was washed with 45 mL of distilled water and ultrafiltrated to starting volume) to remove impurities, such as salts used as a bacteria growth media that might change the ionic strength of the suspension affecting the binding of aMNPs to the bacteria surface.

The attachment between the negatively charged bacteria cells and positively charged aMNPs occurred in aqueous suspension at pH 4, when the suspension of bacteria cells (pH 4) was vigorously admixed into the suspension of aMNPs (1 mg/mL, pH 4). To study the efficiency of the attachment of the aMNPs onto the bacteria cell surface in an aqueous media, two different concentrations of bacteria cells and two different aMNPs/bacteria ratios were taken. The attachment was studied at higher concentration of bacteria cells, i.e., $5 \cdot 10^9$ cells/mL (B1), and lower concentration, i.e., $5 \cdot 10^7$ cells/mL (B2). Assuming full coverage of bacteria cell with aMNPs, the higher ratio was set to 1:8745 (R1), i.e., 8745 aMNPs per one bacteria cell and lower ratio to 1:3336 (R2). The combinations of the

bacteria concentrations and the aMNP/bacteria ratios with detailed volumes are listed in Table 4.

Table 4: *Applied concentrations of bacteria cell and aMNP/bacteria ratios.*

Sample name	Bacteria concentration [cells / mL]	Bacteria suspension volume [mL]	aMNP/bacteria ratio	aMNP (1 mg / mL) volume added [mL]
B1R1	$5 \cdot 10^9$	1	1:8745	0.5
B2R1	$5 \cdot 10^7$	1	1:8745	0.005
B1R2	$5 \cdot 10^9$	1	1:3336	0.2
B2R2	$5 \cdot 10^7$	1	1:3336	0.002

For viability tests and fermentation applications the higher concentration of bacteria and the higher ratio were used.

3.2.2.1 Adsorption of magnetic nanoparticles onto bacteria during the fermentation

Positively charged magnetic nanoparticles can also be also attached onto the bacteria cells at a certain stage of the MLF. After 7 days after the inoculation of wine I added aMNPs into wine where the pristine bacteria, without the magnetic nanoparticles grew. The bacteria concentration in wine was estimated to be approximately 10^8 cells/mL. During vigorously mixing (900 rpm) 6 mL aMNPs (1 mg/mL, pH 4) was added dropwisely into 400 mL of wine with pH 3.1 and left mixing for 30 min at room temperature. So prepared "postmagneto-responsive" *O. oeni* were then separated from wine using HGMS.

3.2.3 Characterization

Electron microscopy methods provide possibility for investigation of the morphological and ultrastructural properties of prokaryotic cells as well as their interactions with surroundings. The magnetic responsive bacteria were characterized using transmission electron microscopy (TEM; JEOL 2100) and scanning electron microscopy (SEM; JEOL 7600F). For the TEM and SEM analysis the bacterial suspensions were 10 times diluted in mixture ethanol (20 % (v/v))/distilled water. For the TEM analysis the diluted suspensions were deposited by drying the suspension on a copper-grid-supported transparent carbon foil and for the SEM analysis the diluted suspensions were deposited by drying on a graphite specimen mount and observed with an additional 3-nm platinum surface coating.

The cell number of the bacteria cells was characterized by flow cytometry (Partec) and counting on the plates.

3.2.3.1 Flow cytometry analyses

For flow cytometry, a CyFlow Space cytometer (Partec, Münster, Germany) equipped with a 50-mW blue laser emitting at 488 nm. A forward scatter (FSC, for cell size) and side scatter (SSC, for cell granularity) were used to define the population of cells. Optical filters were: for detecting PI dye 675/25 nm (FL3) and for SYTO9 dye 590/50 nm (FL2). Setting region on FSC/SSC was used to discriminate bacteria from the background. Gates were defined in the histogram plots of green fluorescence and red fluorescence. Gated cells were analysed at low rate settings of approximately 200 cells s^{-1}, and at least

20,000 cells were analysed. Data were analysed using the FlowJo software (Tree Star, Ashland, OR, USA). A high precision of better than 5 % is guaranteed by precise counting and mechanical volume measurement. The counting reproducibility is better than 2 % relative standard deviation [239].

3.2.3.1.1 Staining procedure

Stock solutions of the dyes were prepared as follows: red-fluorescent nucleic acid stain propidium iodide (PI) and green-fluorescent nucleic acid stain SYTO9 were used from the LIVE/DEAD® BacLight™ Bacterial Viability kit (Molecular Probes) as proposed by the manufacturer. The SYTO9 dye enters all cells, PI was internalised only in dead cells.

All stock solutions were stored at -20°C. 6 µL of the stock solution was added to 2 mL of culture containing approximately 10^6 cell and mix thoroughly by pipetting up and down several times. So prepared sample was incubate at room temperature in the dark for 15 min.

3.2.3.2 Enumeration *O. oeni* on agar plates

The number of *O. oeni* cells was determined by plate count method. 1 mL of starting suspension for dilutions contained 50 mg of freeze-dried bacteria. Serial decimal dilutions of the culture were prepared in Milli-Q water and spread plated on MRS agar (Biolife Italiana, Italia) in duplicates. MRS agar is nutritionally rich and was developed for the general isolation of LAB [168]. The approximate composition of this medium before steam sterilization (121°C, 15 min) is presented in Table 5 (in g/L of distilled water)

Table 5: *The approximate composition of MRS medium before steam sterilization.*

Component	[g/L]
peptone	10
beef extract	10
yeast extract	5
glucose	20
Tween 80	1 mL
ammonium citrate	2
$MgSO_4$	0.2
$MnSO_4$	0.05
sodium acetate	5
K_2HPO_4	5

After sterilization the pH of the medium was 6.25. Inoculated plates were incubated at 30°C for 7 days under anaerobic conditions. These anaerobic conditions were used to prevent the growth of acetic acid bacteria and to accelerate LAB growth. The number of colony-forming units per millilitre (CFU/mL) was estimated by averaging colony counts on each plate and multiplying by dilution factors. Plates with less than 35 or more than 350 colonies were excluded from the analysis.

3.2.3.3 Analytical methods

3.2.3.3.1 WineScan analysis

WSC analysis were performed by Kmetijsko-gozdarski zavod Nova Gorica. Organic acids were measured using a WineScan FT 120 Fourier Transform Infrared Spectrophotometer (Foss, Hillerød, Denmark) that employs a Michelson interferometer was used to generate the

FT-IR spectra. Because the WineScan FT120 is a specialized instrument designed specifically to generate quantitative data against the background matrix of wine, the number of scans generated per sample, the selection of wavenumbers, and the processing of the spectra have been pre-selected by the manufacturer and are not accessible to change by the user.

3.2.3.3.2 Enzymatic analysis

Concentrations of L-malic and L-lactic acid were determined with enzymatic test kits (specific for the determination of L-malic acid or L-lactic acid) from Oenolab Diagnostics and were performed at the Kmetijski inštitut Slovenije.

The most commonly used quantitative analytical method for monitoring MLF is the enzymatic determination of L-malic acid and/or L-lactic acid. This method uses an enzyme that specifically reacts with L-malic acid or L-lactic acid (the principles of determination are described in Section A1.6 in Appendix) and a UV-visible spectrophotometer to monitor the progress of the analytical reaction. The determination is based on the formation of NADH measured by the increase in light in light absorbance at 340 nm. My analysis were performed by BS-200 Chemistry Analyzer (Mindray). The estimated relative error of measurement is below 10 %. The results of enzymatic analysis are expressed as mean value of triplicates.

3.2.4 HGMS of magneto-responsive bacteria

HGMS experiments were performed with a model L-1CN Frantz canister separator, supplied by S. G. Frantz Co., Inc. (Trenton, NJ). The HGMS system consisted of a nonmagnetic stainless column with working space 0.6 cm in width by 2.5 cm in depth and 22.2 cm in length, for a volume of 35.3 cm^3 filled with type 430 fine grade stainless steel wool also supplied by S. G. Frantz Co., Inc. The column was packed with approximately 5 vol. % (15 g) of matrix material, which is the maximum packing fraction that could be obtained manually. For magnetic separation, the canister was placed in the 1 cm gap between the two metal plates of the separator horizontally. A magnetic field between the two plates, which could be varied in strength, was generated with an attached electromagnet. The direction of the magnetic field was transverse to the direction of flow through the column. The maximum flux density generated between the two plates was 1 T, as measured with a handheld magnetometer. In all experiments, the maximum magnetic flux density was used.

A continuous magnetic separation experiments were performed at room temperature by passing 250 mL of the suspension (magneto-responsive bacteria/synthetic media or magneto-responsive bacteria/wine) from the reaction vessel, through the HGMS column with the electromagnet on, into filtrate vessel (Figure 14). The suspension was first roughly shaken and then pumped at 4.3 mL/min steadily with peristaltic pump (Watson Marlow 400, United Kingdom) through the HGMS column.

The separation of magneto-responsive or postmagneto-responsive *O. oeni* from wine during the MLF was achieved by pumping the wine through the HGMS column with the electromagnet on (1T) with peristaltic pump (4.3 mL/min). The total volume of bioreactors was pumped twice through the HGMS column. To clean the HGMS column after each separation, the electromagnet was switched off and the column was back flushed (190 mL/min steadily with peristaltic pump) with cold distilled water (2L) and ethanol absolute (0.2L). To see if the MLF would continue after the HGMS, the bioreactors containing filtrate were blown through with N_2 for 5 min and then closed with fermentation bung.

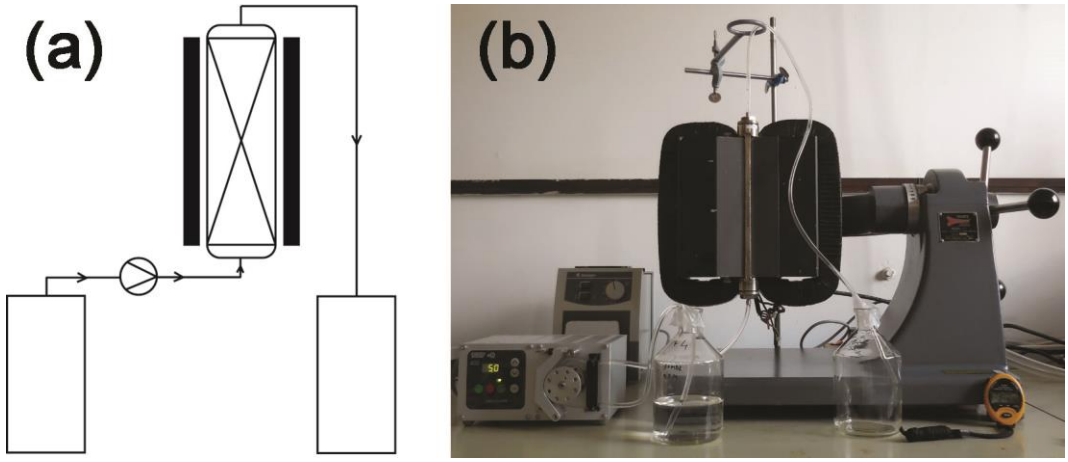

Figure 14: *The HGMS setup.* Scheme (a) and practical setup (b) of continuous HGMS. The suspension is pumped with peristaltic pump through the column, with the electromagnet on, into filtrate vessel.

4 Results

The results in Chapter 4 are divided into material and biotechnology part. The material part was devoted to the synthesis of nanoclusters using controlled heteroaggregation of superparamagnetic iron-oxide nanoparticles in the aqueous suspensions. The nanoclusters can be used in magnetic separation. The majority of research represents a direct comparison between the heteroaggregation controlled by the two types of interactions between the nanoparticles in the suspensions, i.e., electrostatic and chemical, in the same system of the two types of functionalized nanoparticles. The results of this research are also important for synthesis of multifunctional composite nanoparticles and for the control of magnetic nanoparticles bonding onto larger targets, e.g., bacteria in the process of their magnetic separation. The second part describes a possible application of magnetic separation in biotechnology. New method was developed for magnetic separation of LAB at certain stage of MLF of wine. The method includes bonding of functionalized magnetic nanoparticles onto bacteria cell membranes in the suspensions, application of the so "magnetized" bacteria in the fermentation and their magnetic separation from wine using the HGMS.

4.1 Synthesis of magnetic carriers using colloidal processing of nanoparticles

The purpose of the first part of this Chapter was to study the interactions between nanoparticles in aqueous suspensions in order to synthesize magnetic carriers or multifunctional composite nanoparticles. On the other hand, the understanding of interactions between nanoparticles in the aqueous suspension is important for bonding of smaller nanoparticles onto larger objects, e.g., microorganisms, which is a crucial part of the process of their magnetic separation.

The study of interactions between the two types of nanoparticles in an aqueous suspension was based on the model system composed of smaller cMNPs and larger aSNP. The cMNPs and the aSNPs were assembled into heteroaggregates in the aqueous suspension applying electrostatic interactions between the nanoparticles displaying an opposite electrical surface charge, or chemical interactions, resulted from direct covalent bonding between activated carboxyl groups and amino groups of the functionalization molecules at the nanoparticle surfaces. For the synthesis of the superparamagnetic heteroaggregates that could be used in magnetic separation applications the two types of superparamagnetic nanoparticles, i.e., aMNPs and cMNPs were assembled in an aqueous suspension.

This section starts with the characterization of the starting suspensions used in experiments, continues with controlled heteroaggregation of two types of nanoparticles in aqueous suspensions and concludes with the synthesis of superparamagnetic heteroaggregates.

4.1.1 Characterization of the starting suspensions

The TEM analysis showed that the globular aSNPs were of a uniform size of 92±5 nm

(equivalent diameter), corresponding to a calculated specific surface area of 30 m^2/g (Figure 15).

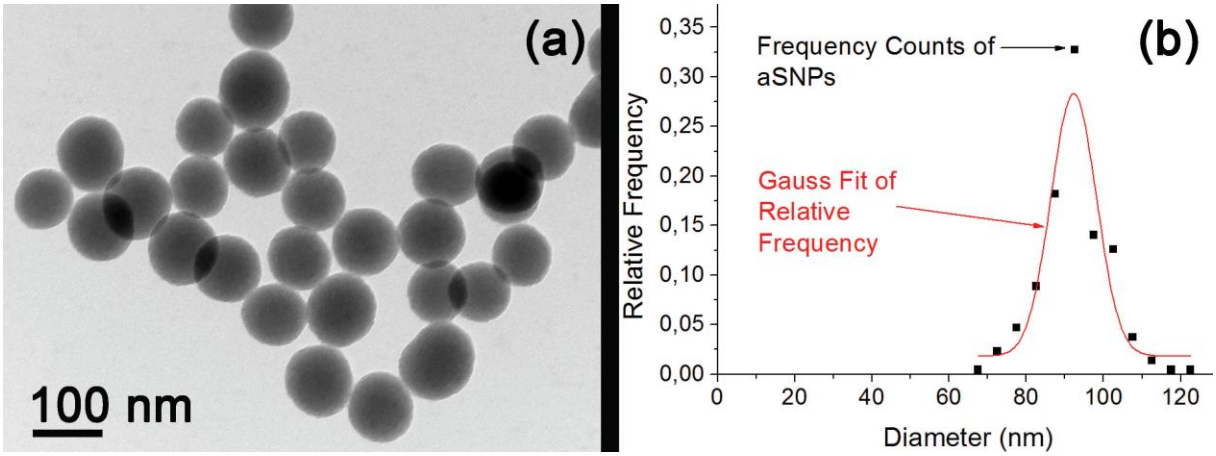

Figure 15: *TEM image of aSNPs (a) and measured distribution of particle size expressed as equivalent diameter (squares) and a corresponding Gaussian fit (line) (b).*

The average cluster size of globular shape a-iNANO estimated from TEM images was 92±16 nm and the thickness of the amorphous silica shell was approximately 11±1 nm (Figure 16). The specific surface area of the a-iNANO was estimated to be 26 m^2/g. The a-iNANO were superparamagnetic with a saturation magnetization of 25 Am^2/kg (Figure A14, Appendix).

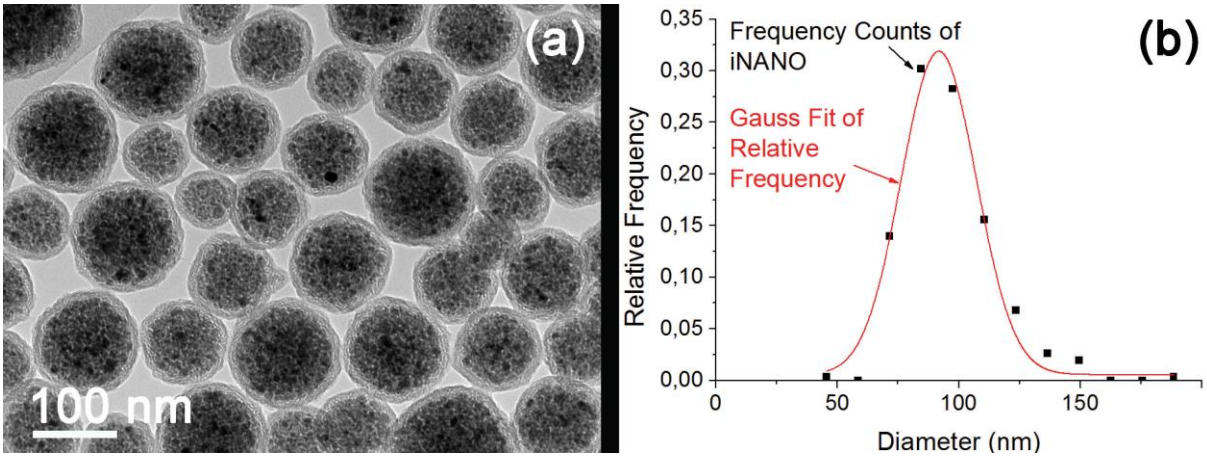

Figure 16: *TEM image of a-iNANO (a) and measured distribution of particle size expressed as equivalent diameter (squares) and a corresponding Gaussian fit (line) (b).*

The average particle size of the maghemite nanoparticles before the coating with the silica layer was estimated from the TEM images to be 11±3 nm (Figure 17).

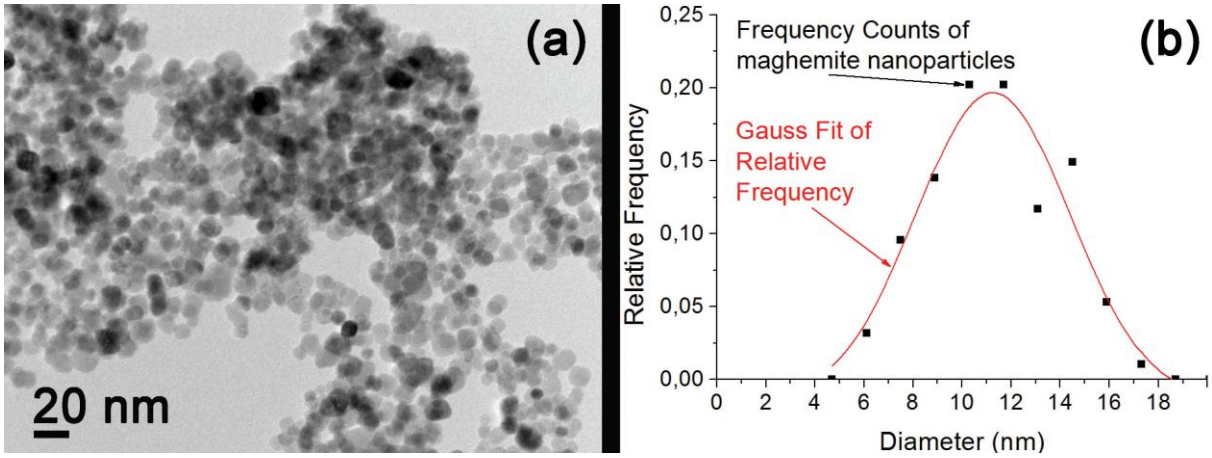

Figure 17: *TEM image of maghemite nanoparticles (a) and measured distribution of particle size expressed as an equivalent diameter (squares) and a corresponding Gaussian fit (line) (b).*

An equivalent nanoparticle diameter of the globular cMNP was estimated from the TEM images to be 24±4 nm (Figure 18). The specific surface area of the cMNPs was estimated by considering the size and the spherical shape of the cMNPs to be 100 m^2/g. The cMNPs were superparamagnetic with a saturation magnetization of 32 Am^2/kg (Figure A13, Appendix). There was no significant difference between the cMNPs and aMNPs in particle diameter or saturated magnetization.

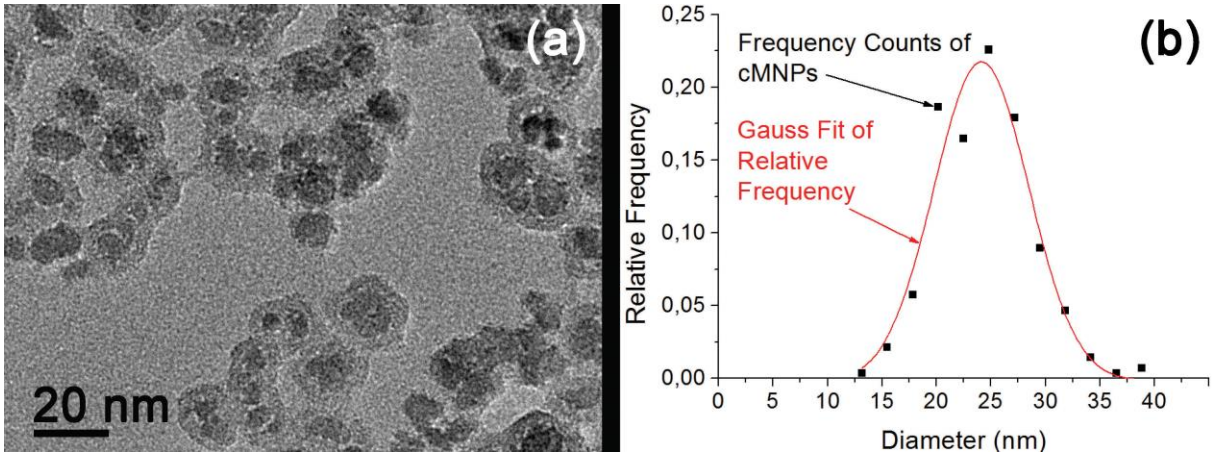

Figure 18: *TEM image of cMNPs (a) and measured distribution of particle size expressed as equivalent diameter (squares) and a corresponding Gaussian fit (line) (b).*

The bare SNPs show a relatively acidic character, because their structure is terminated with negatively charged silanol Si-OH surface groups. Due to the negatively charged -OH surface groups, the MNPs and SNPs show a negative ζ-potential above the isoelectric point (IEP) at pH 3.5. The presence of amino groups of the APMS molecules at the surfaces of aSNPs (Figure 19), aMNPs (Figure 41) or a-iNANO (Figure A14, Appendix) results in a shift of the IEP to a higher pH value of 7.5 [74].

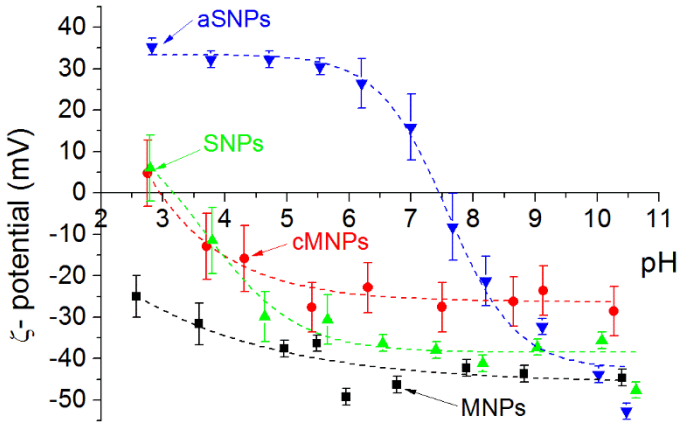

Figure 19: *ζ-potential as a function of pH for MNPs (black squares), cMNPs (red circles), SNPs (green triangles) and aSNPs (blue triangle).*

The cMNPs with the covalently bonded, pre-synthesized, carboxyl-terminated silane molecules at their surfaces showed a highly negative ζ-potential at a pH above the IEP at approximately 3 due to the negatively charged carboxyl groups. The high absolute values of the ζ-potential provided strong electrostatic repulsive forces between the nanoparticles in the suspensions, providing a good colloidal stability over a broad region of pH, except close to the IEP.

Figure 20 compares changing of the ζ-potential with pH for the cMNPs, MNP-PEG8 and MNP-PEG24. The cMNPs display a negative ζ-potential. After bonding the heterolinker to their surfaces the MNP-PEG8 and MNP-PEG24 still show a negative ζ-potential, due to the negatively charged carboxyl groups on the cMNPs surfaces. In the case of PEG with a higher molecular weight, the carboxyl groups are shielded by the longer polymer chains that cover the carboxyl groups at the cMNP surfaces and cause a decrease of the ζ-potential values. For the case of PEG with a lower molecular weight the carboxyl groups might not be as shielded as in the case of the high-molecular-weight PEG because of the different thickness of the polymer shell, also affected by the different conformations of the PEG molecules. For high molecular weights, the PEG is mainly present as a helix, whereas at low molecular weights, its conformation has been reported as an expanded random coil [240].

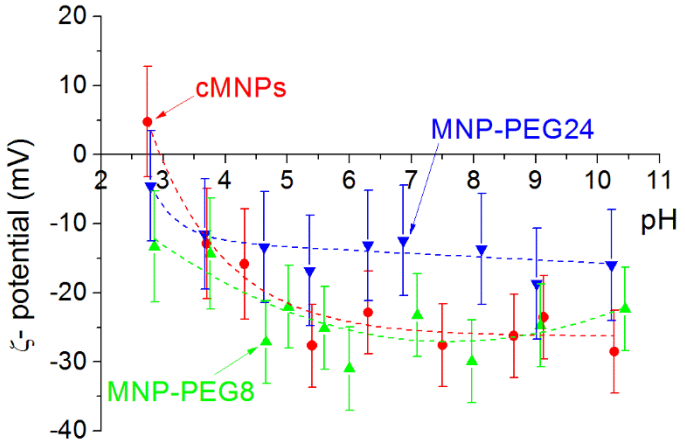

Figure 20: *ζ-potential as a function of pH for cMNPs (red circles), MNP-PEG8 (green triangles) and MNP-PEG24 (blue triangles).*

The nanoparticle hydrodynamic size distributions in the stable aqueous suspensions of a-iNANO (8 mg/mL, pH 4), aSNPs (11 mg/mL, pH 5.5), aMNPs (8 mg/mL, pH 9),

cMNPs (15 mg/mL, pH 5.5), MNP-PEG8 (15 mg/mL, pH 5.5), and MNP-PEG24 (15 mg/mL, pH 5.5) were measured with DLS (Fritsch, ANALYSETTE 12 DynaSizer) (Figure 21). The aSNPs showed a wide size distribution, ranging from 100 to 500 nm, with the peak at around 250 nm (Figure 21a). The smallest sizes correspond well to the aSNPs sizes determined from the TEM images, whereas the majority of the aSNPs were present in the form of small agglomerates. The a-iNANO show narrow hydrodynamic size distribution with the majority of a-iNANO around 110 nm that corresponds well to the a-iNANO size determined from the TEM analysis. The cMNPs and the aMNPs had a narrow hydrodynamic size distribution with the majority of cMNPs and aMNPs being below 20 nm, which is in good agreement with the average diameter of the MNPs determined from the TEM analysis. The MNP-PEG8 and MNP-PEG24 synthesized by attachment of heterobifunctional crosslinker molecule of different lengths onto cMNPs increased the hydrodynamic diameter of cMNPs (Figure 21e and f).

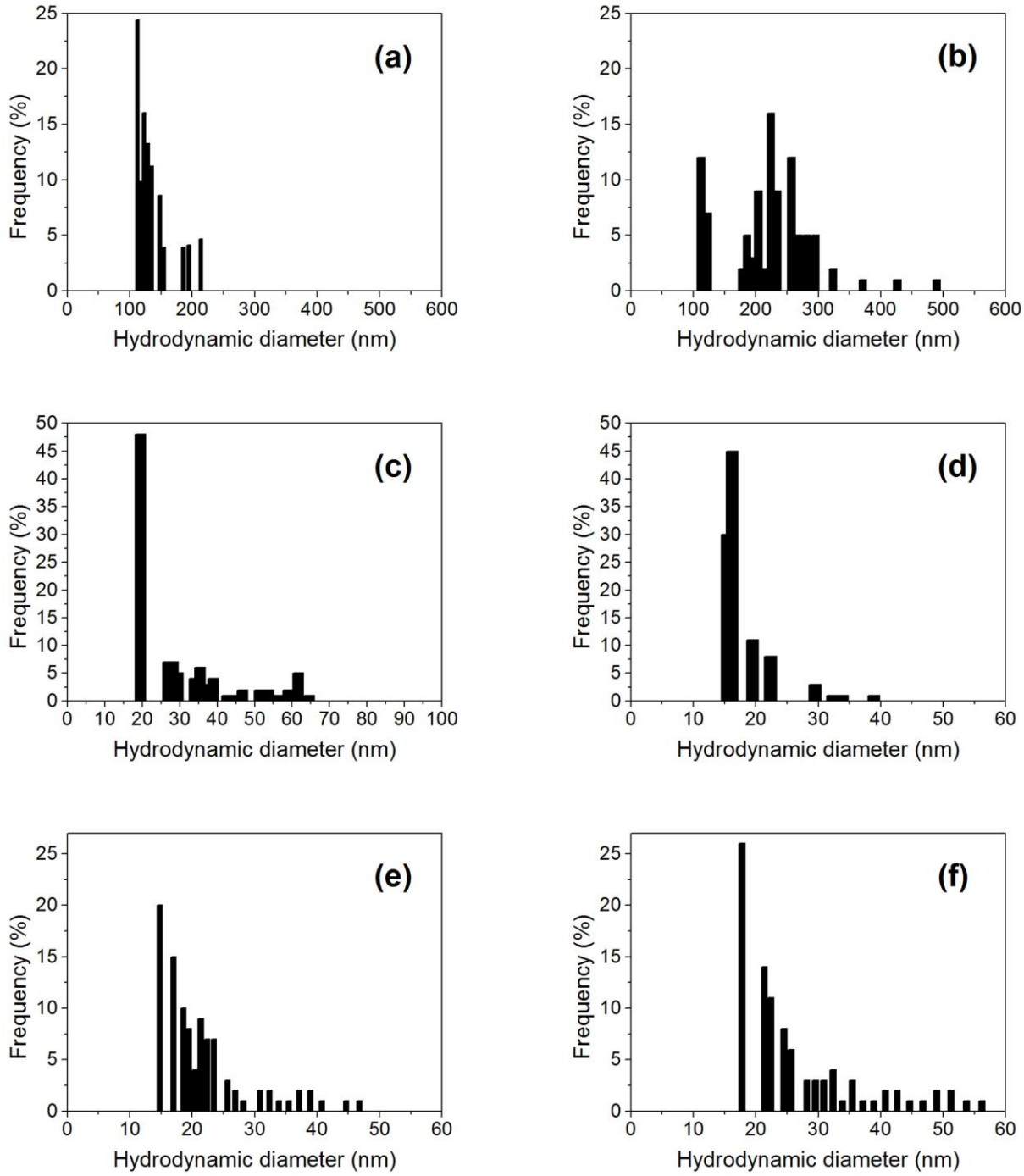

Figure 21: *Number-weighted size distribution of hydrodynamic size for a-iNANO (8 mg/mL, pH 4) (a), aSNPs (11 mg/mL, pH 5.5) (b), aMNPs (8 mg/mL, pH 9) (c), cMNPs (15 mg/mL, pH 5.5) (d), MNP-PEG8 (15 mg/mL, pH 5.5) (e), and MNP-PEG24 (15 mg/mL, pH 5.5) (f).* The plots were generated by statistical method obtained by instrument software nanoQ™ which uses Pade Laplace method to obtain the size distributions from the raw data.

Continuous DLS measurements of the aqueous suspensions of the functionalized nanoparticles at pH 5.5, i.e., the pH at which the heteroaggregation by applying electrostatic interactions between amino- and carboxyl-functionalized nanoparticles were applied, over time showed no increase in the hydrodynamic diameter, proving that the nanoparticles do not agglomerate (Figure A16, Appendix). However, by increasing the ionic strength (0.1-150 mM KCl) of the suspensions the ζ-potential values decreased (Table 6) and as a consequence the nanoparticles started to agglomerate (Figure 22).

Table 6: *Changing of ζ-potential for cMNPs, aSNPs and aMNPs by changing the ionic strength of the nanoparticle suspensions.*

Ionic strength (mM)	cMNP ζ-potential (mV)	aSNP ζ-potential (mV)	aMNP ζ-potential (mV)
0	-29.1	41.9	10.12
0.1	-28.8	54.1	6.7
1	-23.1	47.4	3
10	-24.0	22.2	-5
100	-23.9	13.4	-16.45
1000	-6.9	7.9	-17.28

The influence of increased ionic strength for the cMNPs suspension are presented on the graphs showing normalized hydrodynamic diameter D(t)/D(0) (where D(t) is the average hydrodynamic size at a certain time (t) and D(0) is the average hydrodynamic size for the first measurement) as a function of time (Figure 22). If the value of the normalized hydrodynamic diameter is higher than 1, the aggregation of nanoparticles appears. The shorter time of collecting data by the continuous DLS measurement resulted in a large scattering of normalized hydrodynamic diameter values in the first 10 min (Figure 22). I expected that the agglomeration of nanoparticles in the nanoparticles' suspension would appear immediately when I add the sufficient amount of salt. In order to detect the fast start of the aggregation the time of collecting data by the continuous DLS measurement was shorter in the first 10 min than from 10 min on.

The relative change of the hydrodynamic diameter for the cMNPs started to increase above 100 mM of KCl, suggesting the agglomeration. In contrast to cMNPs aggregation caused by the relatively large increase in ionic strength, the aggregation of aSNPs and aMNPs appeared already at a small increase in the ionic strength (less than 10 mM KCl) of the suspension (data not shown).

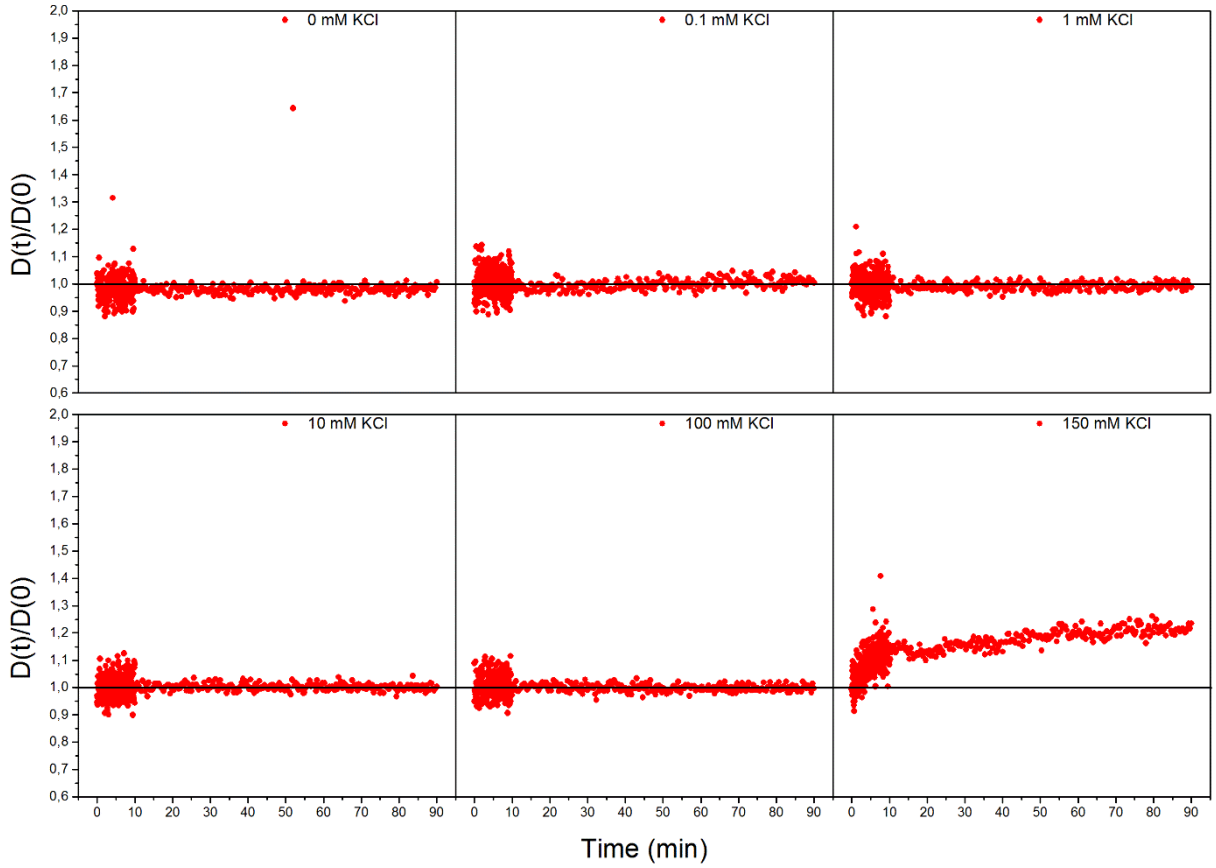

Figure 22: *Kinetic measurement of aggregation for cMNPs (0.7 mg/mL, pH=5.5) by different ionic strengths (0, 0.1, 1, 10, 100, 150 mM of KCl).*

For the heteroaggregation using chemical interactions the carboxyl groups on the surfaces of cMNPs in the suspension were activated with EDC, which might increase the ionic strength of the nanoparticles' suspension and caused the aggregation of cMNPs. Continuous DLS measurements of the suspension of the activated cMNPs at pH 5.5 used during the chemical heteroaggregation showed no increase in the normalized hydrodynamic diameter (Figure 23). This result indicates that the addition of EDC does not cause the agglomeration between nanoparticles in the cMNPs suspension.

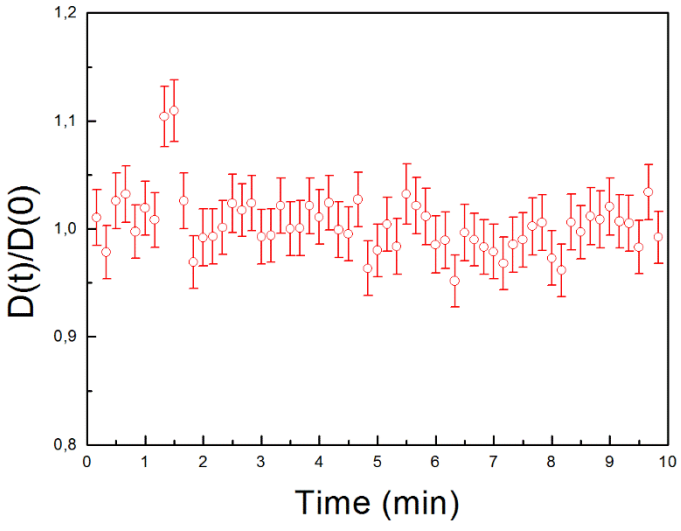

Figure 23: *The influence of added EDC (0.133 mg) on the aggregation of cMNPs (0.7 mg/mL, 0.6 mL) at pH 5.5.*

4.1.2 Controlled heteroaggregation of two types of nanoparticles in an aqueous suspensions

Nanoparticles were assembled into heteroaggregates in an aqueous suspension applying electrostatic interactions or chemical interactions between the nanoparticles. The two types of mentioned interactions were studied by changing different parameters, such as nanoparticle concentration, nanoparticle number ratios and ionic strength of the suspension, as a method for the controlled synthesis of heteroaggregates.

This subsection starts with the study of heteroaggregation due to attractive electrostatic interactions between two types of nanoparticles in a suspension, continues with the study of heteroaggregation by chemical interactions between the two types of the nanoparticles in the suspension and concludes with the kinetics of heteroaggregate formation in the suspensions.

4.1.2.1 Heteroaggregation by electrostatic interactions

Heteroaggregation by applying attractive electrostatic interactions occurs between two types of nanoparticles displaying an opposite surface charge. If the nanoparticles display the same surface charge, they repulse and no heteroaggregation is expected. In order to prove this, I admixed SNPs (45 mg/mL) into cMNPs (15 mg/mL) with the cMNPs/SNP number ratio R = 15 and at pH 9. At pH 9 both types of used nanoparticles in the suspensions display a negative surface charge (Figure 19). No aggregation was observed by DLS measurements for both starting suspensions of nanoparticles, suggesting that both starting suspensions were in dispersed state.

The TEM analysis of mixed suspension (Figure 24) indicates that there was no heteroaggregation between the SNPs and the cMNPs at pH 9, where both types of the nanoparticles displaying a negative surface charge. After drying the suspension of the mixed nanoparticles on a TEM specimen support, the larger SNPs were only sporadically covered with the smaller cMNPs. Observed larger agglomerates of the cMNPs in contact with the SNPs' surfaces could be formed during the preparation of the TEM specimen. Although the cMNPs were in a dispersed state in the suspension at pH 9, they came into contact when the suspension dried on the TEM specimen support.

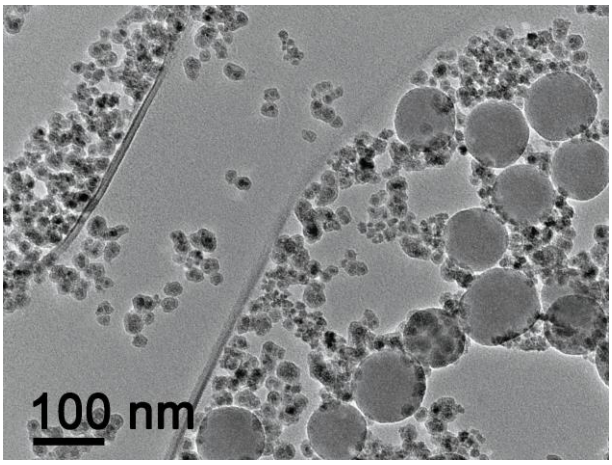

Figure 24: *TEM image of cMNPs and SNPs mixture.*

To confirm that there was no heteroaggregation between SNPs and cMNPs the mixture was analysed by DLS measurements. Figure 25 (a) and (b) show the number distribution of the hydrodynamic radius for the particles in the starting suspensions and Figure 25 (c) for the mixture of cMNP/SNP. The two peaks on the Figure 25 (c) clearly indicates the

two populations of the nanoparticles. The first peak is in good correspondence with larger number of the smaller cMNPs and the second one with the larger SNPs. There was no change in the number distribution of the cMNP/SNP mixture over time (graphs not shown). The influence of the suspensions' concentrations on the heteroaggregation was tested by diluting the starting suspensions for 100 times (i.e., 0.45 mg/mL for SNPs and 0.15 mg/mL for cMNPs) and then mixing the two suspensions at the same cMNPs/SNP number ratio R = 15. Also in this case no aggregation was observed. The two peaks on graph (c) of Figure 25 proved that there was no heteroaggregation between SNPs and cMNPs.

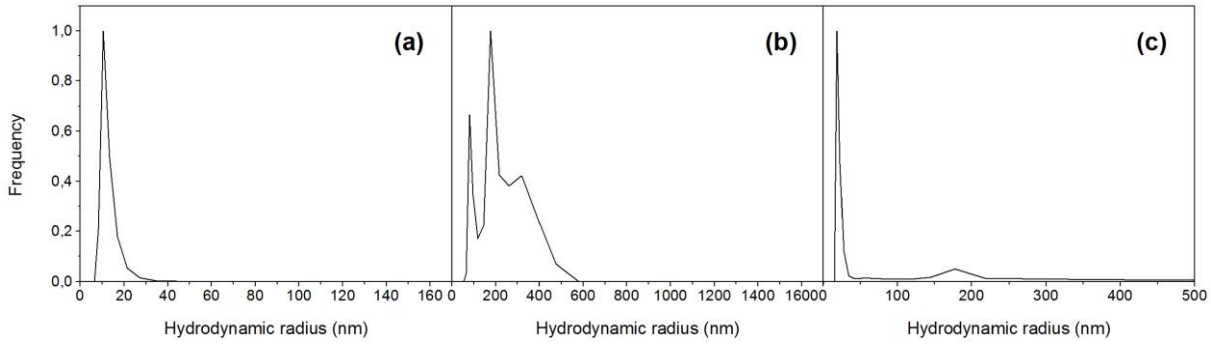

Figure 25: *DLS measurement of hydrodynamic radius size distribution for: (a) cMNPs suspension (15 mg/mL, pH 9), (b) SNPs suspension (15 mg/mL, pH 9) and (c) mixture of cMNP/SNP suspension (R = 15).*

The purpose of this PhD work was to develop a method for the controlled synthesis of nanoparticles clusters in the aqueous suspensions by the process of heteroaggregation. The heteroaggregation by applying attractive electrostatic interactions, i.e., interactions between the negatively charged cMNPs and the positively charged aSNPs, was carried out by mixing the two aqueous suspensions at pH 5.5, where the absolute difference in their ζ-potential was the largest (Figure 19).

First, the heteroaggregation between the aSNPs and the cMNPs was studied at the lower (0.7 mg/mL) concentration of the cMNPs and the cMNPs/aSNPs number ratio R = 89. Figure 26 (a) and (b) show TEM images of the heteroaggregates of the aSNPs and the cMNPs formed at the lower (0.7 mg/mL) concentration of the cMNPs and the cMNPs/aSNPs number ratio R = 89. After the drying of the highly diluted suspension on the TEM specimen support, the larger aSNPs were covered with the smaller cMNPs. Such heteroaggregates were situated on the support individually or in small groups, while the rest of the unbound cMNPs formed agglomerates. Since there was no agglomeration observed by the continuous DLS measurement of the starting cMNP suspension over time (for details see graph (a) on Figure A16 in Appendix), I concluded that the cMNPs were in a dispersed state in the suspension at pH 5.5, and they came into contact when the suspension dried on the TEM specimen support. The analysis of a large number of heteroaggregates revealed that the coverage of the aSNPs with cMNPs was relatively non-uniform. The cMNPs mainly attached to the larger aSNPs as individual nanoparticles; however, they were quite frequently in close contact with each other or even in the form of small agglomerates, while larger areas of the aSNPs' surfaces were uncovered. The larger agglomerates of the cMNPs in contact with the aSNPs' surfaces can form during the preparation of the TEM specimen. However, the cMNPs were also observed in close contact at the surfaces of the individual aSNPs lying on the specimen support with no other cMNPs in the proximity, strongly suggesting that they came into contact already during heteroaggregation in the suspension.

It is known from the literature, that the concentration of nanoparticles in the

suspension has an influence on the surface coverage of larger particles with smaller ones [241]. The influence of the nanoparticle concentration was investigated by changing the cMNPs concentrations (0.007, 0.07, 0.7, 15 mg/mL) and keeping a constant cMNPs/aSNPs number ratio R = 89. TEM analysis revealed that the surface coverage of the larger aSNPs with the smaller cMNPs was nonhomogeneous at the lower concentrations. At the lowest concentration of the cMNPs (0.007 mg/mL), the majority of aSNPs were uncovered or poorly covered, having attached just a few cMNPs. By increasing the cMNPs concentration the surface coverage of the larger aSNPs was improving. When the concentration of cMNPs in the suspension was increased to the highest value (15 mg/mL), the coverage of the central aSNPs with cMNPs improved; however, it was still relatively nonhomogeneous, with the cMNPs frequently present at the aSNPs' surfaces in the form of small agglomerates (Figure 26c).

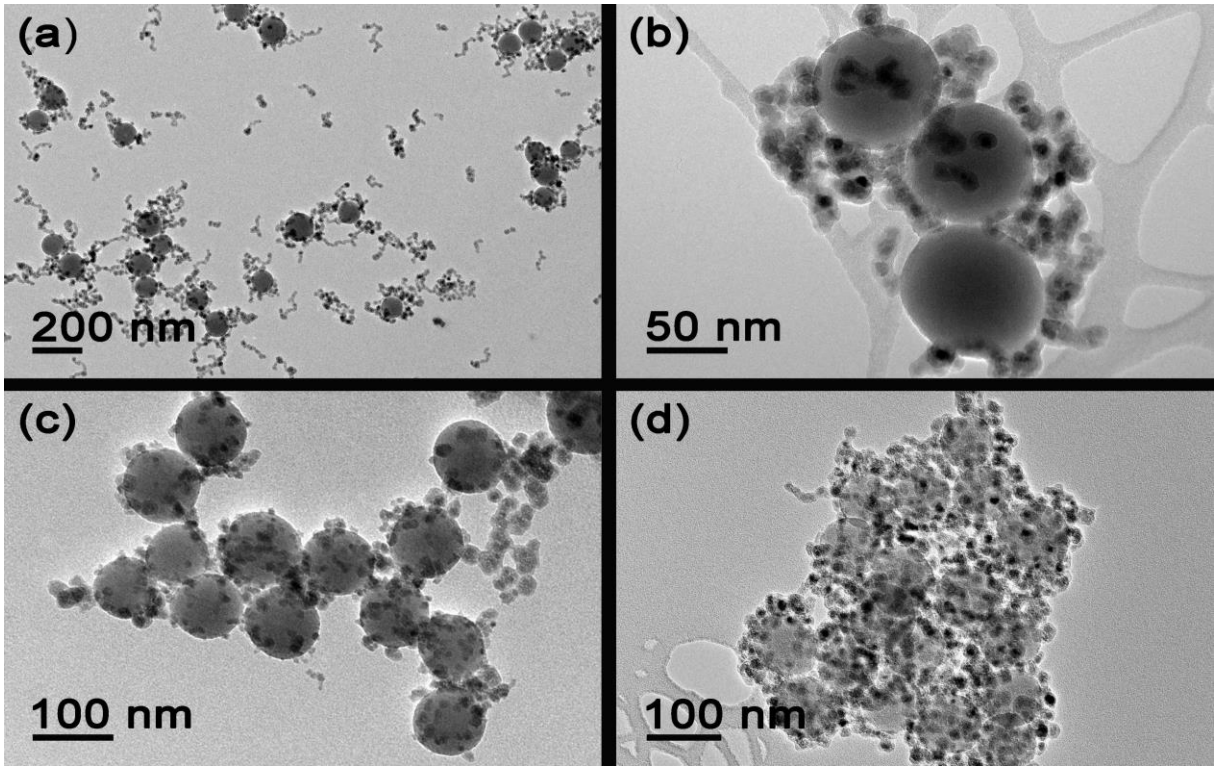

Figure 26: *TEM images of heteroaggregates formed by attractive electrostatic interactions.* At lower (0.7 mg/mL) cMNPs concentration (a,b), at the higher (15 mg/mL) cMNPs concentration (c), and at the increased ionic strength (50 mM KCl, 0.7 mg cMNPs/mL) (d). The cMNPs/aSNPs number ratio was maintained at R = 89 in all the samples.

During electrostatic heteroaggregation the change of the nanoparticle number ratio R can strongly influence the coverage of larger nanoparticles with smaller ones [242]. To investigate the influence of the nanoparticle number ratio on the coverage of larger aSNPs with smaller cMNPs, the cMNPs concentration was kept constant (15 mg/mL) and different cMNPs/aSNPs number ratio R (15, 89 and 450) were used. At R = 15 the sedimentation of particles from the suspension was observed immediately after mixing the two suspensions. The coverage was nonhomogeneous and similar to the one obtained where cMNPs concentration was 0.7 mg/mL and R = 89. By increasing R to 89 the surface coverage of aSNPs improved, but the coverage of aSNPs was still relatively nonhomogeneous. To improve the coverage of the central aSNP the nanoparticle ratio R was further raised from R = 89 to R = 450; however, no significant improvement in the aSNPs coverage by the cMNPs was observed. Obviously, in my experiment the ratio R = 89 was already high enough, and therefore a further increase did not have any

influence on the coverage.

Nanoparticles in aqueous suspensions normally carry an electric surface charge due to charged surface groups. The DLVO theory states that dispersions of such nanoparticles are stable at low salt concentrations due to the repulsive electrostatic forces caused by the overlap of the diffuse layers. Addition of salt destabilizes such suspensions, whereby aggregation is induced by attractive van der Waals forces due to screening of repulsive electrostatic interactions by salt. By screening of repulsive electrostatic interactions between cMNPs, the nanoparticles come closer and as a result the coverage of the larger aSNPs could be improved. To verify this, I studied the influence of the increased ionic strength of the suspension (50 mM and 75 mM of KCl) on the coverage of aSNPs.

To determine the critical amount of added salt, where the nanoparticles start to aggregate, at concentrations and pH value where the heteroaggregation by electrostatic interactions was studied, I did the continuous DLS measurements of an individual aqueous suspensions of cMNPs (0.7 mg/mL, pH 5.5) or aSNPs (0.5 mg/mL, pH 5.5) without and with different amounts of added KCl. No aggregation was observed over the wide range of ionic strength (up to 100 mM KCl) for the cMNPs suspension (Figure 22). The aggregation of the nanoparticles in the suspension appears immediately when the critical aggregation concentration is reached. In the case of the cMNPs suspension the aggregation was observed above 100 mM KCl of ionic strength. In contrast, aSNPs started to aggregate already at a very low (0.1 mM KCl) ionic strength.

Next, the heteroaggregation by electrostatic interactions at the three different ionic strengths (0, 50, 75 mM KCl) was done. First, I added the calculated amount of KCl into the cMNPs suspension and then vigorously admixed the aSNPs suspension into cMNPs suspension. The total ionic strength of the cMNP/aSNP mixture was 50 or 75 mM.

The coverage of the central aSNP with the cMNPs (0.7 mg/mL, R = 89), was clearly improved at the increased ionic strength of the suspension (50 mM KCl) (Figure 26d) compared to the coverage of aSNPs where ionic strength was not increased (Figure 26b). Increasing ionic strength to the higher value (75 mM KCl) did not change significantly the coverage of the central aSNP with the cMNPs. However, it seemed from TEM analysis that the aggregated cMNPs attached onto the central aSNPs. This could be explained by the aggregation of cMNPs, caused by too high ionic strength, before the aSNPs were admixed. The experiment showed that the change of ionic strength has an influence on the coverage of central aSNP with cMNPs.

4.1.2.2 Heteroaggregation by chemical interactions

Controlled process of heteroaggregation between nanoparticles in an aqueous suspension can be achieved by chemical interactions between surface groups of functionalized nanoparticles. In the following experiment I studied the influence of chemical interactions on the surface coverage of the larger aSNPs with the smaller cMNPs.

The covalent bonding between the activated carboxyl groups (single-step EDC activation) at the cMNPs and the amino groups at the aSNPs was more effective in the formation of the heteroaggregates compared to the simple electrostatic interactions. Figure 27 shows TEM and SEM images of the sample obtained by reacting the activated cMNPs with the aSNPs in the suspension at the higher concentration of the cMNPs (15 mg/mL) and R = 89. The aSNPs were homogeneously covered by the cMNPs. A statistical analysis of the TEM images showed that each aSNP was covered, on average, by approximately 23±4 cMNPs, leading to a calculated average surface coverage of the larger aSNPs with the smaller cMNPs of 38±7 %. Besides the individual cMNPs, small agglomerates of the cMNPs were seldom visible on the aSNPs.

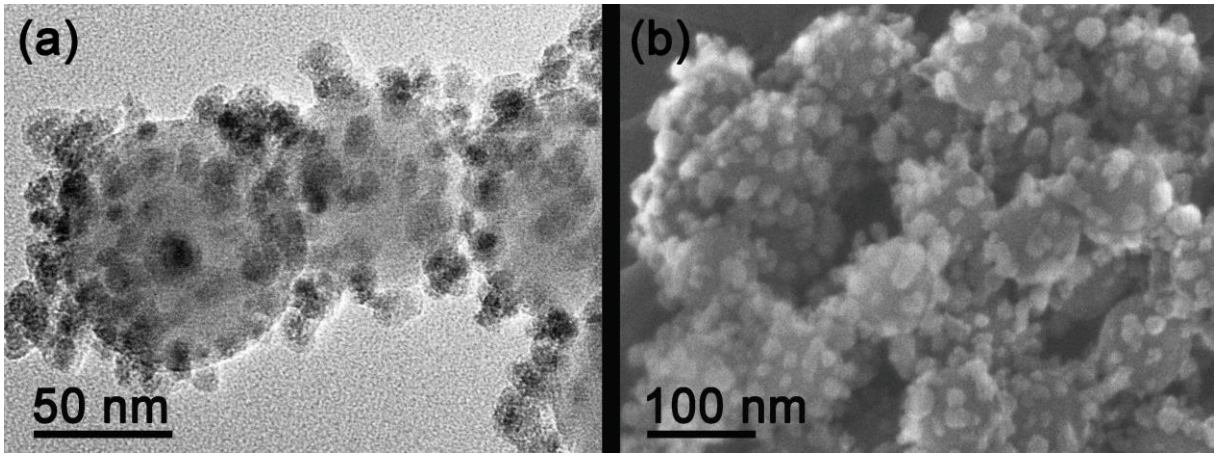

Figure 27: *TEM (a) and SEM (b) image of the heteroaggregates formed between the aSNPs and the cMNPs (15 mg/mL, R = 89) by activating the carboxyl surface groups of cMNPs with EDC.*

The bonding between the two types of nanoparticles takes place after mixing the two stable suspensions: the suspension of activated cMNP at pH = 5.5 and the suspension of aSNP at pH = 9. The pH of the resulting suspension was close to 7 and was further increased to the value of 7.3 required for the reaction between the activated carboxyl groups and the amino groups. At pH = 7.3 the aSNPs are close to the IEP and therefore they tend to agglomerate (Figure 19). However, the aSNPs were always homogeneously covered with cMNPs, the two aSNPs were never in a direct contact, and it seems that the smaller cMNP never reacted with the two aSNPs bridging them together. It can be concluded that the chemical reaction between the two types of nanoparticles is faster than the spontaneous agglomeration of the aSNPs due to van der Waals forces. The two types of nanoparticles probably still display an opposite surface charge at that pH = 7.3; however, the zeta-potential of the aSNPs is very low, so additional electrostatic interactions, if they exist, should be small.

When the lower concentration of cMNPs (0.7 mg/mL) in the suspensions and R = 89 was applied, the appearance of the formed heteroaggregates was similar to that of the heteroaggregates formed by the electrostatic interactions. The reason probably lies in the rapid hydrolysis of the active ester leaving group (o-acylisourea) formed when the EDC reacts with the carboxylate group on the cMNPs. Because of the lower concentration of the cMNPs in the suspension and the required constant ratio between the EDC and the cMNPs, the EDC concentration was too low to effectively activate the carboxyl groups. It is known that the single-step EDC coupling protocol for the activation of carboxyl groups is not effective at low concentrations of nanoparticles [63].

To improve the surface coverage of the central aSNPs, I also tried with the two-step activation process at lower (0.7 mg/mL) and higher (15 mg/mL) concentration and constant R = 89 for cMNPs, where Sulfo-NHS was added after the addition of EDC to increase the solubility and stability of the active intermediate, which ultimately reacts with the attacking amine [63]. TEM analysis of formed heteroaggregates by lower cMNPs concentration showed that the larger aSNPs were poorly, nonhomogeneous covered, similar to single-step EDC activation at lower concentration. However, by increasing the cMNP concentration (15 mg/mL) the coverage of central aSNPs improved, but it was similar to the one of the single-step EDC activation at higher cMNP concentration. In contrast, the DLS measurement of formed heteroaggregates by two-step activation process showed differences. The distribution of single-step activation process gave a broader hydrodynamic diameter size distribution, ranging from 100 to 470 nm. In contrast, the use of the two-step activation process, the hydrodynamic diameter size

distribution was narrower, ranging from 110 to 180 nm. This result suggests that the formed heteroaggregates were more uniform by the two-step activation process.

The influence of nanoparticles' number ratio on the coverage of the larger aSNPs with the smaller cMNPs was tested at the constant cMNPs concentration (15 mg/mL) and different cMNPs/aSNPs number ratio R (15 and 89). Similar to the heteroaggregation by electrostatic interactions, by lowering the cMNPs/aSNPs number ratio (R = 15), the sedimentation of particles from the suspension was observed immediately after mixing the two suspensions. The coverage of the central aSNPs was nonhomogeneous (Figure 28) compared to higher R = 89 (Figure 27).

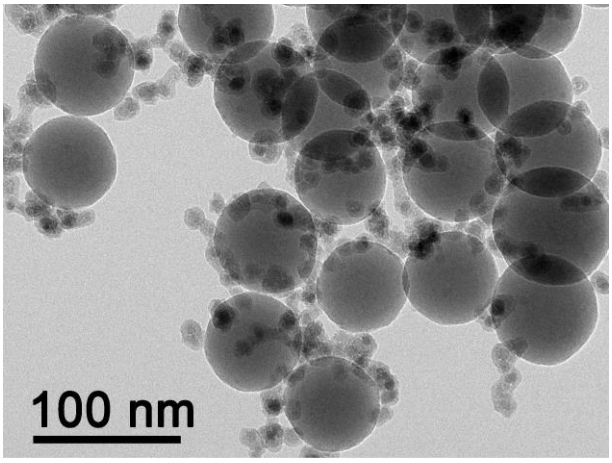

Figure 28: *Heteroaggregates formed by the chemical interaction between aSNPs (11 mg/mL, 4 mL) and cMNPs (15 mg/mL, 4 mL) at R = 15.*

The influence of increased ionic strength of the nanoparticles' suspension was not expected to have a significant improvement on the coverage of larger aSNPs with smaller cMNPs in the process of heteroaggregation by the chemical interactions. To verify this statement, I tested covalent bonding between the activated carboxyl groups (single-step EDC activation) at the cMNPs and the amino groups at the aSNPs, where I added KCl (1 mM) to the starting suspension of cMNPs (0.7 mg/mL). The final ionic strength of the mixture was 50 mM KCl. TEM analysis of the heteroaggregates formed at the increased ionic strength showed no significant improvement of the coverage of the larger aSNPs with the smaller cMNPs. The result indicates that the increased ionic strength has no significant influence on the coverage, unlike it had in the case heteroaggregation by applying attractive electrostatic interactions between oppositely charged nanoparticles.

4.1.2.2.1 The use of a heterobifunctional crosslinker

The heteroaggregation by using heterobifunctional crosslinkers of different lengths was also studied. In the experiments the concentration of cMNPs (15 mg/mL) and R = 89 were constant, while the length of the crosslinker molecule was different (3 nm for PEG8 and 9 nm for PEG24).

The surface coverage of the larger aSNPs with the smaller MNP-PEG8 or MNP-PEG24 was similar to that obtained by direct bonding between the activated carboxyl and the amino groups. Figure 29 shows heteroaggregates formed between the aSNPs and the MNP-PEG24. The estimated average surface coverage of the larger aSNPs with the smaller MNP-PEG24 from the TEM images was equal to that obtained by direct bonding between the activated carboxyl and the amino groups, 37±7 %, whereas the average surface coverage of the aSNPs covered with MNP-PEG8 was somewhat lower, i.e., 34±6 %.

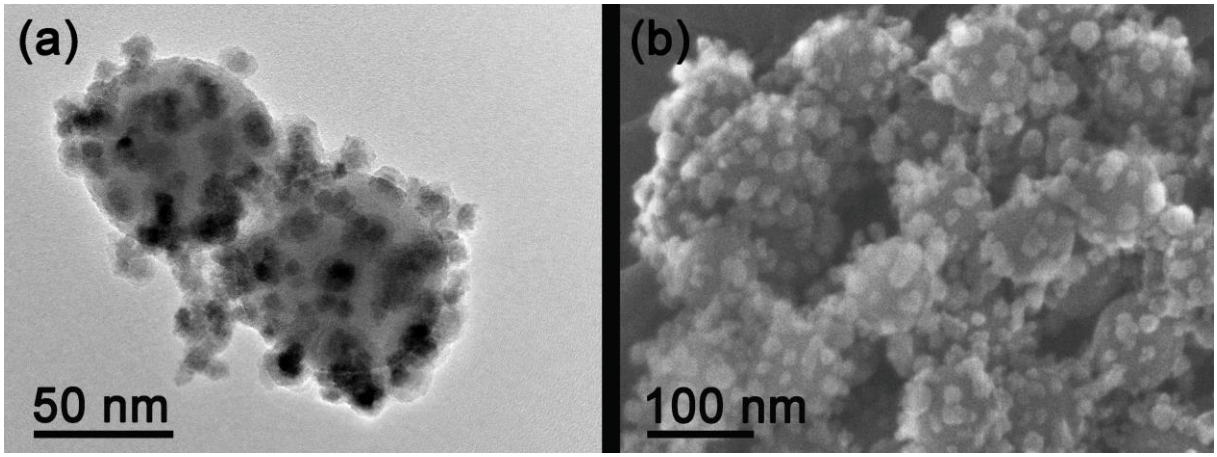

Figure 29: *TEM (a) and SEM (b) image of the heteroaggregates formed between the aSNPs and the MNP-PEG24 (15 mg/mL, R = 89).*

However, the DLS measurement of the hydrodynamic diameter of formed heteroaggregates by using heterobifunctional crosslinker of different lengths showed differences (Figure 30). The distribution of formed heteroaggregates between the aSNPs and the MNP-PEG24 gave a broader hydrodynamic diameter size distribution, ranging from 100 to 600 nm, and majority of heteroaggregates around 400 nm (Figure 30a). In contrast, the hydrodynamic diameter size distribution was narrower for the formed heteroaggregates between aSNPs and MNP-PEG8, ranging from 100 to 400 nm and majority of heteroaggregates around 250 nm (Figure 30b). The results suggest that the length of crosslinker molecule influence on hydrodynamic size of formed heteroaggregates, i.e., the longer length of crosslinker molecule gave broader hydrodynamic size distribution.

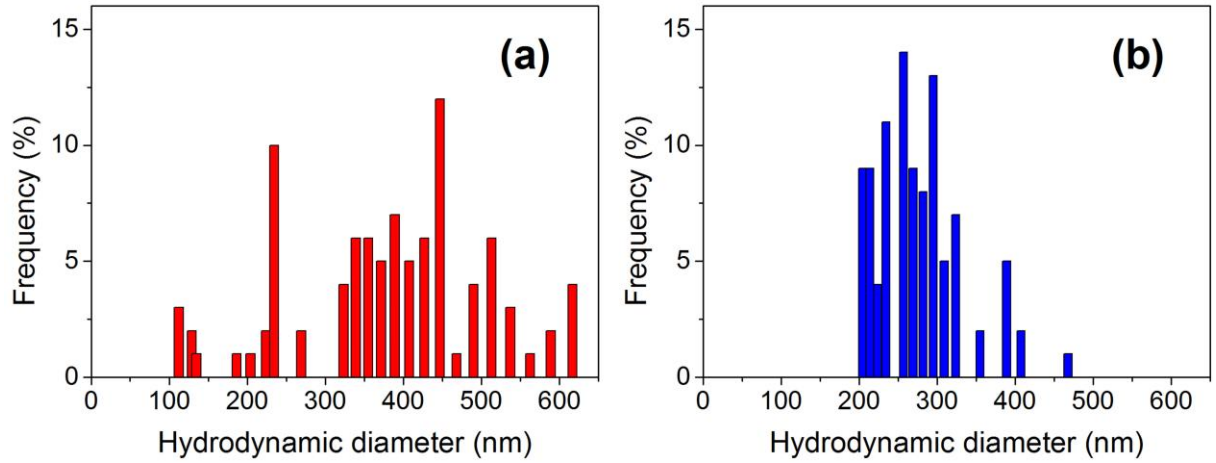

Figure 30: *DLS graphs showing number-weighted size distribution of formed heteroaggregates between aSNPs and MNP-PEG24 (15 mg/mL, R = 89) (a), MNP-PEG8 (15 mg/mL, R = 89) (b).*

4.1.2.3 Kinetics of heteroaggregation

The surface coverage of central nanoparticle might be governed by the kinetics of heteroaggregation. To verify this, the kinetics of heteroaggregation was followed by measuring changes in the relative ratio of the hydrodynamic diameter D(t)/D(0) of the particles in the suspension with time using in-situ DLS measurements. The D(t)/D(0) ratio can change due to interactions between the different nanoparticles; it can increase with

heteroaggregation or with the spontaneous agglomeration of the particles due to van der Waals forces, or it can decrease due to the sedimentation of larger particles. The increase of D(t)/D(0) only with heteroaggregation, i.e., bonding of the single layer of smaller cMNPs onto the larger aSNPs, should be relatively small, because the aSNPs are considerably larger than the cMNPs. Moreover, to detect the kinetics of heteroaggregation the time of the individual DLS measurement should be short, resulting in a large scattering of the results. Thus, the formation of the heteroaggregates due to electrostatic interactions could not be detected. Most probably, the process of heteroaggregation was too fast to be detected.

When the two suspensions containing nanoparticles displaying an opposite surface charge were mixed at the cMNPs concentration of 0.7 mg/mL and R = 89, the D(t)/D(0) remained inside the scatter of the results (Figure 31). The same result was also obtained when the cMNPs concentration was decreased by 10 or 100 times. Most probably, the heteroaggregation due to the electrostatic interactions is too fast to be detected with DLS. It is well known that, in the absence of any steric barrier, oppositely charged particles aggregate due to the attractive electrostatic interactions immediately upon mixing [40]. The time needed to finish the first measurement after the mixing of the two suspensions was approximately one minute.

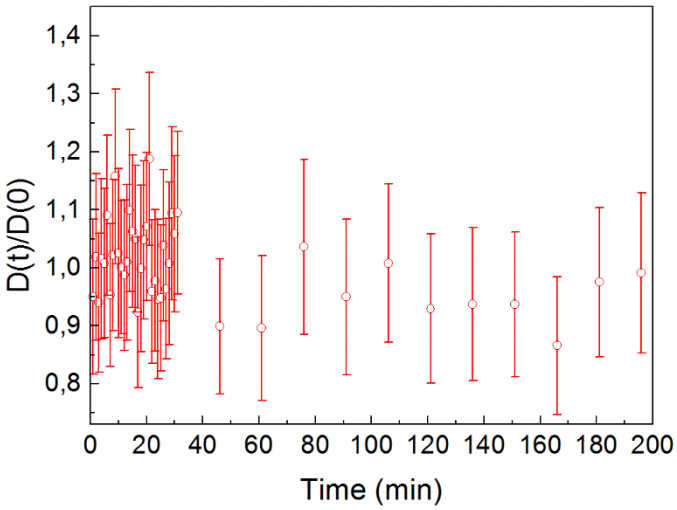

Figure 31: *The kinetics of formed heteroaggregates by electrostatic interaction between aSNP (0.5 mg/mL) and cMNP (0.7 mg/mL) at pH 5.5 and R = 89.*

In contrast, when the chemical interactions are applied to the heteroaggregation of the two types of nanoparticles at the cMNPs concentration of 0.7 mg/mL and R = 89, the initial increase in D(t)/D(0) was clearly visible in the DLS measurements (Figure 32).

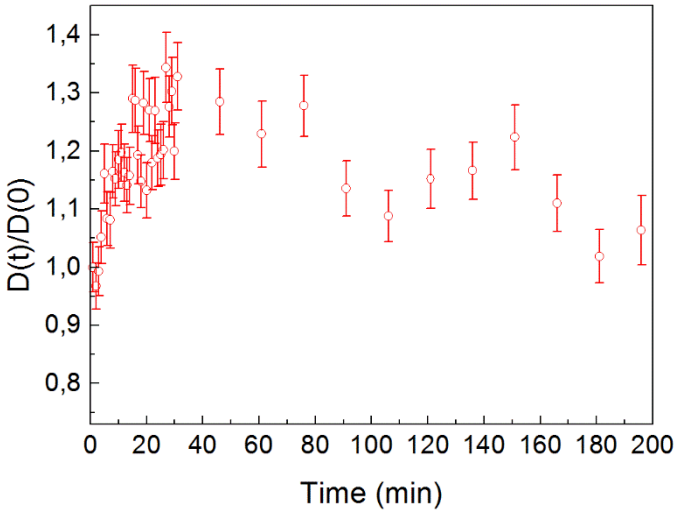

Figure 32: *The kinetics of formed heteroaggregates by chemical interaction between aSNP (0.5 mg/mL) and cMNP (0.7 mg/mL) at R = 89.*

Figure 33a shows the changing of D(t)/D(0) with time after the suspension of the aSNPs was mixed with the suspension of the activated cMNPs (0.7 mg/mL, R = 89). The D(t)/D(0) increased in the initial 20 min and then it remained constant, indicating that the heteroaggregation achieved its steady state. Only after a longer time than 1.5 hours did the D(t)/D(0) start to slowly decrease, indicating the slight sedimentation of the larger particles. To link the increase in D(t)/D(0) with the heteroaggregation, the samples were retracted at different times after the mixing of the two suspensions. The analysis of the sample extracted right after the two suspensions were mixed (Figure 33b) shows that the smaller cMNPs were only seldom in direct contact with the aSNPs. The sample extracted 20 min after the mixing showed a much larger number of cMNPs in direct contact with the aSNPs, i.e., much better coverage of the aSNPs with the cMNPs (Figure 33c). This sample showed no significant difference in terms of the coverage of the sample extracted at the end of the process (Figure 33d). The results indicate that the chemical bonding between the cMNPs and the aSNPs was completed in approximately 20 min.

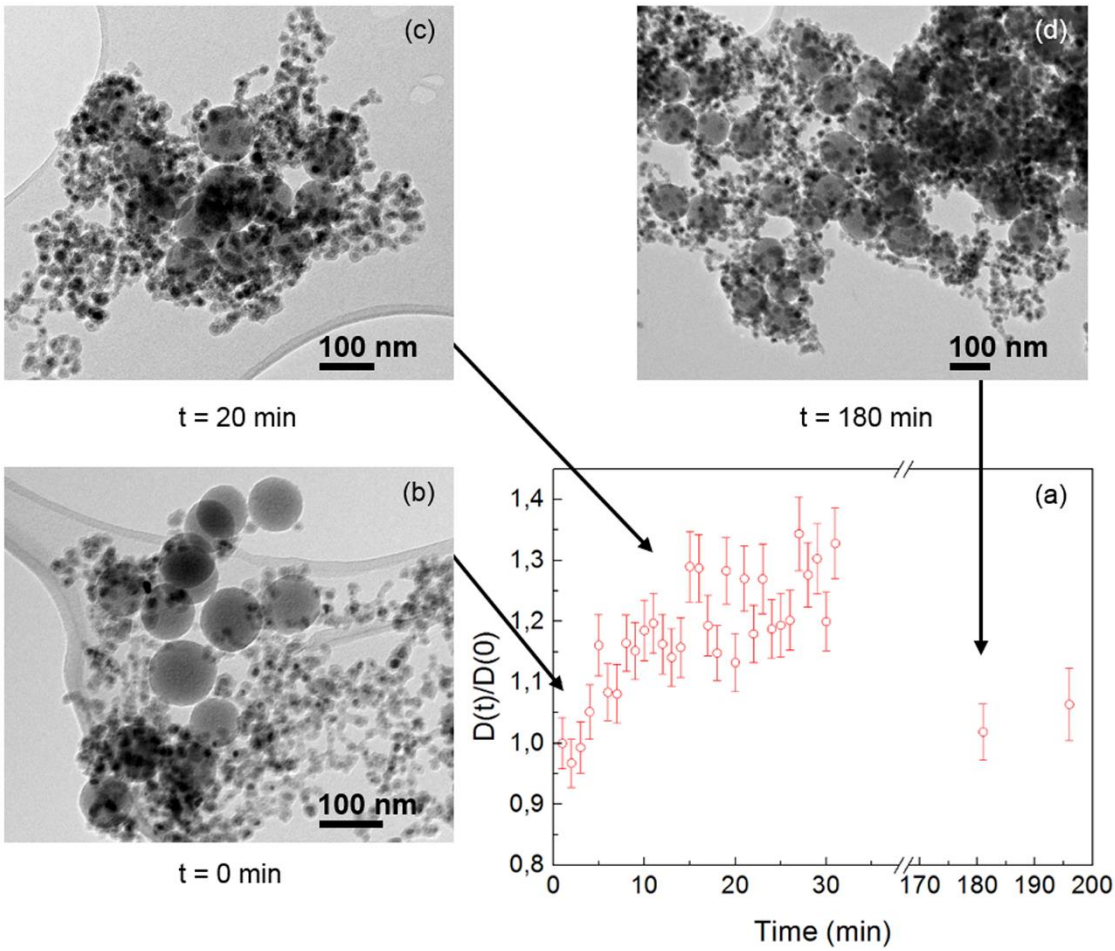

Figure 33: *Relative change of hydrodynamic diameter with time for chemical heteroaggregation at the cMNPs concentration of 0.7 mg/mL and R = 89 (a) and TEM of the samples of heteroaggregates extracted from the reaction mixture right after (t = 0) (b), 20 min (c) and 3 hours (d) after the two suspension were mixed.*

The kinetics of heteroaggregation due to the chemical interactions appears to be slower compared to that involving the electrostatic interactions. The reason is most probably in the slower diffusion in the suspension during the chemical heteroaggregation, where there is almost no influence of the electrostatic forces on the transport of the nanoparticles.

The DLS measurements of the heteroaggregation kinetics in the suspension containing higher concentrations of the nanoparticles (15 mg/mL of cMNPs) were not possible because the suspension was not transparent enough for the laser beam, although the suspension remained stable for a long time.

When the aSNP suspension was admixed to the cMNP suspension at the lower concentration of 0.7 mg/mL and at the lower cMNP/aSNP number ratio R = 15 the continuous DLS measurements showed no initial increase in D(t)/D(0) with time for electrostatic interaction (Figure 34) or chemical interaction (Figure 35) between aSNPs and cMNPs.

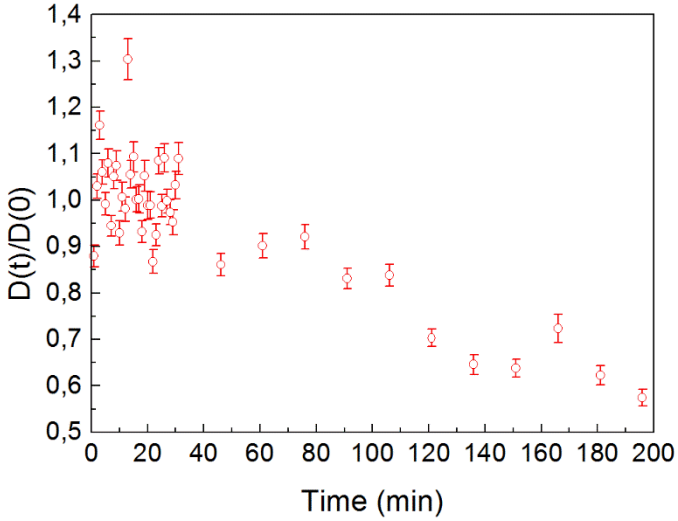

Figure 34: *The kinetics of formed heteroaggregates by electrostatic interaction between aSNP (0.5 mg/mL) and cMNP (0.7 mg/mL) at pH 5.5 and R = 15.* The decrease of D(t)/D(0) after approximately 30 min is the result of the sedimentation of larger heteroaggregates.

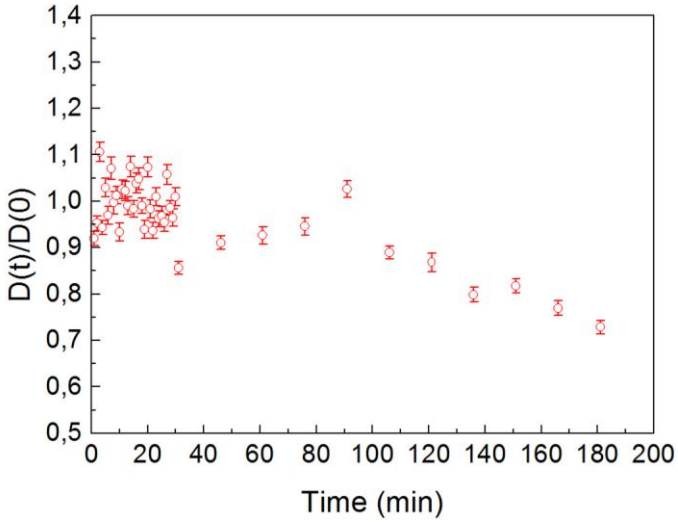

Figure 35: *The kinetics of formed heteroaggregates by chemical interaction between aSNP (0.5 mg/mL) and cMNP (0.7 mg/mL) at R = 15.* The decrease of D(t)/D(0) after approximately 30 min is the result of the sedimentation of larger heteroaggregates.

Initially, the D(t)/D(0) ratio remained inside the fluctuations of the measurements. However, already after approximately 30 min the D(t)/D(0) started to decrease, indicating sedimentation of the larger particles. The sedimentation of the particles from the suspension was also observed immediately after the mixing of the two suspensions at the higher concentration of the cMNPs (15 mg/mL) and at lower R = 15. I assume that in the case when the cMNPs were in larger excess in the reaction suspension, i.e., R = 89, the non-attached cMNPs acted like stabilizers of the suspension of the formed heteroaggregates. In contrast, in the suspension with the smaller nanoparticle number ratio R = 15, the smaller cMNPs make bridges between the larger aSNPs (Figure 29). Thus, instead of separate heteroaggregates with a defined structure, the larger structures are formed, which are relatively large and quickly sediment from the suspension.

4.1.3 Controlled heteroaggregation of functionalized superparamagnetic nanoparticles and superparamagnetic clusters in an aqueous suspension

Knowing the interactions between nanoparticles in aqueous suspensions is also important for the synthesis of multifunctional composite nanoparticles, combining nanoparticles of different materials. By replacing model particles with different materials, the developed method for chemically-driven heteroaggregation by single-step EDC activation could be the preferred method for the synthesis of multifunctional composite nanoparticles. For example, in the model system the nonmagnetic aSNPs served as a support for cMNPs with magnetic properties. The system could be used in catalytic applications, by replacing nonmagnetic aSNPs with magnetic particles for support and by replacing magnetic cMNPs with nanoparticles with catalytic properties. Such multifunctional composite particles could be magnetically separated from the reaction mixture after the reaction, where they were used as catalyst.

In the following experiment, I tried to demonstrate the use of the developed chemically-driven heteroaggregation method for the preparation of composite nanoparticles. To synthesise composite nanoparticles with improved magnetic properties and different surface coverage of larger nanoparticles with smaller cMNPs, I replaced the nonmagnetic aSNP from the model system with the magnetic a-iNANO.

The covalently-driven heteroaggregation between activated carboxyl-functionalized cMNPs (1 mg/mL) and amino-functionalized a-iNANO, was studied at two different cMNP/a-iNANO nanoparticles number ratios, i.e., smaller (R = 10) and higher (R = 100). Figure 36 shows a difference in the coverage of the central a-iNANO with the smaller cMNPs at a) the higher and b) the smaller cMNP/a-iNANO nanoparticles number ratios.

Results showed that the cMNP/a-iNANO system behaved similar to previously studied model system. Like in the model system, the a-iNANO were more homogeneously covered by the cMNPs at the higher R = 100 (Figure 36a), compared to the smaller R = 10 (Figure 36b). Besides the individual cMNPs, small agglomerates of the cMNPs were also seldom visible on the a-iNANO. The suspension of formed heteroaggregates at the higher R = 100 start to sediment approximately one day after the synthesis was finished. In contrast to the model system, the sediment was easily re-dispersed with gentle mixing and no larger aggregates was observed. The observed behaviour at the smaller R = 10 was similar to the one observed at the model system at R = 15. The sedimentation of the particles from the suspension was observed immediately after mixing of the two suspensions.

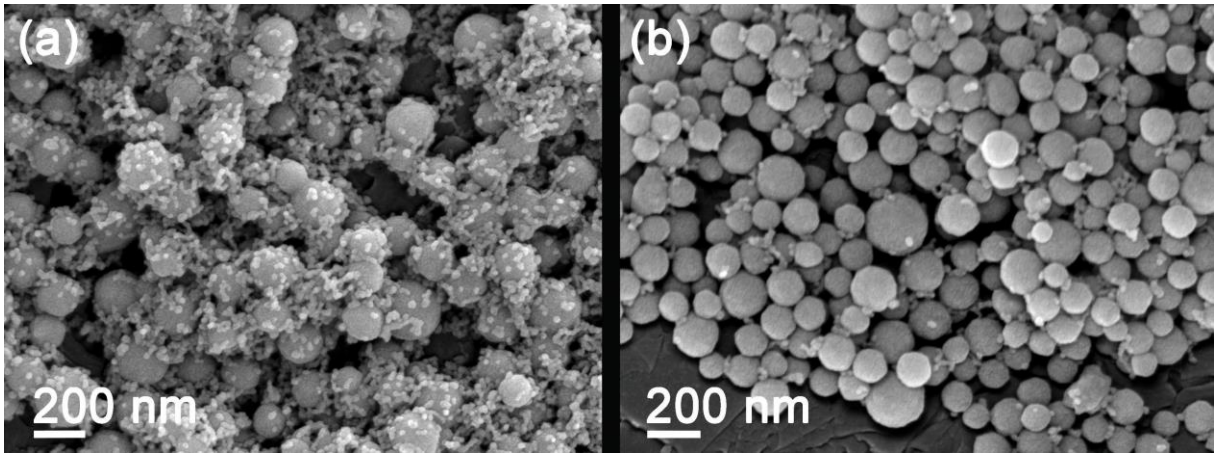

Figure 36: *SEM images of formed heteroaggregates between a-iNANO and cMNPs (1 mg/mL) for R = 100 (a) and R = 10 (b).*

4.1.4 Superparamagnetic heteroaggregates

Superparamagnetic heteroaggregates that could be used as magnetic carriers in magnetic separation applications were synthesised by the heteroaggregation of differently-functionalized superparamagnetic nanoparticles of the same size in the aqueous suspension. Figure 37 shows TEM images of the synthesized superparamagnetic heteroaggregates using covalently driven heteroaggregation between central aMNPs (8 mg/mL) and outer cMNPs (1 mg/mL) at the cMNP/a MNP number ratio R = 6.

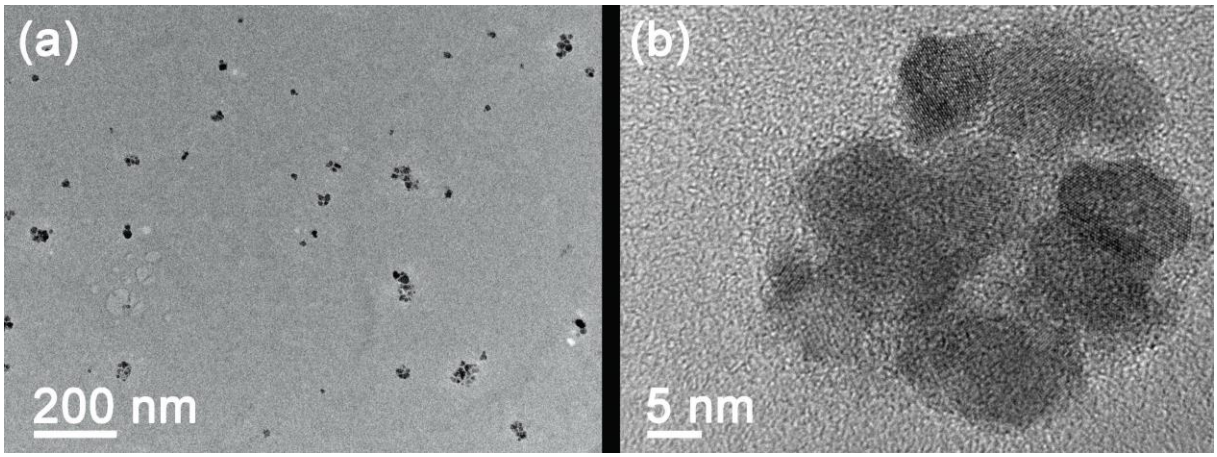

Figure 37: *TEM images of the representative superparamagnetic heteroaggregates at low (a) and high (b) magnification.*

The superparamagnetic heteroaggregates composed of 6-11 nanoparticles had relatively uniform sizes of approximately 50-70 nm, as estimated from TEM images.

The DLS measurement of starting suspensions of the functionalized nanoparticles (Figure 38a and b) had the majority of nanoparticles' hydrodynamic diameter around 20 nm. Some nanoparticles in the starting suspensions might have aggregated over time, which resulted in the broader hydrodynamic size distribution up to 60 nm. The hydrodynamic size distribution of the synthesized superparamagnetic heteroaggregates can be described by two populations, i.e., the first one between 30-40 nm and the second one between 50-90 nm (Figure 38c). The distribution between 30-40 nm presents the majority of nanoparticles in the suspension of formed superparamagnetic

heteroaggregates and can be ascribed to the superparamagnetic heteroaggregates in the early stage of the heteroaggregation process. The increase in the hydrodynamic size (Figure 38c between 30-40 nm) compared to the hydrodynamic size of starting suspensions of the functionalized nanoparticles (Figure 38a and b), where the majority of the nanoparticles was around 20 nm, indicates, that the heteroaggregation between the oppositely functionalized nanoparticles appeared. The distribution between 50-90 nm, could be ascribed to the synthesized superparamagnetic heteroaggregates.

At the aMNPs/cMNPs number ratio R = 12 (data not shown), the formed superparamagnetic heteroaggregates had broader hydrodynamic size distribution (up to 500 nm) compared to the aMNPs/cMNPs number ratio R = 6 (Figure 38c). The superparamagnetic heteroaggregates formed at the higher nanoparticle ratio are more likely to sediment due to gravitation and are difficult to be re-dispersed once the sedimentation occurs. By lowering the aMNPs/cMNPs number ratio to R = 6, the hydrodynamic size distribution of the formed superparamagnetic heteroaggregates decreased. By considering the size of the individual silica-coated nanoparticle and their spherical shape, a specific surface area of the heteroaggregates was calculated to be 78 m^2/g. The specific surface area of formed heteroaggregates is important, because it provides a larger absorptive surface area needed for bonding of targeted species in magnetic separation. The absorptive specific surface area of synthesized superparamagnetic heteroaggregates is larger compared to that of most commercially available superparamagnetic beads [243,244], which are generally used in different magnetic separation applications.

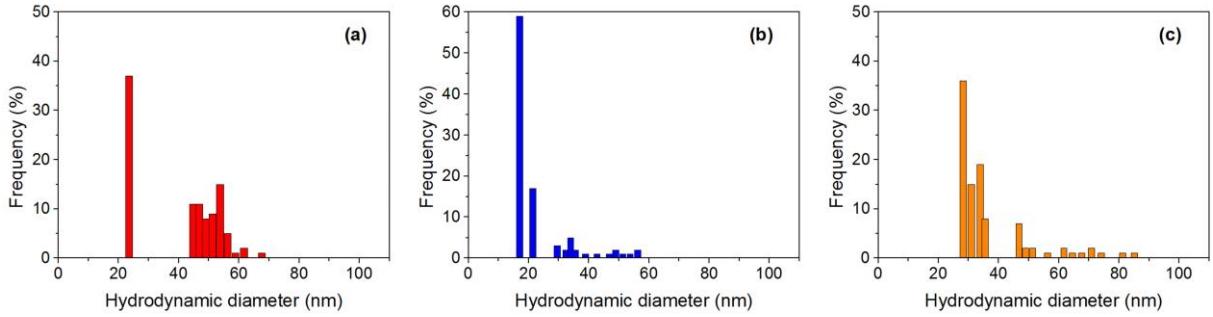

Figure 38: *DLS number distribution of aMNPs (a), cMNP (b) and formed superparamagnetic heteroaggregates (c).*

Besides nanoparticle number ratios, the concentrations of the nanoparticle suspensions were also found to be important for the effective assembly of the superparamagnetic heteroaggregates. In the case of the twice-higher concentration of cMNPs (compared to the concentrations of cMNPs used in the case presented above), the uncontrolled agglomeration took place after the synthesis of the superparamagnetic heteroaggregates, whereas the formation of the superparamagnetic heteroaggregates with the twice-diluted reaction mixture was not effective.

4.2 Preparation and magnetic separation of lactic acid bacteria from fermentation media

In the second part of this chapter I describe a possible application of magnetic separation in biotechnology. The attachment of superparamagnetic nanoparticles onto larger objects, i.e., bacteria, was studied in order to prepare the "magneto-responsive" lactic acid bacteria (LAB) *O. oeni*. The bonding between the magnetic nanoparticles and the bacteria is crucial for their magnetic separation. Generally, the magnetic separation of bacteria is

important for applications where the bacteria need to be removed from the process or in fermentation applications to control the fermentation process. To demonstrate the application of magnetic separation, the malolactic fermentation (MLF) of wine was performed with magneto-responsive bacteria. MLF is so-called secondary fermentation of wine and is performed by the LAB that converts the L-malic acid to L-lactic acid and carbon dioxide. Uncontrolled or spontaneous MLF implies several risks, such as a considerable increase in volatile acidity, consumption of residual sugars, undesirable organoleptic changes, change of wine colour formation of undesirable metabolites, such as biogenic amines, that can affect human health and lead to low quality wines. If MLF is not desired, the growth of LAB in wine must be suppressed by removing or inactivating the bacteria that are present. This can be achieved by employing magnetic separation of LAB from wine.

First, magneto-responsive bacteria were prepared by absorption of magnetic particles onto LAB. Next, the influence of the attached magnetic nanoparticles onto LAB metabolism was investigated by comparing the final conversion of L-malic acid into L-lactic acid by LAB without or with attached magnetic nanoparticles onto the bacteria. Finally, the magneto-responsive bacteria were separated from media using HGMS.

4.2.1 Characterization of bacteria

O. oeni belong to the Gram positive group based on the Gram staining method (Figure A17, Appendix). In the literature the shape of *O. oeni* is described as spherical or slightly elongated [166]. The shape of bacteria used in my experiments (Figure 40 and Figure 43), i.e., *O. oeni* (UVAFERM BETA), could be described as oval shape or by mathematical description as prolate spheroid. Figure 39 shows the SEM analysis of freeze-dried bacteria powder. LAB are incorporated within a some sort of matrix (Figure 39a) composed of larger particles of a plate-like shape. Besides plates with incorporated bacteria, cube-like particles were observed in freeze-dried powder. The EDXS analysis of the cube-like particles showed the presence of aluminium, silica, sodium and oxygen. In my opinion the composition could be ascribed to aluminosilicate zeolits. It is known, that aluminosilicate are good moisture adsorbents [245]. Such particles could be added as molecular sieves to capture moisture that might appear during storage of the freeze-dried bacteria and could cause their damage. SEM image of the matrix with included LAB taken at higher magnification (Figure 39b) reveals that the shape of LAB could be described as a prolate spheroid.

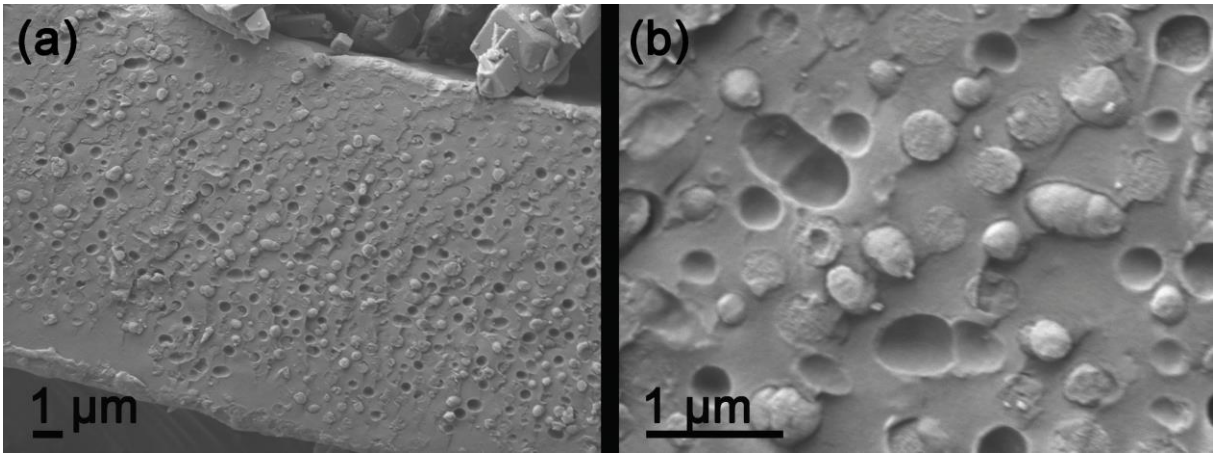

Figure 39: *SEM image of freeze-dried O. oeni.* Figure 39a shows a cross-section of a plate-like particle of the matrix with incorporated *O. oeni*. In the top right corner cube-like particles are also seen. The bacteria cells are better seen at higher magnification in Figure 39b. When the matrix particles was fractured, some of the bacteria were fractured and the others remained intact and their shape can be resolved. A part of bacteria was pulled from the matrix during fracturing leaving the holes with shape that perfectly corresponds to the shape of bacteria

When water was added, the matrix in which the freeze-dried bacteria were incorporated, was dissolved. Analysis of TEM images of the bacteria after washing with water and drying, confirmed their prolate spheroid shape with 1.5±0.3 µm for the long dimension and 0.5±0.07 µm in transverse (Figure 40). By considering these values, the specific surface area of the dry *O. oeni* was estimated to be 2 μm^2. It is expected that the bacteria shrink during drying.

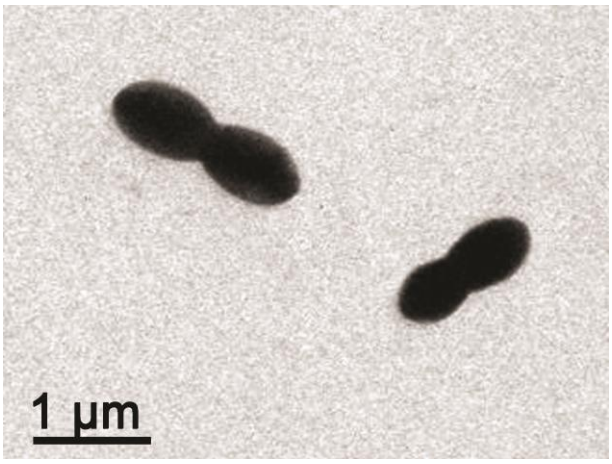

Figure 40: *TEM image of O. oeni.* The freeze-dried bacteria were reactivated in distilled water and deposit by drying suspension on a specimen support. Uranyl acetate was added as a contrast agent for TEM analysis.

A surface charge of aMNPs and *O. oeni* were followed by measurements of the ζ-potential of their aqueous suspensions as a function of pH (Figure 41). The *O. oeni* show an acidic character, because its cell wall consists of several polymers and macromolecules, which possess carboxyl, hydroxyl and phosphate surface groups [246], displaying negatively surface charge.

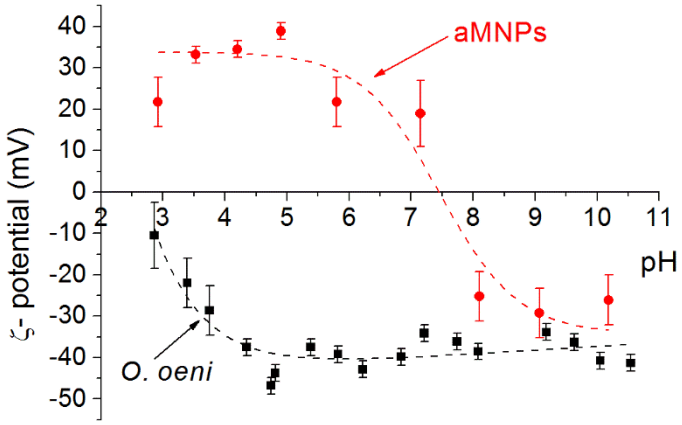

Figure 41: *ζ-potential of the O. oeni and the aMNPs as a function of the pH value of their aqueous suspension.*

The number of bacteria cells in starting bacteria suspension was determined by flow cytometry technique and plate count method. To estimate the number ratio between the functionalized nanoparticles and the bacteria cells I needed the absolute number of the bacteria cells in the suspension. Flow cytometry was used to analyse stained cells at the level of individual cells. For staining of *O. oeni* I used live-dead bacterial viability kit BacLight™, which is composed of two nucleic acid-binding stains, Syto9 that stains all of the bacterial cells (green) (Figure 42a) and PI, that stains dead or dying cells (red) (Figure 42b). Figure 42 shows images obtained by fluorescence microscopy in order to test the stains in viability kit and not to determine the percentage of viable cells.

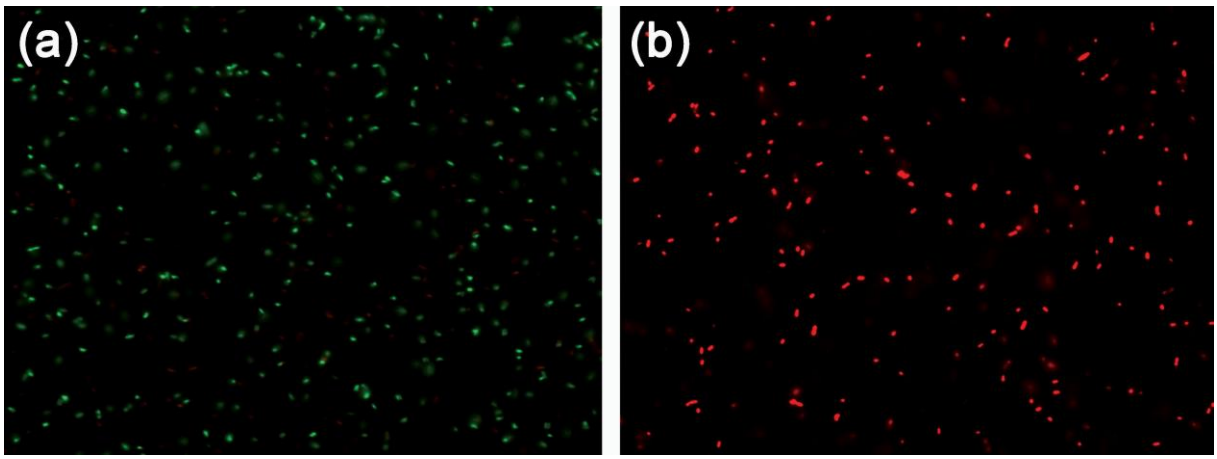

Figure 42: *O. oeni fluorescence detection of (a) all and (b) dead bacteria.* The images were obtained by fluorescence microscopy to test the suitability of viability kit.

By the flow cytometry analyses, the stained *O. oeni* cells were easily detected by their light scattering. In the dot plot of the FSC vs. SSC, a region was subsequently defined that comprised the cell population (flow cytometry method is described Section A1.8 in Appendix). Interfering particles that also had an SSC above the threshold, but were not in the delineated region were thus disregarded. $3 \cdot 10^9$ cells/mL was determined by flow cytometry. The use of fluorescent stains in combination with flow cytometry allows the detection and discrimination of viable culturable, viable nonculturable, and nonviable organisms [247]. The viability for *O. oeni* in bacteria suspension, determined by flow cytometry, was 98 %.

In practice, bacterial viability is measured using the plate count technique and is assimilated to culturability. However, in the case of *O. oeni*, the plate count technique

requires a very long incubation time of about 10 days or more [248]. To verify the number of bacteria cells obtained by flow cytometry, the bacteria were grown on MRS agar plates. The number of $5 \cdot 10^9$ CFU/mL was determined by the plate counting, which is in good agreement with OIV (International Organisation of Vine and Wine) codex that states: »The number should be more or equal to 10^{11} CFU/g for lyophilised or dried bacteria.« [249]. The disadvantage of plate count method is that we only detect viable cells. Since in my experiments the number obtained by plate count method ($5 \cdot 10^9$ CFU/mL) was higher, but of the same order of magnitude (10^9) than the number obtained by flow cytometry analysis, I decided to use it for further planning of experiments.

4.2.2 Preparation of the magneto-responsive bacteria

The preparation of magneto-responsive *O. oeni* was studied by using positively-charged aMNPs, which interact by attractive electrostatic interactions with the *O. oeni* displaying a negative surface charge. The attachment between the negatively-charged *O. oeni* and the positively-charged aMNPs occurred in the aqueous suspension at pH 4, when the suspension of the bacteria cells (pH 4) was vigorously admixed into the suspension of aMNPs (1 mg/mL, pH 4).

First, the influence of the ionic strength, on the coverage of *O. oeni* with aMNPs was investigated. The bacteria suspension, prepared by reactivation of the freeze-dried bacteria powder, might contained salts or some other components form growth media besides bacteria cells (Figure 39). The presence of these water soluble components increases the ionic strength of the suspension and consequently causes the agglomeration of the individual aMNPs. To remove remaining impurities, the bacteria suspension was ultrafiltrated (for details see Section 3.2.2 in Materials and Methods) before they were added to the suspension of aMNPs.

Figure 43a shows the attachment of the aMNPs (1 mg/mL, R1 = 1:8745, pH 4) on the non-ultrafiltrated *O. oeni* (B1 = $5 \cdot 10^9$ cells/mL, pH 4). After drying of the strongly diluted suspension on a SEM specimen support, the *O. oeni* were covered with a low number of the smaller aMNPs non-uniformly. The aMNPs were mainly attached to the larger bacteria cells as small agglomerates, especially at the rim of bacteria cells, while larger areas of the bacteria cells were uncovered. The formed agglomerates and consequently larger uncovered areas might be explained by the influence of an increased ionic strength.

The coverage of the bacteria cell was clearly improved when the bacteria suspension was ultrafiltrated (Figure 43b). The bacteria cells were covered more homogenously with the individual aMNPs, although some agglomerates of aMNPs were also observed.

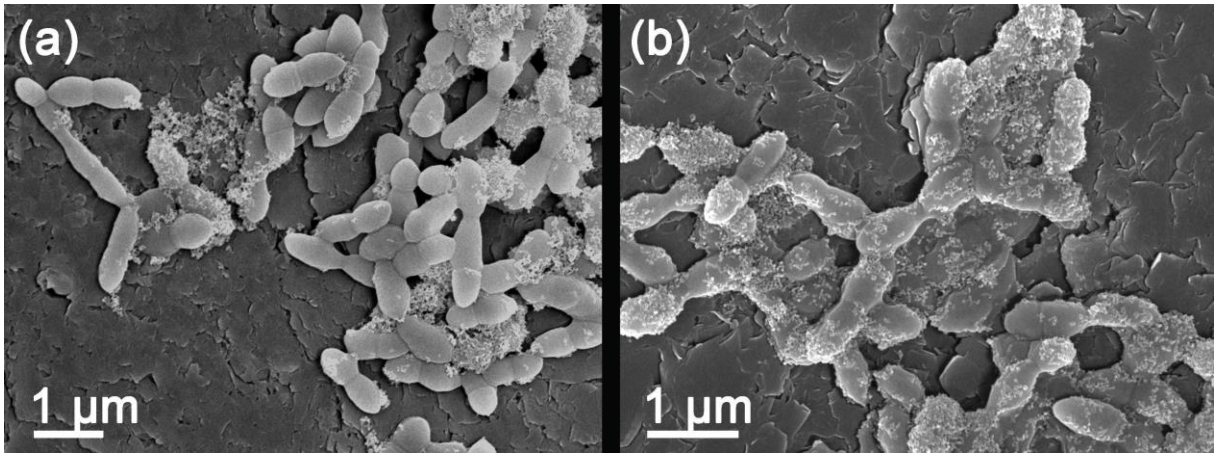

Figure 43: *Attachment of aMNPs onto non-ultrafiltrated (a) and ultrafiltrated (b) O. oeni.*

TEM analysis showed that different aMNPs/bacteria number ratios and different bacteria concentrations influenced the coverage of the ultrafiltrated *O. oeni* with the aMNPs. The aMNPs/bacteria number ratios were chosen according to the specific surface area of bacteria cells determined from microscopic analysis of dry bacteria cells. The coverage of *O. oeni* with the smaller aMNPs was better in the case of the higher (R1 = 1:8745) (Figure 44a and b) compared to the lower (R2 = 1:3336) aMNPs/bacteria ratio (Figure 44c and d). The *O. oeni* were more homogenous covered at the higher ($B1 = 5 \cdot 10^9$ cells/mL) (Figure 44a) compared to the lower ($B2 = 5 \cdot 10^7$ cells/mL) (Figure 44b) bacteria concentration at the same aMNPs/bacteria ratio (R1). In the case of the lower bacteria concentration (B2) the excess of the unbound aMNPs formed agglomerates. It is evident that by decreasing the aMNPs/bacteria ratio less aMNPs were attached to the bacteria cells (Figure 44c and d). I assume that in the case when the aMNPs are in excess (R1), the non-attached aMNPs act like stabilizers preventing aggregation of the magnetically-modified *O. oeni*, whereas in the case of the lower aMNPs/bacteria ratio (R2), the aMNPs act like linkers between the bacteria cells.

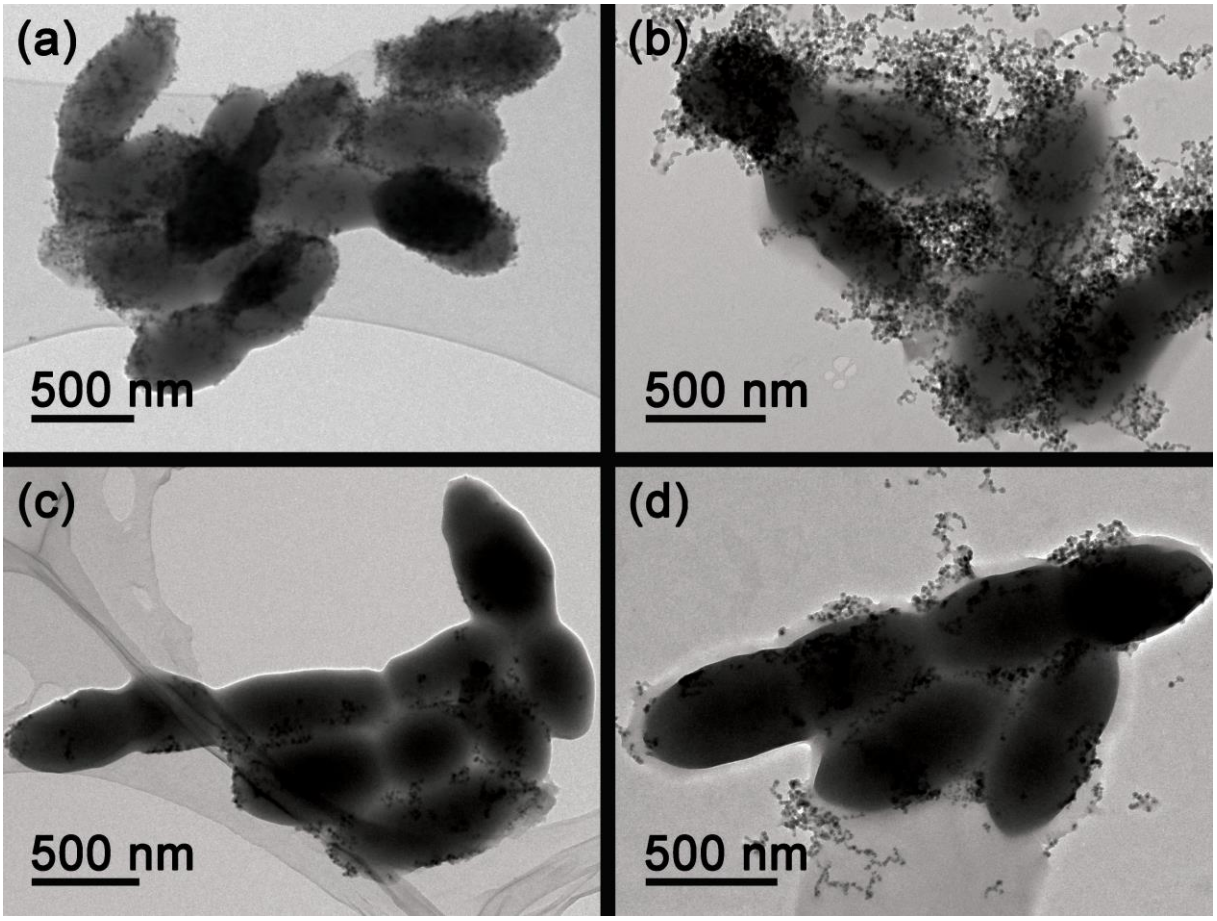

Figure 44: Attachment of aMNPs onto bacteria at d*ifferent bacteria concentrations and different aMNP/bacteria ratios; (a) B1R1, (b) B1R2, (c) B2R1 and (d) B2R2.*

The preparation process of the magneto-responsive bacteria and the attached magnetic nanoparticles onto the bacteria cells might have an influence on the viability of the *O. oeni*. To answer this question the flow cytometry analysis were performed. The flow cytometry results of the bacteria cells that were ultrafiltrated or bacteria cells with attached aMNPs were the same as in the case of the non-ultrafiltrated bacteria suspension. The percentage of live bacteria in the suspension remained the same, i.e., 98 %. The process of preparation magneto-responsive bacteria and the attached magnetic nanoparticles onto the bacteria cells show no antibacterial effect on the *O. oeni*.

If a sufficient surface concentration of the nanoparticles is bonded to the surface of LAB, magneto-responsive bacteria magnetic moment in the magnetic field can be large enough for effective separation, because of its relatively large volume. The difference in the homogenous and non-homogenous coverage of *O. oeni* with aMNPs had an effect on the magnetic separation of magneto-responsive bacteria from the bacteria suspension. The prepared magneto-responsive *O. oeni*, homogenously covered B1R1 (Figure 44a) and non-homogenously covered B1R2 (Figure 44b), were collected from the suspension by the permanent magnet. The flow cytometry was used to determine the number of non-separated bacteria cells remained in the supernatant after 30 minutes of the magnetic separation. 0.5 % in *O. oeni* case of B1R1 and 2 % in *O. oeni* case of B1R2 of the total bacteria cells used in the experiment remained in the suspension. The result suggests that the magnetic separation was more efficient when the *O. oeni* surface was homogenously covered with aMNPs (B1R1), compared to the non-homogenously surface coverage (B1R2).

4.2.3 Influence of the attached magnetic nanoparticles on the *O. oeni* metabolism during MLF

Although it was shown that the attached magnetic nanoparticles accelerate the metabolic activity of the wine yeast by fastening the fermentation process kinetics [88], the attached magnetic nanoparticles onto the surface of *O. oeni* should not have an influence on the bacteria metabolism.

The influence of attached aMNPs on the metabolism of *O. oeni* was tested by performing the MLF in wine after alcoholic fermentation. Results obtained by enzymatic analysis showed that there was practically no differences on the final values of pH and organic acids in wine comparing the inoculation according to the manufacturer's recommendations (control bacteria in Table 7) and inoculation with purified bacteria suspension (centrifuged or ultrafiltrated bacteria) or the magneto-responsive bacteria (centrifuged or ultrafiltrated bacteria with the aMNPs).

The comparison between start (first raw in Table 7) and the end values of pH and organic acids (Table 7) confirmed, that the attached aMNPs does not affect the *O. oeni* metabolism. Results also showed that the purification methods, e.g., centrifugation or ultrafiltration, which were used for the preparation of the magneto-responsive bacteria does not have any influence on the bacteria metabolism.

Table 7: *The comparison between start and end values of pH and organic acids for MLF in wine.* (a) starting values for wine, (b) end values for inoculation according to manufacturer's recommendations, (c) end values for inoculation with purified bacteria and (d) end values for inoculation with magneto-responsive bacteria.

sample	pH	L-malic acid	L-lactic acid	citric acid
(a) control wine	3.07	2.66	<0.05	0.187
(b) control bacteria	3.23	<0.05	2.02	0.045
(c) centrifuged bacteria	3.21	<0.05	2.02	0.054
ultrafiltrated bacteria	3.25	<0.05	2.00	0.034
(d) centrifuged bacteria with aMNPs	3.20	<0.05	1.98	0.047
ultrafiltrated bacteria with aMNPs	3.24	<0.05	1.96	0.053

4.2.4 HGMS of magneto-responsive bacteria

The first aim of the HGMS study was to set up the continuous HGMS that could be scaled up to an industrial scale. The HGMS method was designed in the previous preliminary experiments based on separation of MNPs. First, MNPs (1 mg/mL) were separated from an aqueous suspension using batch or continuous HGMS. To estimate the efficiency of batch HGMS, VSM analysis were used. After the HGMS the column was backflushed

with distilled water to elute the magnetic nanoparticles and to clean the column. The eluted suspension of nanoparticles did not sediment and hydrodynamic diameter determined by the DLS measurement was 18 nm (DLS and VSM measurements are shown in Section A1.9 in Appendix). This result suggests that the HGMS did not cause the aggregation of separated MNPs in the column.

Next, the MNPs in the aqueous suspension were replaced by the magneto-responsive bacteria. The same concentration of the magneto-responsive bacteria (10^8 CFU/mL) were separated either by batch or by continuous HGMS. The efficiency of separation was determined by flow cytometry analysis as a quotient between the number of cells after HGMS divided by the number of cells before the HGMS. To achieve the similar separation efficiency (approximately 96 %), between batch and continuous HGMS, the pump velocity had to be set to the lowest possible achieved by the peristaltic pump Watson Marlow 400, i.e., 4.3 mL/min.

With an aim to develop a method for continuous HGMS of the magneto-responsive bacteria from wine, they were first separated from the synthetic media after the MLF. The synthetic media had the similar composition like wine. Besides inoculated LAB with or without attached magnetic nanoparticles, no other microorganism, e.g., yeast, was present in synthetic media. Due to the exhaust of CO_2, which is one of the two products of L-malic conversion, I can assume that the fermentation process occurred. The efficiency of the HGMS and the number of remained cells was determined by the flow cytometry analysis. No difference in the flow cytometry analysis, e.g., background noise, was observed if the LAB were dispersed in distilled water or in the synthetic media. Figure 45 shows graphs FSC vs. SSC before (a) and after (b) HGMS.

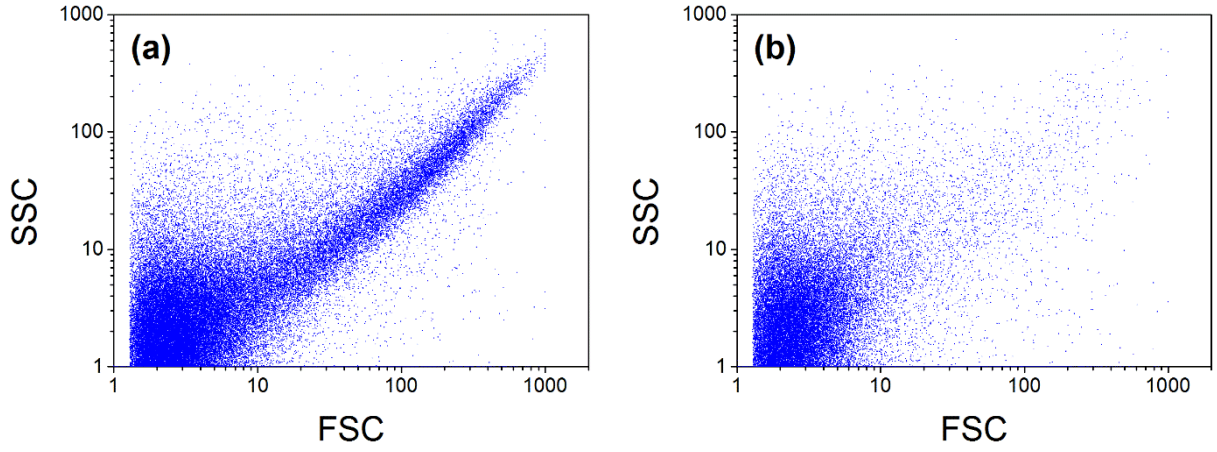

Figure 45: *Graphs FSC vs. SSC before (a) and after (b) HGMS.*

The "tail" shape part, i.e., part between 10 and 1000 FSC, of the graph (a) on the Figure 45 presents the magneto-responsive bacteria (for details look Section A1.9 in Appendix) before the HGMS. It is clearly seen that tail part on the graph corresponding to magneto-responsive bacteria is missing after the HGMS. The achieved efficiency of the HGMS was 96 %. The number of bacteria cells/mL after the HGMS was $4 \cdot 10^3$, which is less than the number of cells needed for the start or continuing the MLF [164]. The result of successful separation was further confirmed by TEM analysis before and after the HGMS separation. Before the HGMS, the magneto-responsive bacteria were seen on the specimen support, whereas after the HGMS the specimen support contained no bacteria cells.

4.2.4.1 Separation of the magneto-responsive bacteria from wine

Finally, HGMS was carried out on the wine sample. Figure 46 presents FSC vs SSC graphs before and after the HGMS in wine sample. Two populations of cells are clearly seen in the graph. The part between 10 and 200 FSC on the FSC vs SSC graph could be ascribed to the magneto-responsive bacteria, whereas the upper right population, i.e., between 200 and 1000 FSC, could be ascribed to yeast according to literature [250]. The second population might be already present in wine, since it was not filtered before experiments or it was added by bioactivators. Due to the two populations and non-specific staining for *O. oeni* the efficiency of the HGMS estimated by flow cytometry analysis was 59%.

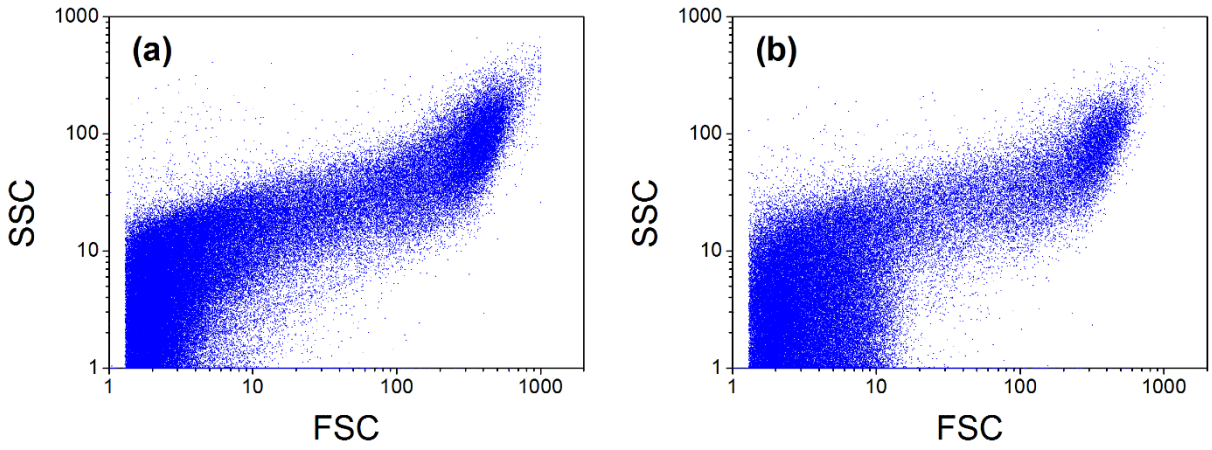

Figure 46: *Graphs FSC vs. SSC before (a) and after (b) HGMS in vine sample.*

The efficiency of the HGMS was further tested with a TEM analysis and by observations of MLF process after the HGMS. No bacteria were observed in the samples after the HGMS with the TEM analysis, whereas some larger cells, e.g., yeast, were observed.

The TEM analysis of the magneto-responsive bacteria after the MLF showed that although the cells multiplied, the nanoparticles remained on their surfaces (Figure 47a, b and c). After drying of the bacteria suspension on a TEM specimen support, the vast majority of the bacteria cells were deposited on the support as clusters containing several bacteria cells.

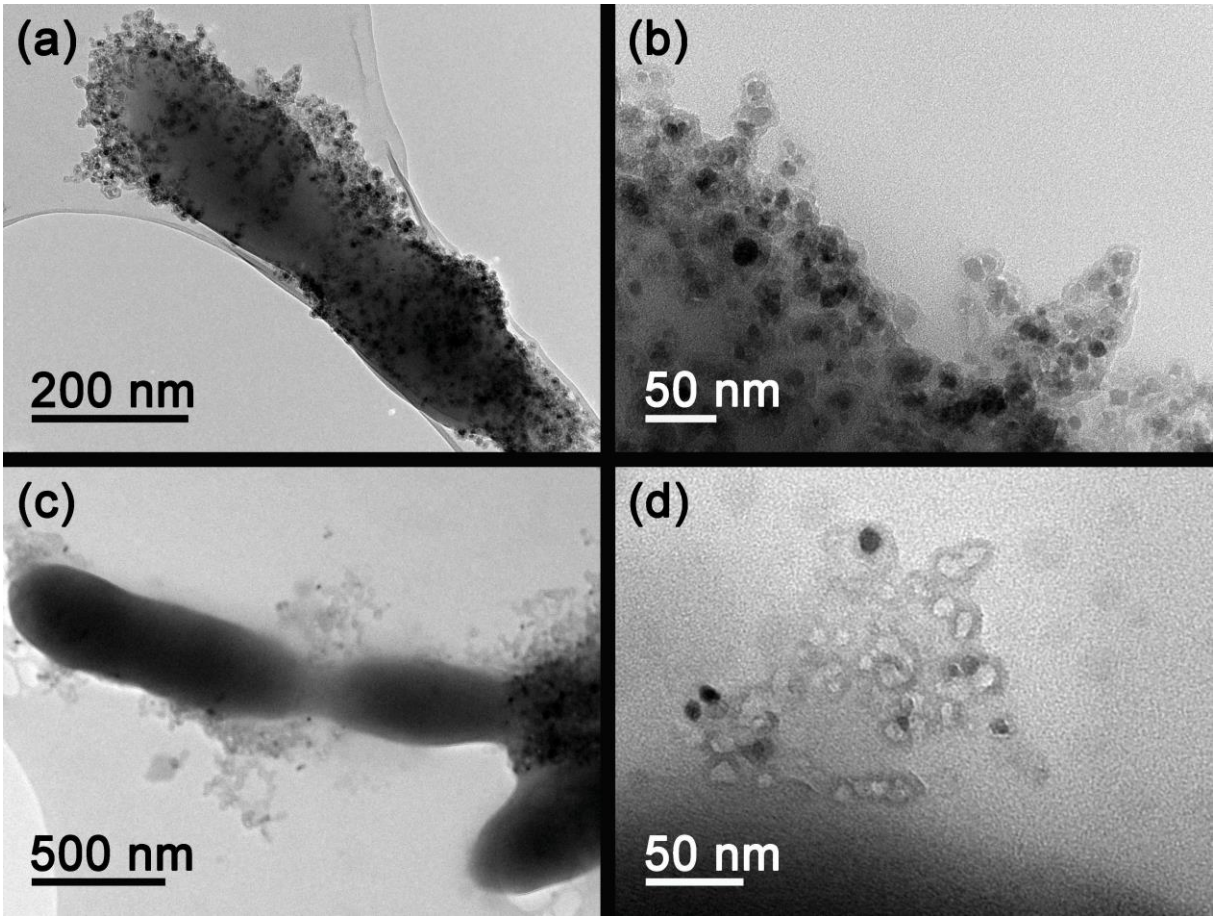

Figure 47: *TEM image of bacteria and aMNPs after the MLF*. Magneto-responsive bacteria after MLF in synthetic media (a), aMNPs at bacteria surface at high magnification in the synthetic media (b), magneto-responsive bacteria after MLF in wine (c) and aMNPs at bacteria surface at high magnification in wine (d).

Detailed TEM analysis of the nanoparticles after the MLF reviled that they partially dissolved in wine. In Figure 47d empty silica shells, which remained after dissolution of the iron-oxide core of the nanoparticles are visible. Dissolution of the attached magnetic nanoparticles was more obvious when the MLF occurred in wine compared to synthetic media. However, the dissolution of the nanoparticles did not significantly decrease the efficiency of the magnetic separation. For practical applications the nanoparticles should be prepared by appropriate surface coating to prevent their dissolution.

The MLF can be controlled by the removal of *O. oeni* at a certain stage of fermentation. The termination of MLF can be monitored by the exhaust of CO_2, which is one of the products in the MLF of the conversion of L-malic acid into L-lactic acid. To stop the fermentation in a certain stage of MLF the HGMS was performed after 7 days after the inoculation of wine with the magneto-responsive *O. oeni*. Furthermore, the aMNPs were adsorbed onto the pristine *O. oeni*, without the magnetic nanoparticles (labelled as "postmagneto-responsive" *O. oeni* in Table 8) after 7 days after their inoculation of the wine. The efficiency of HGMS of the magneto-responsive *O. oeni* was estimated based on the consumption of L-malic acid and citric acid, the production of L-lactic acid and the change of the pH value (Table 8).

Table 8: *Changing of pH and in content of organic acids with MLF of wine*. First raw shows the starting values for the wine. "Pristine *O. oeni*" represent bacteria without attached magnetic nanoparticles (the control). "Magneto-responsive *O. oeni*" represent bacteria with attached magnetic nanoparticles. The measurement were made after the bacteria were magnetically separated from the wine after 7 days of MLF, and after additional 7 days or 14 days after the separation. For "postmagneto-responsive *O. oeni*" the pristine bacteria was used for MLF. After 7 days of ML the magnetic nanoparticles were adsorbed onto the bacteria and they were magnetically separated. "Recycled magneto-responsive *O. oeni*" represent back flushed magneto-responsive *O. oeni* from HGMS column, which were inoculated into a new substrate. (The error of the measurements of the acid content was estimated to be ±10 %).

sample	pH	L-malic acid [g/L]	L-lactic acid [g/L]	citric acid [g/L]	time after inoculation [days]
Control wine	3.07	3	<0.1	0.21	
Pristine *O. oeni*	3.08	1.3	1.3	0.16	7
	3.15	0.1	2.2	0.02	14
	3.17	0.1	2.2	0.01	21
Magneto-responsive *O.oeni*	3.13	0.5	1.7	0.12	7
	3.13	0.5	1.7	0.12	14
	3.13	0.5	1.7	0.12	21
Postmagneto-responsive *O.oeni*	3.09	0.9	1.4	0.14	7
	3.09	0.9	1.4	0.14	14
	3.09	0.8	1.4	0.12	21
Recycled magneto-responsive *O. oeni*	3.08	2.2	0.5	0.19	7
	3.19	0.1	2.1	0.05	14

The starting concentration of L-malic acid and citric acid was decreased after 7 days after the inoculation of wine. In contrast, the concentration of L-lactic acid increased and the exhaust of CO_2 was observed. The results indicate that the MLF proceeded. The concentration of L-malic acid and citric acid continued to decrease and the concentration of L-lactic acid continued to increase in the next 7 days in bioreactors containing the pristine *O. oeni* without attached magnetic nanoparticles. In contrast, the acids concentrations remained the same and no exhaustion of CO_2 was observed in bioreactors after the HGMS of the magneto-responsive *O. oeni*. Results prove that the fermentation process was stopped completely. It is therefore reasonable to expect that the fermentation can be completely stopped in the desired stage of the fermentation with the separation of the magneto-responsive bacteria.

After the HGMS of the magneto-responsive *O. oeni*, the HGMS column containing trapped magneto-responsive *O. oeni*, was back flushed with distilled water. The "recycled" magneto-responsive *O. oeni* were than inoculated into a new bioreactor containing wine. The consumption of L-malic acid and the production of L-lactic acid (last two rows in Table 8) clearly indicate that the MLF occurred. Result proves that the separation process does not have a negative effect on the magneto-responsive *O. oeni* in the HGMS column. Therefore, the recycled magneto-responsive bacteria could be further used in another MLF. The MLF can also be stopped in the desired stage of the process when the pristine bacteria are applied and the magnetic nanoparticles are added just before the separation. The magnetic nanoparticles added in the form of concentrated suspension to the wine with the O. oeni adsorbed onto the bacteria and enabled their

effective HGMS. Also in the case of post addition of the magnetic nanoparticles, the MLF was completely stopped.

5 Discussion

5.1 Controlled heteroaggregation of two types of nanoparticles in an aqueous suspension

Appropriate magnetic carriers for the selective magnetic separation and multifunctional composite nanoparticles can be synthesized by assembly of nanoparticles in the aqueous suspension. To control this process the understanding of interactions between the nanoparticles with different surfaces' properties in the suspensions is crucial. The crucial information about the synthesis of heteroaggregates can be generated by knowing the influence of numerous parameters, such as, relative nanoparticle sizes, nanoparticle number ratios, nanoparticle concentration, and ionic strength, on the heteroaggregation process.

The aim of this thesis was to synthesize magnetic carries with controlled heteroaggregation of superparamagnetic nanoparticles in the aqueous suspension. The study showed that different heteroaggregates can be formed, when the interactions between nanoparticles with different surfaces' properties in the suspension are controlled. First, the influence of attractive electrostatic interactions and chemical interactions between two types of nanoparticles in an aqueous suspension was studied in order to develop a method for the controlled synthesis of the heteroaggregates. The heteroaggregation experiments described in this thesis were based on the model system composed of larger amorphous aSNPs and smaller crystalline cMNPs. The process of heteroaggregation was followed by DLS measurements and by determination of differences in a surface coverage of the central aSNP with the smaller cMNPs based on TEM analysis.

The electrostatic heteroaggregation processes are particularly interesting, but still not well understood [251]. Different parameters, e.g., nanoparticle concentration, nanoparticle number ratios, ionic strength, etc., were reported to have an influence on the heteroaggregate structure formed by applying electrostatic interactions between nanoparticles [28,132,252,253]. The TEM images (Figure 26) of formed heteroaggregates, synthesized by applying attractive electrostatic interactions between oppositely charged nanoparticles, show that the heteroaggregation between aSNP and cMNPs occurred at pH 5.5 and at the constant nanoparticle number ratio (R = 89) at both, i.e., the lower (0.7 mg/mL) and the higher (15 mg/mL) nanoparticle concentration of the cMNPs. An analysis of a large number of heteroaggregates revealed that the coverage of the aSNPs with the cMNPs was relatively non-uniform. The cMNPs mainly attached to the larger aSNPs as individual nanoparticles; however, they were quite frequently in close contact with each other or even in the form of small agglomerates, while larger areas of the aSNPs' surfaces were uncovered. The close contact between the cMNPs was surprising, since they display a strongly negative surface charge and should therefore repulse each other. The reason for the close contact between the cMNPs at the surfaces of the aSNPs, even though repulsive electrostatic forces are expected between them, is not clear. It can be explained by formation of small aggregates already during synthesis of the cMNPs. During the synthesis of MNPs, the silica layer might be formed around two or

more maghemite nanoparticles. Such “mini” clusters of the MNPs further functionalized with carboxyl groups, are still too small to be separated from the suspension by applying an external magnetic field, when washing the suspension of cMNPs with distilled water. Since they are usually in minority compared to the individual MNPs population, the DLS analysis might not characterize them properly. However, their behaviour in the nanoparticle suspensions will be similar to individual maghemite nanoparticles with a thin layer of silica. These clusters of cMNPs are having the same surface charge as an individual cMNP at pH 5.5, i.e., negative. During the process of heteroaggregation applying the attractive electrostatic interactions between the oppositely charged nanoparticles, such cluster might attach to the aSNP surface. Using TEM analysis the attachment of such cluster might look like the individual cMNPs are in close contact at the surfaces of the aSNPs. The close contact between the cMNPs at the surfaces of the aSNPs can also be explained by the change in the overall surface charge of the formed heteroaggregate. When the negatively charged cMNP attaches to the positively charged aSNP, its ζ-potential can locally change to become positive and this represents the preferred location for the next adsorbing cMNP. The attachment of the nanoparticles with a high surface charge in the form of smaller agglomerates onto the surfaces of larger, oppositely charged particles was also observed by others [122,152,242]. However, it has never been observed in the electrostatically driven heteroaggregation of larger, micron-sized particles.

The surface coverage of the larger aSNPs can be varied by changing the concentration of the nanoparticles in the suspensions or by the nanoparticle number ratio. By increasing the cMNP concentration and keeping the same nanoparticle number ratio, the surface coverage of the larger aSNPs was improved. Better, but still non-uniform coverage with the increasing cMNPs’ concentration can be explained by larger possibility for the collisions between the oppositely-charged nanoparticles in the suspension. When the nanoparticle suspension is diluted the electrostatic forces between the nanoparticles are decreased due to larger average distance between the oppositely charged nanoparticles’ surfaces (Equation 7) [96]. It is known, that the magnitude and length scale of electrostatic interactions can be tuned controllably through the choice of solvent (e.g., dielectric constant) as well as the concentration of the charged nanoparticles [145].

The increase of the number ratio between the nanoparticles of the two different sizes has been reported to improve the coverage of the larger nanoparticles with the smaller ones during electrostatic heteroaggregation [242]. This was, for example, observed in the electrostatic heteroaggregation of multi-walled carbon nanotubes and hematite particles [103]. My experiments showed no significant improvement of the surface coverage when the nanoparticle number ratio was increased from $R = 89$ to $R = 450$. It seems that the $R = 89$ was already high enough, and therefore a further increase did not have any influence on the coverage. However, if I compare the result of the surface coverage at $R = 15$ with $R = 89$, an improvement in surface coverage at $R = 89$ was observed. Therefore, I can conclude that the nanoparticle number ratio improves the surface coverage.

An improvement of surface coverage of aSNPs with cMNP by electrostatic interactions by increasing the ionic strength of the suspension was clearly seen (Figure 26d). There are several reports on the influence of the ionic strength on the formation of heteroaggregates between oppositely charged particles [156,253-256]. Although the stability of starting nanoparticles’ suspensions is decreased by increasing the ionic strength (Figure 22), the coverage of nanoparticles can generally be improved [156,257,258]. Electrostatic screening effects at the increased ionic strength decrease the effective electrostatic interaction [259,260]. Thus, the decrease in the repulsive interaction between the like-charged cMNPs can improve their surface density at the surfaces of the

aSNPs while the decrease in attractive interaction between the oppositely-charged nanoparticles can make the kinetics of heteroaggregation slower, also observed by the continuous DLS measurements in my experiments, and thus improve the homogeneity. However, also the agglomeration of the formed heteroaggregates in the suspension was more intensive at the increased ionic strength. Therefore, I can conclude that the increased ionic strength of the nanoparticle suspension does influence the surface coverage of larger nanoparticles with smaller one.

Compared to electrostatic interactions, the chemical interactions between activated carboxyl groups at the cMNPs and amino groups at the aSNPs ware more effective in the formation of the heteroaggregates and the surface coverage of the aSNPs with the cMNPs was more uniform (Figure 27). The significant difference in the appearance of the heteroaggregates obtained by the chemical interactions (Figure 27) compared to that obtained by the electrostatic interactions (Figure 26) strongly suggests that the covalent bonds between the two types of the functionalization molecules at the nanoparticles successfully formed.

The nanoparticle concentration in the experiments of the covalently-driven heteroaggregation influenced the activation of carboxyl groups of the cMNPs with the EDC activator molecule. Due to this effect of the concentration on the activation of the carboxyl groups, the effect on the surface coverage of aSNPs cannot be resolved. The results obtained by TEM analysis support this by observed better coverage of aSNPs with cMNPs in experiment with higher cMNP concentration (15 mg/mL) where carboxyl groups ware successfully activated, whereas in case of lower cMNP concentration (0.7 mg/mL) the coverage of aSNP was poor, suggesting that the concentration of cMNP was too low for successful activation of carboxyl groups. It is known that the single-step EDC coupling protocol for the activation of carboxyl groups is not effective at low concentrations of nanoparticles [76]. Due to effect on the activation, the influence of the nanoparticles concentration on the coverage during the covalently-driven heteroaggregation was smaller compared to electrostatic interactions, where the increase of the nanoparticle concentration effectively improved the surface coverage of aSNP.

The influence of the nanoparticle number ratio on the surface coverage of aSNP during the covalently- driven heteroaggregation was clearly seen by TEM analysis on the Figure 27 for the higher (R = 89) and Figure 28 for the lower (R = 15) nanoparticles ratios. In the case of the lower nanoparticle number ratio (R = 15) the sedimentation of the formed heteroaggregates was observed immediately after admixing the aSNPs into the suspension of the activated cMNPs. The fast sedimentation strongly suggests that the smaller cMNPs make bridges between the larger aSNPs. Such heteroaggregates are expected to be larger and have more branched structure [131]. In contrast, at R = 89, where the cMNPs ware in larger excess in the reaction suspension, the non-attached cMNPs acted like stabilizers of the suspension of the formed heteroaggregates. Furthermore, the heteroaggregate structure at R = 15 was expected to be more branched [131], while the obtained structure of the formed heteroaggregates at R = 89 could be described as raspberry-like. The raspberry-like heteroaggregates were also observed by others, when higher nanoparticles number ratio and large size difference between two types of nanoparticles were applied [131,261].

Using heterobifunctional crosslinkers (MNP-PEGn) as binding molecules no significant improvement of the surface coverage of the aSNP was observed (Figure 29) compared to direct bonding between the activated carboxyl and amino groups (Figure 27). The difference in crosslinker molecule length had no significant effect on the surface coverage. However, the influence of the crosslinkers of different length was observed by DLS analysis (Figure 30). The difference in the hydrodynamic size distribution due to different lengths of attached crosslinker molecules to the nanoparticle surface was also

reported by other researchers [240]. Results obtained by DLS measurements of the formed heteroaggregates support the idea that the longer crosslinker molecule would result in a broader hydrodynamic size distribution (Figure 30a) and the shorter crosslinker molecule would result in more narrow hydrodynamic size distribution (Figure 30b).

The kinetics of the heteroaggregation has a decisive influence on the appearance of the heteroaggregates. In general, apart from the relative size [256], the number ratio R between the two types of particles defines the morphology of the heteroaggregates. When the difference in the sizes of the particles is large, the larger particles are usually coated with the smaller ones at the large R values [131], as also observed in my experiments (Figure 27). With a decrease in the R value such heteroaggregates first start to form colloidal clusters through bridging the larger particles with the smaller ones (Figure 28). With a further decrease in the R value the ring-like and elongated chains are preferred [131]. However, when the process is too fast, non-uniform, disordered, colloidal structures are formed. Only by slowing down the kinetics of heteroaggregation with controlling the inter-particle interactions in the mixed systems, well-ordered hetero-aggregated structures can be obtained [262]. The significant difference in the kinetics of heteroaggregate formation was observed, comparing the continuous DLS measurement of the electrostatically-driven (Figure 31) and the covalently-driven heteroaggregation (Figure 32). I concluded based on continuous DLS measurements (see Figure 31 and Figure 32) that the electrostatic-driven heteroaggregation is very fast. At the nanoparticle concentrations usually applied in the heteroaggregation (0.7 mg/mL of cMNPs and R = 89) the kinetics were too fast to be measured. By decreasing the nanoparticle concentration, the aggregation might be slowed to time scales accessible or measurable by the continuous DLS. However, the same result was obtained when the cMNPs concentration was decreased by 10 or 100 times. Most probably, the heteroaggregation due to the electrostatic interactions is too fast to be detected with DLS. It is well known that, in the absence of any steric barrier, oppositely charged particles aggregate due to the attractive electrostatic interactions immediately upon mixing [107]. In my case, the slower heteroaggregation due to chemical interactions resulted in a much larger and much more homogeneous coverage of the larger aSNPs with the smaller cMNPs compared to the faster heteroaggregation caused by the attractive electrostatic interactions. The reason is most probably in the slower diffusion in the suspension during the chemical heteroaggregation, where there is almost no influence of the electrostatic forces on the transport of the nanoparticles.

Chemical heteroaggregation is therefore the preferred method for the synthesis of clusters of nanoparticles of controlled size, as was demonstrated in the case of superparamagnetic nanoparticle clusters for applications in magnetic separation [241]. The homogenous surface coverage of the larger nonmagnetic aSNPs with the magnetic cMNPs obtained by chemically-driven heteroaggregation on the model system also indicated a promising method for the synthesis of multifunctional composite nanoparticles. The method is relatively simple in terms of experimental conditions and equipment used, needing no high temperatures or external electric or magnetic fields. The multifunctional composite nanoparticles with raspberry-like structure bearing smaller nanoparticles over the larger central nanoparticle have been found in wide range of applications [263,264]. To estimate the developed method for the controlled synthesis of heteroaggregates in an aqueous suspension by the process of the covalently-driven heteroaggregation, the non-magnetic aSNPs in the model system were replaced with superparamagnetic nanoclusters a-iNANO. Analogous results, in terms of surface coverage of the larger nanoparticles by the smaller ones at different nanoparticle number ratios (Figure 36), were obtained as in the case of the model system. Based on the different surface coverage of the larger nanoparticles with the smaller ones, the developed

method has the potential to be used as the synthesis method for multifunctional composite nanoparticles.

A superparamagnetic heteroaggregates were synthesised with the control of interactions between differently functionalized superparamagnetic nanoparticles in an aqueous suspension. The superparamagnetic heteroaggregates were synthesised using chemical bonding between the central aMNPs and the outer cMNPs. The surplus of the cMNPs in the reaction mixture ensured that each of the aMNPs was surrounded by as many of the cMNPs as possible. However, at the higher nanoparticle number ratio (R = 12), they were more likely to sediment and were difficult to be re-dispersed once the sedimentation accrued. In contrast, at the same nanoparticles' concentration but with lower nanoparticle number ratio (R = 6) the suspension of formed superparamagnetic heteroaggregates was more stable. The superparamagnetic heteroaggregates were composed of 6-11 nanoparticles and had relatively uniform sizes of approximately 50-70 nm, as estimated from TEM images (Figure 37). Using only TEM analysis we cannot distinguish, which nanoparticle is the amino- and which is the carboxyl- functionalized, since they are composed of the same material with the same size. Based on analogy with the results obtained on the model system, where the aSNP present in the suspension in a lower number were situated in the centre of the heteroaggregate, I can speculate that also the formed superparamagnetic heteroaggregate shown in the Figure 21b aMNP is in the centre and is surrounded by the cMNP.

5.2 Controlled attachment of magnetic nanoparticles onto bacteria

The described method for the controlled synthesis of heteroaggregates by the process of heteroaggregation is not limited to the synthesis of magnetic carriers described in this study. In principle, by the control of interactions between magnetic nanoparticles and the surface of larger objects that are frequent targets of a magnetic separation process, e.g., bacteria, magnetic nanoparticles can be attached to the objects' surfaces. The attachment of the magnetic nanoparticles on such objects is an important part of their magnetic separation. The attachment of magnetic nanoparticles (aMNPs) onto the LAB *O. oeni* surface was studied in order to develop a method for the preparation of magneto-responsive bacteria that could be used in the winemaking. The wine industry is a branch, where large quantities of final product are produced. To minimize the expenses during the production of wine the method for the preparation of magneto-responsive bacteria should be an inexpensive process. The electrostatically-driven attachment of magnetic nanoparticles can be the method of choice, mainly for the economic reasons.

The preparation of magneto-responsive bacteria was based on electrostatic interactions between negatively-charged *O. oeni* and positively-charged aMNPs at pH 4 (Figure 41). Bonding of nanoparticles onto cell wall can damage the cell membrane of microorganism [265,266]. The cell membrane of *O. oeni* used in my experiments was reinforced by the MBR® process developed by Lallemand to adapt the cells to the harsh conditions in MLF, e.g., high amount of ethanol, low pH, etc. [209]. This allowed me to rehydrate bacteria in distilled water, where other cells without reinforced cell membrane can swell due to hypotonic environment [267], and washed the *O. oeni* suspension with centrifugation or ultrafiltration, without causing any damaged to the *O. oeni* cell membrane. The adsorption of the magnetic nanoparticles onto the non-ultrafiltrated bacteria was non-uniform compared to attachment onto the ultrafiltrated *O. oeni* (Figure 43). The result suggests that freeze dried bacteria besides bacteria cell might contain some rest of growth media (rich in nutrients) that might increase the ionic strength of the bacteria suspension. Although no difference in ζ-potential values was observed between non-ultrafiltrated and ultrafiltrated *O. oeni*, the ionic strength of non-

ultrafiltrated bacteria suspension could be high enough to cause the aggregation of the aMNPs and cause the nonhomogeneous surface coverage of the *O. oeni.*

Previous researches dealing with the adsorption of magnetic nanoparticle onto microorganism surfaces show that apart from the suspension pH [268], the nanoparticle concentration influences the surface coverage of the microorganisms [158]. There are very few reports investigating the number ratio R between the magnetic nanoparticles and the microorganisms [88,265]. The number ratio between bacteria and magnetic nanoparticles decisively affected the surface coverage of the bacteria with the magnetic nanoparticles (Figure 44). Similar to synthesized heteroaggregates at higher R, the surface of the bacteria was more homogenously covered (Figure 44a) compared to the coverage at the lower R (Figure 44b). It is worth mentioning that at the lower R, the absorbed nanoparticles make bridges between bacteria cells (Figure 44c), similar to the situation observed with the chemically-driven heteroaggregation at R = 15 (Figure 28). The difference in the behaviour of the magneto-responsive *O. oeni* covered with the nanoparticles at different number ratios was investigated by a direct assay of *O. oeni* removal from the suspension by a permanent magnet. The higher concentration of the attached nanoparticles onto the bacteria cell increases the efficiency of the magneto-responsive bacteria removal from the suspension [265]. In my experiment, the separation efficiency of homogenously covered bacteria with aMNPs ($5 \cdot 10^9$ cells/mL, R = 8745) was slightly higher (99.5±2%) compared non-homogenously covered bacteria ($5 \cdot 10^9$ cells/mL, R = 3336) (98±2%). Small difference can be also ascribed to experimental error. However, the high separation efficiency suggests that the developed method could be used to prepare magneto-responsive bacteria that can be further magnetically separated from the reaction mixture.

Results in Table 7 show that the preparation method for the magneto-responsive *O. oeni* or adsorption of the aMNPs onto the bacteria cell did not have an influence on the *O. oeni* metabolism. The known main factors influencing metabolism of *O. oeni* are temperature, pH, ethanol and sulphur dioxide concentration [269]. A literature review of the influence of attached nanoparticles on the bacteria metabolism in general shows that this topic is not well researched yet. The influence of the attached nanoparticles on the growth of bacteria was studied by other researchers in order to see the cytotoxic effect [270-272]. In my opinion, although the surface of the LAB is fully covered with nanoparticles, there is still enough space for the transport of material needed for bacteria growth. Due to occupied bacteria surface with magnetic nanoparticles, the transport might be slower compared to LAB without attached magnetic nanoparticles. By fully cover the LAB surface, the weight of bacteria increase, resulting in faster sedimentation of the bacteria compared to LAB without attached nanoparticles. In this case, the transport of material needed for growth might be more difficult compared to the floating cells, which might be seen as slower metabolism. Therefore, the attachment of magnetic nanoparticles onto LAB might result in slower kinetics of metabolism compared to bacteria cells without attached nanoparticles.

5.3 HGMS separation of magneto-responsive LAB

A deep understanding of heteroaggregation is also a key issue for development of novel biotechnological applications, such as bacteria separation [148] and industrial extraction of enzymes from culture fungi [93]. In the last part of this chapter I will discuss the hypothesis that the MLF can be controlled by magnetic separation of magneto-responsive *O. oeni* in a certain stage of MLF.

To estimate the efficiency of the continuous HGMS of the magneto-responsive *O. oeni* from the fermentation media the flow cytometry analysis was used. The difference before

and after the HGMS separation of the magneto-responsive *O. oeni* from the synthetic media is clearly seen on the Figure 45. The number of unseparated bacteria after the HGMS was $4 \cdot 10^3$ bacteria cells/mL, which is less than the number of cells needed for the start or continuing the MLF [164].

By changing the fermentation media from synthetic to wine I demonstrated the HGMS of the magneto-responsive *O. oeni* on a practical case. Unfortunately, the flow cytometry analysis of HGMS of the magneto-responsive *O. oeni* from wine after HGMS was not the appropriate method for determining the separation efficiency. The flow cytometry results before and after HGMS show two populations of cells (Figure 46) due to non-specific staining of *O. oeni*. The second population could be ascribed to yeast [178], since the wine was not filtrated before the inoculation with the magneto-responsive bacteria. The carbon dioxide is one of two major products by LAB conversion of L-malic acid into L-lactic acid (Equation 8), and also the parameter for monitoring the process of MLF [166]. Since there was no exhaust of CO_2 observed in the bioreactor containing the separation filtrate after the HGMS of the magneto-responsive bacteria from wine I can conclude that the MLF process was stopped by the HGMS.

Unfortunately, the time of MLF could also affect the HGMS process. The maghemite cores of aMNPs start to dissolve at a certain time in wine (Figure 47d). This could decrease the HGMS effectiveness. The aMNPs in synthetic media also start to dissolve, but much slower than in wine (Figure 47b). Besides malic and citric acid used in the synthetic media, there are others acids that might speed up the dissolution of maghemite cores of aMNPs [269]. Therefore, to prevent the dissolution of maghemite, a porous silica layer [273] covering maghemite nanoparticles should be replaced by another non-porous and insoluble material. In practice, this problem of maghemite dissolution can be solved by applying appropriate protective coatings at the nanoparticles, for example, made of carbon or amphiphilic molecules.

The MLF in wine starts when the *O. oeni* reach the population of 10^6 cells/mL [176,209,274]. The cell multiplying stops when bacteria reach a stationary phase. The cell concentration at the stationary phase can reach up to 10^8 cells/mL [170,274], but usually is lower as reported by other researchers [168,275]. The *O. oeni* are known to grow slowly compare to other bacteria [176]. Their slow growth and chain-like structures formed during multiplication [176] could be advantages in magnetic separation. During the MLF the magneto-responsive bacteria cells multiply and their magnetization decreases because of the increase in the number of non-magnetized bacteria. Although the *O. oeni* multiply during fermentation process, the magnetic nanoparticles remained on their surfaces in a relatively high concentration (Figure 48).

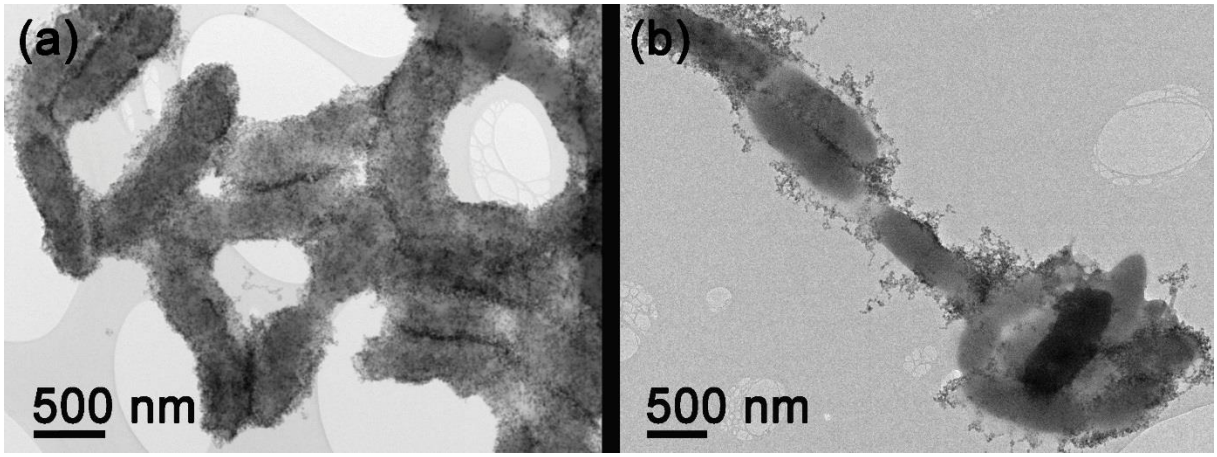

Figure 48: *TEM image of magneto-responsive bacteria before (a) and after (b) MLF*. Before MLF (a) the surface of *O. oeni* was densely covered with aMNPs. The chain like structure of *O. oeni* formed when bacteria multiply (b) resulted in decrease in number of aMNPs on the bacteria surface.

However, the newly formed bacteria cells might not contain the attached magnetic nanoparticles on their surface and can therefore not be magnetically separated. However, the multiplied cells are usually linked into chain-like structure, where only the first cell, i.e., original magneto-responsive bacteria, has attached magnetic nanoparticles. To ensure the efficient magnetic separation of such bacteria chains, the surface of the original magneto-responsive bacteria should be covered with magnetic nanoparticles in surface concentration as high as possible. Regarding this, in my fermentation experiments the magneto-responsive bacteria surfaces were densely covered with aMNPs. Although the cells multiplied during MLF, they were efficiently separated after MLF using the HGMS. Therefore, the high surface coverage of bacteria with the magnetic nanoparticles plays an important role in the magnetic separation.

Results in Table 8 prove that the MLF in wine was stopped by the magnetic separation of magneto-responsive bacteria. In the first 7 days of the MLF, the conversion of L-malic acid into L-lactic acid is clearly seen. Also the pH values had increased and the exhaust of CO_2 from bioreactors was observed. These are the indices that the MLF in bioreactors occurred. In the next 7 days the indices continued to change in bioreactors containing *O. oeni* without attached magnetic nanoparticles. In contrast, the concentration of acids, pH values did not change and no exhaust of CO_2 was observed in bioreactors containing HGMS filtrate. The same values were obtained at the end of MLF experiment. These results prove that the MLF stopped after the HGMS of magneto-responsive *O. oeni*. Regarding to the obtained results I can conclude that the fermentation process can be controlled by the magnetic separation of the magneto-responsive bacteria in the desired stage of the fermentation.

The trapped magneto-responsive bacteria in the HGMS column were successfully used in another MLF experiment. During the HGMS the bacteria were exposed to the high magnetic field. The exposure of microorganisms to the magnetic field could have an influence on the metabolism or viability of microorganism [276]). Although the magneto-responsive bacteria were exposed to high magnetic field during their magnetic separation, it seem that the effect of high magnetic field had no effect on their metabolism. The concentrations of L-malic acid and citric acid decreased, whereas concentrations the L-lactic acid increased (last two rows in Table 8). It is therefore reasonable to expect that the recycled magneto-responsive bacteria could be further used in another MLF.

6 Conclusions

In this thesis the study of the heteroaggregation of different nanoparticles in an aqueous suspension was experimentally studied as a possible method for the synthesis of superparamagnetic nanoclusters of a controlled size that can be applied as magnetic carriers in magnetic separation. The same method can be also used for the synthesis of multifunctional composite particles combing nanoparticles of different materials. The work represents a rare direct comparison between the heteroaggregation controlled by two types of interactions, electrostatic or chemical, in the same system of the two types of functionalized-nanoparticles. The heteroaggregation controlled by the electrostatic or by the chemical interactions is directly compared on the model system consisting of larger, amino-functionalized silica nanoparticles (aSNPs) and much smaller, superparamagnetic, carboxyl-functionalized, silica-coated maghemite nanoparticles (cMNPs). The influence of the electrostatic interactions between the two types of nanoparticles displaying an opposite surface charge on the heteroaggregation was compared to the influence of the chemical interactions originating from direct covalent bonding between the activated carboxyl functional groups at the cMNPs and the amino groups of the aSNPs. TEM analysis showed that the attractive electrostatic interactions result in a low and non-uniform coverage of the larger aSNPs with the smaller cMNPs, independent of the experimental conditions used, e.g., the concentration of the nanoparticles and the cMNPs/aSNPs number ratio. In contrast, chemical bonding between the functionalized molecules at the nanoparticle surfaces led to a much greater and more homogeneous coverage of the aSNPs with the cMNPs. The use of heterobifunctional crosslinkers (CAPEGn) as binding molecules had no significant influence on the coverage. In-situ DLS measurements strongly suggested that the higher and more homogeneous coverage in the case of the chemical heteroaggregation is related to the slower kinetics of heteroaggregates formation compared to the electrostatic aggregation. For the synthesis of the clusters/composites using the heteroaggregation of the nanoparticles in the aqueous suspensions, rapid chemical reactions at the surfaces of the two different types of nanoparticles have to be ensured and the heteroaggregation has to be performed at the pH of the suspension where there are no strong electrostatic attractions between the nanoparticles that would increase the kinetics of the interactions. The chemical heteroaggregation would therefore be the preferred method for the synthesis of clusters of superparamagnetic nanoparticles of controlled size needed in magnetic separation, as well as for the synthesis of multifunctional composite nanoparticles, combining nanoparticles of different functional materials.

For the synthesis of the superparamagnetic heteroaggregates for applications in magnetic separation the two types of superparamagnetic maghemite nanoparticles, i.e., amino-functionalized (aMNP) and carboxyl-functionalized (cMNP), were assembled in the aqueous suspensions due to chemical bonding between the activated carboxyl functional groups at the cMNPs and the amino groups of the aMNPs. The heteroaggregates of a controlled size were only obtained at the appropriate nanoparticle concentration and the nanoparticle number ratio. Therefore, can conclude that the chemically-driven heteroaggregation is appropriate method for the synthesis of the superparamagnetic heteroaggregates of controlled size for magnetic separation, if the

nanoparticle concentration and the nanoparticle number ratio is controlled during the synthesis.

On the other hand, the bonding of smaller maghemite nanoparticles onto larger silica nanoparticles represents a model for bonding individual superparamagnetic nanoparticles onto larger objects, for example, microorganisms, which is a crucial part in the process of their magnetic separation. The electrostatic interactions between aMNPs and lactic acid bacteria *O. oeni* were used to prepare magneto-responsive bacteria. TEM analysis showed that the ionic strength of the bacteria suspension, the nanoparticle concentration, and the nanoparticle number-to-bacteria ratio influence the surface coverage of the *O. oeni* with the aMNPs. The difference of the surface coverage of the *O. oeni* with the aMNPs also effected the separation of the magneto-responsive bacteria from the suspension using a permanent magnet. The method used for the magneto-responsive bacteria preparation and attachment of the aMNPs onto the bacteria cell did not have a negative influence on the *O. oeni* metabolism, as shown in Table 7. The electrostatic interactions between the negatively-charged *O. oeni* and the positively-charged aMNPs would therefore be the appropriate method for the preparation of the magneto-responsive bacteria that could be used in wine industry.

The magneto-responsive bacteria can be separated from fermentation media at a certain stage of the fermentation process using high gradient magnetic separation (HGMS). The developed separation method does not have a negative influence on the metabolism of the magneto-responsive *O. oeni* trapped in the HGMS column, since the MLF also occurred by using recycled magneto-responsive *O. oeni*. Flow cytometry analysis of the synthetic media containing the magneto-responsive bacteria before and after the HGMS showed successful separation. The used flow cytometry method was not appropriate for determining separation efficiency of the magneto-responsive bacteria from wine because too pore selectivity. However, the exhaust of CO_2 from bioreactor containing wine stopped after the HGMS and the analysis of acids concentration showed no change (Table 8). These results proves that the fermentation process stopped. Therefore, can conclude that the HGMS was successful in the separation of magneto-responsive bacteria from wine. Furthermore, the fermentation process can be controlled with the separation of magneto-responsive bacteria.

In this thesis I showed that heteroaggregates of controlled size can be prepared by understanding the interactions and parameters between nanoparticles with different surfaces' properties in the aqueous suspension. The method for the controlled synthesis of heteroaggregates described in thesis can be used for the synthesis of magnetic carriers appropriate for application in a magnetic separation of specific targets such as, bacteria or proteins. The same method can also be applied for the synthesis of multifunctional composite nanoparticles combining nanoparticles of different materials.

7 Acknowledgements

I would like to thank my supervisor and head of the Department for Synthesis of Materials at the Jožef Stefan Institute Prof. Dr. Darko Makovec: firstly for giving me the opportunity to work at K8; and secondly for his guidance, support and advice. I have learned a number of new things in these years and, especially, I had the privilege to work in an environment where high-class scientific research is done. I would like to thank Prof. Dr. Marin Berovič, co-supervisor of this dissertation, for help on biotechnology part of this dissertation.

Next, I have to thank the people with whom I did the majority of the work presented in this dissertation. Dr. Alenka Mertelj from Complex Matter of Jožef Stefan Institute, Dr. Martina Turk from Department of Biology at the Biotechnical Faculty, Dr. Mojca Benčina from Laboratory of Biotechnology, National Institute of Chemistry, Prof. Dr. Rok Kostanjšek from Department of Biology at the Biotechnical Faculty, Dr. Tatjana Košmrl from Department of Food Technology at the Biotechnical Faculty, are acknowledged for their support, discussions, analysis, and great ideas.

There is one persons who would fit into the category above on the first place, but I think that he deserves a special place. This is my »working mentor« Dr. Slavko Kralj. Thank you for your help with advices, discussions, suggestions, the microscopy analysis and all the other stuff. It is cool to work with a person with who you can laugh at jokes in one minute and in the next minute you are analysing scientific data together. I really enjoy to work with you because it was fun and in most cases fruitful. When we were together new ideas were just popping up.

I would also thank Dr. Marjan Bele from the National Institute of Chemistry, Slovenia, for providing silica nanoparticles, Bojan Kobal from Ptujska klet for providing wine samples and Gordana Veber from Jurana d.o.o for providing freeze-dried bacteria. For analysis of wine samples I would like to thank Dr. Dejan Bavčar from Kmetijski inštitut Slovenije for enzymatic analysis and Dr. Tjaša Jug from Kmetijsko-gozdarski zavod Nova Gorica for WSC analysis.

Special thanks go to Klemen Birtič from Faculty for chemistry and chemical technology for help with the preparation of fermentation experiments and Barbara Kastelic-Bokal from the Biotechnical Faculty for help with the microbiological experiments.

I also need to thank all my colleagues from the Department for Material Synthesis for providing a positive and working atmosphere and to all other friends from Jožef Stefan Institute, for the support and nice moments that we spent together.
I would like to thank to the committee members Dr. Darja Lisjak and Prof. Dr. Josep López Santín, for the detailed review of my doctoral dissertation. Their valuable comments helped to improve this dissertation.

The Ministry of Higher Education, Science and Technology of the Republic of Slovenia within the National Research Program P2-0089 is gratefully acknowledged for financially supporting my work. I acknowledge the use of equipment in the Center of Excellence on Nanoscience and Nanotechnology-Nanocenter.

Last, but not least, I would like to thank to everyone, who helped me on scientific area,

for the support and encouragement during my years of study. A thank also to my friends for their support and all the unforgettable moments that we spent together. So, thank you all.

8 References

1. Kishikawa N, Kuroda N. Analytical techniques for the determination of biologically active quinones in biological and environmental samples. *Journal of pharmaceutical and biomedical analysis.* Jan 2014;87:261-270.

2. Zhang Z, Tan W, Hu Y, Li G, Zan S. Microwave synthesis of gibberellin acid 3 magnetic molecularly imprinted polymer beads for the trace analysis of gibberellin acids in plant samples by liquid chromatography-mass spectrometry detection. *The Analyst.* Feb 21 2012;137(4):968-977.

3. Zhou C, Du Z, Li G, Zhang Y, Cai Z. Oligomers matrix-assisted dispersion of high content of carbon nanotubes into monolithic column for online separation and enrichment of proteins from complex biological samples. *The Analyst.* Oct 7 2013;138(19):5783-5790.

4. Jiang TF, Liang TT, Wang YH, Zhang WH, Lv ZH. Immobilized capillary tyrosinase microreactor for inhibitor screening in natural extracts by capillary electrophoresis. *Journal of pharmaceutical and biomedical analysis.* Oct 2013;84:36-40.

5. Xie N, Ding X, Wang X, Wang P, Zhao S, Wang Z. Determination of thioglycolic acid in cosmetics by capillary electrophoresis. *Journal of pharmaceutical and biomedical analysis.* Jan 2014;88:509-512.

6. Wisniewski JR, Zielinska DF, Mann M. Comparison of ultrafiltration units for proteomic and N-glycoproteomic analysis by the filter-aided sample preparation method. *Analytical biochemistry.* Mar 15 2011;410(2):307-309.

7. Leskinen SD, Brownell M, Lim DV, Harwood VJ. Hollow-fiber ultrafiltration and PCR detection of human-associated genetic markers from various types of surface water in Florida. *Applied and environmental microbiology.* Jun 2010;76(12):4116-4117.

8. Xu X, Sherry RA, Niu S, Li D, Luo Y. Net primary productivity and rain-use efficiency as affected by warming, altered precipitation, and clipping in a mixed-grass prairie. *Global change biology.* Sep 2013;19(9):2753-2764.

9. Zhao X, Bi K, Wang X, et al. A UFLC-MS/MS method coupled with one-step protein precipitation for determination of docetaxel in rat plasma: comparative pharmacokinetic study of modified nanostructured lipid carrier. *Journal of pharmaceutical and biomedical analysis.* Sep 2013;83:202-208.

10. Rabilloud T, Chevallet M, Luche S, Lelong C. Two-dimensional gel electrophoresis in proteomics: Past, present and future. *Journal of proteomics.* Oct 10 2010;73(11):2064-2077.

11. Shi Y, Zhang JH, Shi D, et al. Selective solid-phase extraction of cholesterol using molecularly imprinted polymers and its application in different biological samples. *Journal of pharmaceutical and biomedical analysis.* Nov 16 2006;42(5):549-555.

12. Cao Y, Bai G, Chen J, Tian W, Wang S, Yang W. Preparation and characterization of magnetic microspheres for the purification of interferon alpha-2b. *Journal of chromatography. B, Analytical technologies in the biomedical and life*

sciences. Apr 3 2006;833(2):236-244.

13. Wierucka M, Biziuk M. Application of magnetic nanoparticles for magnetic solid-phase extraction in preparing biological, environmental and food samples. *TrAC Trends in Analytical Chemistry.* 2014;59:50-58.

14. Veiseh O, Gunn JW, Zhang M. Design and fabrication of magnetic nanoparticles for targeted drug delivery and imaging. *Advanced drug delivery reviews.* Mar 8 2010;62(3):284-304.

15. Gunther CG. *Electro-magnetic ore separation.* New York [etc.]: Hill publishing company; 1909.

16. Parker MR. The physics of magnetic separation. *Contemporary Physics.* 1977/05/01 1977;18(3):279-306.

17. Yavuz CT, Prakash A, Mayo JT, Colvin VL. Magnetic separations: From steel plants to biotechnology. *Chemical Engineering Science.* 2009;64(10):2510-2521.

18. Horak D, Babic M, Mackova H, Benes MJ. Preparation and properties of magnetic nano- and microsized particles for biological and environmental separations. *Journal of separation science.* Jul 2007;30(11):1751-1772.

19. Chang SC, Anderson TI, Bahrman SE, Gruden CL, Khijniak AI, Adriaens P. Comparing recovering efficiency of immunomagnetic separation and centrifugation of mycobacteria in metalworking fluids. *Journal of industrial microbiology & biotechnology.* Dec 2005;32(11-12):629-638.

20. Yavuz CT, Mayo JT, Yu WW, et al. Low-field magnetic separation of monodisperse Fe3O4 nanocrystals. *Science.* Nov 10 2006;314(5801):964-967.

21. Kappler TE, Hickstein B, Peuker UA, Posten C. Characterization of magnetic ion-exchange composites for protein separation from biosuspensions. *Journal of bioscience and bioengineering.* Jun 2008;105(6):579-585.

22. Franzreb M, Siemann-Herzberg M, Hobley TJ, Thomas OR. Protein purification using magnetic adsorbent particles. *Applied microbiology and biotechnology.* May 2006;70(5):505-516.

23. Šafařík I, Šafaříková M. Use of magnetic techniques for the isolation of cells. *Journal of Chromatography B: Biomedical Sciences and Applications.* 1999;722(1–2):33-53.

24. Iacob G, Ciochina AD, Bredetean O. High gradient magnetic separation ordered matrices. *European Cells and Materials.* 2002;3(2):167-169.

25. Pankhurst QA, Connolly J, Jones SK, Dobson J. Applications of magnetic nanoparticles in biomedicine. *J Phys D Appl Phys.* Jul 7 2003;36(13):R167-R181.

26. Safarikova M, Safarik I. The Application of Magnetic Techniques in Biosciences. *Magnetic and Electrical Separation.* 2001;10(4):223-252.

27. He J, Huang M, Wang D, Zhang Z, Li G. Magnetic separation techniques in sample preparation for biological analysis: A review. *Journal of pharmaceutical and biomedical analysis.* Apr 24 2014.

28. Rheinländer T, Kötitz R, Weitschies W, Semmler W. Magnetic fractionation of magnetic fluids. *Journal of Magnetism and Magnetic Materials.* 2000;219(2):219-228.

29. Moeser GD, Roach KA, Green WH, Alan Hatton T, Laibinis PE. High-gradient magnetic separation of coated magnetic nanoparticles. *AIChE Journal.* 2004;50(11):2835-2848.

30. Ditsch A, Lindenmann S, Laibinis PE, Wang DIC, Hatton TA. High-Gradient

Magnetic Separation of Magnetic Nanoclusters. *Industrial & Engineering Chemistry Research.* 2005/08/01 2005;44(17):6824-6836.

31. Hatch GP, Stelter RE. Magnetic design considerations for devices and particles used for biological high-gradient magnetic separation (HGMS) systems. *Journal of Magnetism and Magnetic Materials.* 2001;225(1–2):262-276.

32. Hubbuch JJ, Thomas ORT. High-gradient magnetic affinity separation of trypsin from porcine pancreatin. *Biotechnology and bioengineering.* 2002;79(3):301-313.

33. Leun D, SenGupta AK. Preparation and Characterization of Magnetically Active Polymeric Particles (MAPPs) for Complex Environmental Separations. *Environmental science & technology.* 2000/08/01 2000;34(15):3276-3282.

34. Kappler T, Cerff M, Ottow K, Hobley T, Posten C. In situ magnetic separation for extracellular protein production. *Biotechnology and bioengineering.* Feb 1 2009;102(2):535-545.

35. He X, Chen Y, Wang K, Wu P, Gong P, Huo H. Selective separation of proteins with pH-dependent magnetic nanoadsorbents. *Nanotechnology.* 2007;18(36):365604.

36. Bucak S, Jones DA, Laibinis PE, Hatton TA. Protein separations using colloidal magnetic nanoparticles. *Biotechnol Progr.* Mar-Apr 2003;19(2):477-484.

37. Shieh DB, Su CH, Chang FY, et al. Aqueous nickel-nitrilotriacetate modified Fe(3)O(4)-NH(3)(+) nanoparticles for protein purification and cell targeting. *Nanotechnology.* Aug 28 2006;17(16):4174-4182.

38. Borlido L, Azevedo AM, Roque AC, Aires-Barros MR. Magnetic separations in biotechnology. *Biotechnology advances.* Dec 2013;31(8):1374-1385.

39. Neurauter AA, Bonyhadi M, Lien E, et al. Cell isolation and expansion using Dynabeads. *Advances in biochemical engineering/biotechnology.* 2007;106:41-73.

40. Gómez-Pastora J, Bringas E, Ortiz I. Recent progress and future challenges on the use of high performance magnetic nano-adsorbents in environmental applications. *Chemical Engineering Journal.* 2014;256:187-204.

41. Hu J, Chen G, Lo IM. Removal and recovery of Cr(VI) from wastewater by maghemite nanoparticles. *Water research.* Nov 2005;39(18):4528-4536.

42. Miltenyi S, Muller W, Weichel W, Radbruch A. High-Gradient Magnetic Cell-Separation with Macs. *Cytometry.* 1990;11(2):231-238.

43. Kumar CSSR. *Magnetic Nanomaterials.* Wiley; 2009.

44. Svoboda J, Fujita T. Recent developments in magnetic methods of material separation. *Minerals Engineering.* 2003;16(9):785-792.

45. Häfeli U. *Scientific and Clinical Applications of Magnetic Carriers.* Springer; 1997.

46. Cole AJ, Yang VC, David AE. Cancer theranostics: the rise of targeted magnetic nanoparticles. *Trends in biotechnology.* Jul 2011;29(7):323-332.

47. Xu C, Sun S. New forms of superparamagnetic nanoparticles for biomedical applications. *Advanced drug delivery reviews.* Nov 2 2012.

48. Kralj S, Rojnik M, Kos J, Makovec D. Targeting EGFR-overexpressed A431 cells with EGF-labeled silica-coated magnetic nanoparticles. *Journal of Nanoparticle Research.* 2013;15(5).

49. Kocbek P, Kralj S, Kreft ME, Kristl J. Targeting intracellular compartments by magnetic polymeric nanoparticles. *European journal of pharmaceutical sciences : official journal of the European Federation for Pharmaceutical Sciences.* Sep 27

2013;50(1):130-138.

50. Wang LX, Li JC, Jiang Q, Zhao LJ. Water-soluble Fe3O4 nanoparticles with high solubility for removal of heavy-metal ions from waste water. *Dalton T.* 2012;41(15):4544-4551.

51. Makovec D, Sajko M, Selišnik A, Drofenik M. Magnetically recoverable photocatalytic nanocomposite particles for water treatment. *Materials Chemistry and Physics.* 2011;129(1-2):83-89.

52. Zhang F, Liu N, Zhao P, et al. Gold on amine-functionalized magnetic nanoparticles: A novel and efficient catalyst for hydrogenation reactions. *Applied Surface Science.* 2012;263:471-475.

53. Long Y, Xie M, Niu J, Wang P, Ma J. Preparation of acid–base bifunctional core–shell structured Fe3O4@SiO2 nanoparticles and their cooperative catalytic activity. *Applied Surface Science.* 2013;277:288-292.

54. Safarik I, Safarikova M. Magnetic techniques for the isolation and purification of proteins and peptides. *Biomagnetic research and technology.* Nov 26 2004;2(1):7.

55. Meyer A, Hansen DB, Gomes CSG, Hobley TJ, Thomas ORT, Franzreb M. Demonstration of a strategy for product purification by high-gradient magnetic fishing: Recovery of superoxide dismutase from unconditioned whey. *Biotechnol Progr.* Jan-Feb 2005;21(1):244-254.

56. Ditsch A, Yin J, Laibinis PE, Wang DIC, Hatton TA. Ion-exchange purification of proteins using magnetic nanoclusters. *Biotechnol Progr.* Aug 2006;22(4):1153-1162.

57. Huber DL. Synthesis, properties, and applications of iron nanoparticles. *Small.* May 2005;1(5):482-501.

58. Lu AH, Salabas EL, Schuth F. Magnetic nanoparticles: synthesis, protection, functionalization, and application. *Angew Chem Int Ed Engl.* 2007;46(8):1222-1244.

59. Thanh NTK. *Magnetic Nanoparticles: From Fabrication to Clinical Applications : Theory to Therapy, Chemistry to Clinic, Bench to Bedside.* CRC PressINC; 2012.

60. Cornell RM, Schwertmann U. Transformations. *The Iron Oxides*: Wiley-VCH Verlag GmbH & Co. KGaA; 2004:365-407.

61. Ma Z, Liu H. Synthesis and surface modification of magnetic particles for application in biotechnology and biomedicine. *China Particuology.* 2007;5(1-2):1-10.

62. Mahmoudi M, Sant S, Wang B, Laurent S, Sen T. Superparamagnetic iron oxide nanoparticles (SPIONs): development, surface modification and applications in chemotherapy. *Advanced drug delivery reviews.* Jan-Feb 2011;63(1-2):24-46.

63. Gupta AK, Gupta M. Synthesis and surface engineering of iron oxide nanoparticles for biomedical applications. *Biomaterials.* Jun 2005;26(18):3995-4021.

64. Gubin SP. *Magnetic Nanoparticles.* John Wiley & Sons; 2009.

65. Sun Z-X, Su F-W, Forsling W, Samskog P-O. Surface Characteristics of Magnetite in Aqueous Suspension. *Journal of Colloid and Interface Science.* 1998;197(1):151-159.

66. Gupta AK, Gupta M. Cytotoxicity suppression and cellular uptake enhancement of surface modified magnetic nanoparticles. *Biomaterials.* May 2005;26(13):1565-1573.

67. Liu X, Guan Y, Ma Z, Liu H. Surface Modification and Characterization of Magnetic Polymer Nanospheres Prepared by Miniemulsion Polymerization. *Langmuir : the ACS journal of surfaces and colloids.* 2004/11/01 2004;20(23):10278-10282.

68. Shao D, Xia A, Hu J, Wang C, Yu W. Monodispersed magnetite/silica composite microspheres: Preparation and application for plasmid DNA purification. *Colloids and Surfaces A: Physicochemical and Engineering Aspects.* 2008;322(1-3):61-65.

69. Kralj S, Makovec D, Čampelj S, Drofenik M. Producing ultra-thin silica coatings on iron-oxide nanoparticles to improve their surface reactivity. *Journal of Magnetism and Magnetic Materials.* 2010;322(13):1847-1853.

70. Campelj S, Makovec D, Drofenik M. Preparation and properties of water-based magnetic fluids. *Journal of physics. Condensed matter : an Institute of Physics journal.* May 21 2008;20(20):204101.

71. Racuciu M, Creanga DE, Airinei A. Citric-acid-coated magnetite nanoparticles for biological applications. *The European physical journal. E, Soft matter.* Oct 2006;21(2):117-121.

72. Nagao D, Yokoyama M, Yamauchi N, Matsumoto H, Kobayashi Y, Konno M. Synthesis of Highly Monodisperse Particles Composed of a Magnetic Core and Fluorescent Shell. *Langmuir : the ACS journal of surfaces and colloids.* 2008/09/02 2008;24(17):9804-9808.

73. Čampelj S, Makovec D, Drofenik M. Functionalization of magnetic nanoparticles with 3-aminopropyl silane. *Journal of Magnetism and Magnetic Materials.* 2009;321(10):1346-1350.

74. Kralj S, Drofenik M, Makovec D. Controlled surface functionalization of silica-coated magnetic nanoparticles with terminal amino and carboxyl groups. *Journal of Nanoparticle Research.* 2010;13(7):2829-2841.

75. Colombo M, Carregal-Romero S, Casula MF, et al. Biological applications of magnetic nanoparticles. *Chemical Society reviews.* Jun 7 2012;41(11):4306-4334.

76. Hermanson GT. *Bioconjugate Techniques.* Academic Press; 2008.

77. Lee J, Lee Y, Youn JK, et al. Simple synthesis of functionalized superparamagnetic magnetite/silica core/shell nanoparticles and their application as magnetically separable high-performance biocatalysts. *Small.* Jan 2008;4(1):143-152.

78. Sun S, Ma M, Qiu N, et al. Affinity adsorption and separation behaviors of avidin on biofunctional magnetic nanoparticles binding to iminobiotin. *Colloids and surfaces. B, Biointerfaces.* Nov 1 2011;88(1):246-253.

79. Marszall MP, Bucinski A. A protein-coated magnetic beads as a tool for the rapid drug-protein binding study. *Journal of pharmaceutical and biomedical analysis.* Jul 8 2010;52(3):420-424.

80. Xu H, Aguilar ZP, Yang L, et al. Antibody conjugated magnetic iron oxide nanoparticles for cancer cell separation in fresh whole blood. *Biomaterials.* Dec 2011;32(36):9758-9765.

81. Ma Z-Y, Liu X-Q, Guan Y-P, Liu H-Z. Synthesis of magnetic silica nanospheres with metal ligands and application in affinity separation of proteins. *Colloids and Surfaces A: Physicochemical and Engineering Aspects.* 2006;275(1-3):87-91.

82. Xu X, Rosi NL, Wang Y, Huo F, Mirkin CA. Asymmetric Functionalization of Gold Nanoparticles with Oligonucleotides. *Journal of the American Chemical Society.* 2006/07/01 2006;128(29):9286-9287.

83. Chen T, Shukoor MI, Wang R, et al. Smart Multifunctional Nanostructure for Targeted Cancer Chemotherapy and Magnetic Resonance Imaging. *ACS Nano.* 2011/10/25 2011;5(10):7866-7873.

84. Dai X, Xu H, Zhang X, Zhu W, Gu H, Wei M. Determination of the affinity

constant of streptavidin-coupled magnetic particles and a biotinylated antibody for high performance of magnetic solid carrier in immunoassays. *Materials science & engineering. C, Materials for biological applications.* Jan 1 2014;34:422-428.

85. Lee YC, Block G, Chen H, et al. One-step isolation of plasma membrane proteins using magnetic beads with immobilized concanavalin A. *Protein expression and purification.* Dec 2008;62(2):223-229.

86. Leslie-Pelecky DL, Rieke RD. Magnetic Properties of Nanostructured Materials. *Chemistry of Materials.* 1996/01/01 1996;8(8):1770-1783.

87. Ditsch A, Laibinis PE, Wang DIC, Hatton TA. Controlled clustering and enhanced stability of polymer-coated magnetic nanoparticles. *Langmuir : the ACS journal of surfaces and colloids.* Jun 21 2005;21(13):6006-6018.

88. Berovic M, Berlot M, Kralj S, Makovec D. A new method for the rapid separation of magnetized yeast in sparkling wine. *Biochemical Engineering Journal.* 2014;88:77-84.

89. Masliyah JH, Bhattacharjee SUhbgsbiGVYQEC. *Electrokinetic and Colloid Transport Phenomena.* Wiley; 2006.

90. Shaw DJUhbgsbin. *Introduction to Colloid and Surface Chemistry.* Butterworth-Heinemann; 1992.

91. Behrens SH, Christl DI, Emmerzael R, Schurtenberger P, Borkovec M. Charging and Aggregation Properties of Carboxyl Latex Particles: Experiments versus DLVO Theory. *Langmuir : the ACS journal of surfaces and colloids.* 2000/03/01 2000;16(6):2566-2575.

92. Jia X, Gregory J, Williams RUhbgsbiv. *Particle Deposition & Aggregation: Measurement, Modelling and Simulation.* Elsevier Science; 1998.

93. Cosgrove TUhbgsbiELL. *Colloid Science: Principles, Methods and Applications.* John Wiley & Sons; 2010.

94. Malvern Instruments Ltd. Zetasizer Nano Series User Manual. 2004; http://www.biozentrum.unibas.ch/fileadmin/redaktion/Forschung/Research_Groups/BF/instruments/zetasizer_manual.pdf.

95. Israelachvili J. Solvation forces and liquid structure, as probed by direct force measurements. *Accounts of chemical research.* 1987/11/01 1987;20(11):415-421.

96. Lewis JA. Colloidal Processing of Ceramics. *Journal of the American Ceramic Society.* 2000;83(10):2341-2359.

97. Tuinier R, Vliegenthart GA, Lekkerkerker HNW. Depletion interaction between spheres immersed in a solution of ideal polymer chains. *The Journal of Chemical Physics.* 2000;113(23):10768-10775.

98. Dzubiella J, Likos CN, Löwen H. Star-polymers as depleting agents of colloidal hard spheres. *Europhys. Lett.* 2002;58(1):133-139.

99. Holdich RGUhbgsbiB. *Fundamentals of Particle Technology.* Midland Information Technology and Publishing; 2002.

100. Kalantari M, Kazemeini M, Tabandeh F, Arpanaei A. Lipase immobilisation on magnetic silica nanocomposite particles: effects of the silica structure on properties of the immobilised enzyme. *Journal of Materials Chemistry.* 2012;22(17):8385.

101. Gyergyek S, Makovec D, Mertelj A, Huskic M, Drofenik M. Superparamagnetic nanocomposite particles synthesized using the mini-emulsion technique. *Colloid Surface A.* Aug 20 2010;366(1-3):113-119.

102. Gyergyek S, Huskić M, Makovec D, Drofenik M. Superparamagnetic nanocomposites of iron oxide in a polymethyl methacrylate matrix synthesized by in situ polymerization. *Colloids and Surfaces A: Physicochemical and Engineering Aspects.* 2008;317(1–3):49-55.

103. Huynh KA, McCaffery JM, Chen KL. Heteroaggregation of multiwalled carbon nanotubes and hematite nanoparticles: rates and mechanisms. *Environmental science & technology.* Jun 5 2012;46(11):5912-5920.

104. Wang J, Chen C. Biosorbents for heavy metals removal and their future. *Biotechnology advances.* Mar-Apr 2009;27(2):195-226.

105. Zamani F, Hosseini SM. Palladium nanoparticles supported on Fe3O4/amino acid nanocomposite: Highly active magnetic catalyst for solvent-free aerobic oxidation of alcohols. *Catalysis Communications.* 2014;43:164-168.

106. HidalgoAlvarez R, Martin A, Fernandez A, Bastos D, Martinez F, delasNieves FJ. Electrokinetic properties, colloidal stability and aggregation kinetics of polymer colloids. *Advances in colloid and interface science.* Sep 2 1996;67:1-118.

107. López-López JM, Schmitt A, Moncho-Jordá A, Hidalgo-Álvarez R. Stability of binary colloids: kinetic and structural aspects of heteroaggregation processes. *Soft Matter.* 2006;2(12):1025.

108. Lin MY, Lindsay HM, Weitz DA, Klein R, Ball RC, Meakin P. Universal Diffusion-Limited Colloid Aggregation. *J Phys-Condens Mat.* Apr 2 1990;2(13):3093-3113.

109. Lebovka NI. Aggregation of Charged Colloidal Particles. *Adv Polym Sci.* 2014;255:57-96.

110. Witten TA, Sander LM. Diffusion-Limited Aggregation, a Kinetic Critical Phenomenon. *Physical Review Letters.* 1981;47(19):1400-1403.

111. Sander LM. Diffusion-limited aggregation: a kinetic critical phenomenon? *Contemporary Physics.* Jul-Aug 2000;41(4):203-218.

112. Buffle J, Wilkinson KJ, Stoll S, Filella M, Zhang JW. A generalized description of aquatic colloidal interactions: The three-colloidal component approach. *Environmental science & technology.* Oct 1 1998;32(19):2887-2899.

113. Islam AM, Chowdhry BZ, Snowden MJ. Heteroaggregation in colloidal dispersions. *Advances in colloid and interface science.* Dec 1 1995;62(2-3):109-136.

114. Hidalgo-Álvarez R, Martín A, Fernández A, Bastos D, Martínez F, de las Nieves FJ. Electrokinetic properties, colloidal stability and aggregation kinetics of polymer colloids. *Advances in colloid and interface science.* 1996;67(0):1-118.

115. Buffle J, Wilkinson KJ, Stoll S, Filella M, Zhang J. A Generalized Description of Aquatic Colloidal Interactions: The Three-colloidal Component Approach. *Environmental science & technology.* 1998/10/01 1998;32(19):2887-2899.

116. Ambashta RD, Sillanpaa M. Water purification using magnetic assistance: a review. *Journal of hazardous materials.* Aug 15 2010;180(1-3):38-49.

117. Lim CW, Lee IS. Magnetically recyclable nanocatalyst systems for the organic reactions. *Nano Today.* 2010;5(5):412-434.

118. Biesheuvel PM, Lindhoud S, Stuart MAC, de Vries R. Phase behavior of mixtures of oppositely charged protein nanoparticles at asymmetric charge ratios. *Physical Review E.* Apr 2006;73(4).

119. Jadhav S, Bochner BS, Konstantopoulos K. Hydrodynamic shear regulates the

kinetics and receptor specificity of polymorphonuclear leukocyte-colon carcinoma cell adhesive interactions. *J Immunol.* Nov 15 2001;167(10):5986-5993.

120. McCarty OJT, Jadhav S, Burdick MM, Bell WR, Konstantopoulos K. Fluid shear regulates the kinetics and molecular mechanisms of activation-dependent platelet binding to colon carcinoma cells. *Biophys J.* Aug 2002;83(2):836-848.

121. Hong L, Cacciuto A, Luijten E, Granick S. Clusters of Charged Janus Spheres. *Nano letters.* 2006/11/01 2006;6(11):2510-2514.

122. Claesson EM, Philipse AP. Monodisperse Magnetizable Composite Silica Spheres with Tunable Dipolar Interactions. *Langmuir : the ACS journal of surfaces and colloids.* 2005/10/01 2005;21(21):9412-9419.

123. Wagner CS, Shehata S, Henzler K, Yuan J, Wittemann A. Towards nanoscale composite particles of dual complexity. *J Colloid Interface Sci.* Mar 1 2011;355(1):115-123.

124. Westcott SL, Oldenburg SJ, Lee TR, Halas NJ. Formation and Adsorption of Clusters of Gold Nanoparticles onto Functionalized Silica Nanoparticle Surfaces. *Langmuir : the ACS journal of surfaces and colloids.* 1998/09/01 1998;14(19):5396-5401.

125. Caruso F, Spasova M, Susha A, Giersig M, Caruso RA. Magnetic Nanocomposite Particles and Hollow Spheres Constructed by a Sequential Layering Approach. *Chemistry of Materials.* 2001/01/01 2000;13(1):109-116.

126. Stoeva SI, Huo F, Lee J-S, Mirkin CA. Three-Layer Composite Magnetic Nanoparticle Probes for DNA. *Journal of the American Chemical Society.* 2005/11/01 2005;127(44):15362-15363.

127. Caruso F, Susha AS, Giersig M, Möhwald H. Magnetic Core–Shell Particles: Preparation of Magnetite Multilayers on Polymer Latex Microspheres. *Advanced Materials.* 1999;11(11):950-953.

128. Salgueiriño-Maceira V, Correa-Duarte MA, Farle M. Manipulation of Chemically Synthesized FePt Nanoparticles in Water: Core–Shell Silica/FePt Nanocomposites. *Small.* 2005;1(11):1073-1076.

129. Rogach A, Susha A, Caruso F, et al. Nano- and Microengineering: 3-D Colloidal Photonic Crystals Prepared from Sub-μm-sized Polystyrene Latex Spheres Pre-Coated with Luminescent Polyelectrolyte/Nanocrystal Shells. *Advanced Materials.* 2000;12(5):333-337.

130. Zhang D, Pelton R. Controlling the assembly of nanoparticle mixtures with two orthogonal polymer complexation reactions. *Langmuir : the ACS journal of surfaces and colloids.* Feb 14 2012;28(6):3112-3119.

131. Hiddessen AL, Rodgers SD, Weitz DA, Hammer DA. Assembly of binary colloidal structures via specific biological adhesion . *Langmuir : the ACS journal of surfaces and colloids.* 2000;16(25):9744-9753.

132. Dušak P, Mertelj A, Kralj S, Makovec D. Controlled heteroaggregation of two types of nanoparticles in an aqueous suspension. *Journal of Colloid and Interface Science.* 2015;438(0):235-243.

133. Wang J, Yang X. Synthesis of Core−Corona Polymer Hybrids with a Raspberry-like Structure by the Heterocoagulated Pyridinium Reaction. *Langmuir : the ACS journal of surfaces and colloids.* 2008/04/01 2008;24(7):3358-3364.

134. Starck P, Vincent B. Heteroflocculation of particle mixtures by a coacervation mechanism. A rheological study. *Langmuir : the ACS journal of surfaces and colloids.*

Jun 6 2006;22(12):5294-5300.

135. Li GL, Yang XL, Bai F, Huang WQ. Raspberry-like composite polymer particles by self-assemble heterocoagulation based on a charge compensation process. *Journal of Colloid and Interface Science.* May 15 2006;297(2):705-710.

136. Chak C-P, Xuan S, Mendes PM, Yu JC, Cheng CHK, Leung KC-F. Discrete Functional Gold Nanoparticles: Hydrogen Bond-Assisted Synthesis, Magnetic Purification, Supramolecular Dimer and Trimer Formation. *ACS Nano.* 2009/08/25 2009;3(8):2129-2138.

137. Li X, Liu Y, Xu Z, Yan H. Preparation of magnetic microspheres with thiol-containing polymer brushes and immobilization of gold nanoparticles in the brush layer. *European Polymer Journal.* 2011;47(10):1877-1884.

138. Lee KS, Woo MH, Kim HS, Lee EY, Lee IS. Synthesis of hybrid Fe(3)O(4)-silica-NiO superstructures and their application as magnetically separable high-performance biocatalysts. *Chem Commun (Camb).* Jul 7 2009(25):3780-3782.

139. Gude K, Narayanan R. Synthesis and Characterization of Colloidal-Supported Metal Nanoparticles as Potential Intermediate Nanocatalysts. *The Journal of Physical Chemistry C.* 2010/04/15 2010;114(14):6356-6362.

140. Kim J, Lee JE, Lee J, et al. Generalized fabrication of multifunctional nanoparticle assemblies on silica spheres. *Angew Chem Int Ed Engl.* Jul 17 2006;45(29):4789-4793.

141. Mirkin CA, Letsinger RL, Mucic RC, Storhoff JJ. A DNA-based method for rationally assembling nanoparticles into macroscopic materials. *Nature.* Aug 15 1996;382(6592):607-609.

142. Alivisatos AP, Johnsson KP, Peng XG, et al. Organization of 'nanocrystal molecules' using DNA. *Nature.* Aug 15 1996;382(6592):609-611.

143. Li M, Wong KKW, Mann S. Organization of Inorganic Nanoparticles Using Biotin−Streptavidin Connectors. *Chemistry of Materials.* 1999/01/01 1998;11(1):23-26.

144. Shenton W, Davis SA, Mann S. Directed self-assembly of nanoparticles into macroscopic materials using antibody-antigen recognition. *Advanced Materials.* Apr 16 1999;11(6):449-+.

145. Bishop KJ, Wilmer CE, Soh S, Grzybowski BA. Nanoscale forces and their uses in self-assembly. *Small.* Jul 2009;5(14):1600-1630.

146. Lee JH, Jun YW, Yeon SI, Shin JS, Cheon J. Dual-mode nanoparticle probes for high-performance magnetic resonance and fluorescence imaging of neuroblastoma. *Angew Chem Int Ed Engl.* Dec 11 2006;45(48):8160-8162.

147. Liu B, Zhou M, Liu H, Wang X, Yang X. Binary colloidal hetero-coagulation for raspberry-like particles through azide–alkyne click reaction. *Colloids and Surfaces A: Physicochemical and Engineering Aspects.* 2013;436:1027-1033.

148. Such GK, Johnston APR, Liang K, Caruso F. Synthesis and functionalization of nanoengineered materials using click chemistry. *Progress in Polymer Science.* Jul 2012;37(7):985-1003.

149. Viota JL, Rasa M, Sacanna S, Philipse AP. Stability of mixtures of charged silica, silica-alumina, and magnetite colloids. *Journal of Colloid and Interface Science.* Oct 15 2005;290(2):419-425.

150. Fernández-Barbero A, Vincent B. Charge heteroaggregation between hard and soft particles. *Physical Review E.* 2000;63(1).

151. Kim AY, Berg JC. Fractal heteroaggregation of oppositely charged colloids. *Journal of Colloid and Interface Science.* Sep 15 2000;229(2):607-614.

152. Perko S, Dakskobler A, Kosmac T. High-Performance Porous Nanostructured Ceramics. *Journal of the American Ceramic Society.* 2010;93(9):2499-2502.

153. DiFeo A, Finch JA, Xu ZH. Sphalerite-silica interactions: effect of pH and calcium ions. *Int J Miner Process.* Jan 2001;61(1):57-71.

154. Starck P, Ducker WA. Simple Method for Controlled Association of Colloidal-Particle Mixtures using pH-Dependent Hydrogen Bonding. *Langmuir : the ACS journal of surfaces and colloids.* Feb 17 2009;25(4):2114-2120.

155. Snoswell DRE, Rogers TJ, Howe AM, Vincent B. Controlling porosity within colloidal heteroaggregates. *Langmuir : the ACS journal of surfaces and colloids.* Nov 22 2005;21(24):11439-11445.

156. Lin W, Kobayashi M, Skarba M, Mu C, Galletto P, Borkovec M. Heteroaggregation in Binary Mixtures of Oppositely Charged Colloidal Particles. *Langmuir : the ACS journal of surfaces and colloids.* 2006/01/01 2005;22(3):1038-1047.

157. Pospiskova K, Prochazkova G, Safarik I. One-step magnetic modification of yeast cells by microwave-synthesized iron oxide microparticles. *Lett Appl Microbiol.* Jun 2013;56(6):456-461.

158. Singh S, Barick KC, Bahadur D. Surface engineered magnetic nanoparticles for removal of toxic metal ions and bacterial pathogens. *Journal of hazardous materials.* Sep 15 2011;192(3):1539-1547.

159. Song EQ, Hu J, Wen CY, et al. Fluorescent-magnetic-biotargeting multifunctional nanobioprobes for detecting and isolating multiple types of tumor cells. *ACS Nano.* Feb 22 2011;5(2):761-770.

160. El-Boubbou K, Gruden C, Huang X. Magnetic glyco-nanoparticles: a unique tool for rapid pathogen detection, decontamination, and strain differentiation. *J Am Chem Soc.* Nov 7 2007;129(44):13392-13393.

161. Kell AJ, Stewart G, Ryan S, et al. Vancomycin-modified nanoparticles for efficient targeting and preconcentration of Gram-positive and Gram-negative bacteria. *ACS Nano.* Sep 23 2008;2(9):1777-1788.

162. Gu H, Xu K, Xu C, Xu B. Biofunctional magnetic nanoparticles for protein separation and pathogen detection. *Chem Commun (Camb).* Mar 7 2006(9):941-949.

163. Chen L. Bioconjugated Magnetic Nanoparticles for Rapid Capture of Gram-positive Bacteria. *Journal of Biosensors & Bioelectronics.* 2012;01(S11).

164. Lonvaud-Funel A. Lactic acid bacteria in the quality improvement and depreciation of wine. *Antonie van Leeuwenhoek.* Jul-Nov 1999;76(1-4):317-331.

165. König H, Unden G, Fröhlich JUhbgsbiCRv-s. *Biology of Microorganisms on Grapes, in Must and in Wine.* Springer; 2009.

166. Ribéreau-Gayon P, Dubourdieu D, Donèche B, Lonvaud A. *Handbook of Enology, The Microbiology of Wine and Vinifications.* Wiley; 2006.

167. Ambrožič M. *Vpliv biološkega razkisa na nastanek hlapnih komponent vina*. Ljubljana: Katedra za vinarstvo na Oddelku za živilstvo Biotehniške fakultete Univerze v Ljubljanai, University of Ljubljana; 2006.

168. Wibowo D, Eschenbruch R, Davis CR, Fleet GH, Lee TH. Occurrence and Growth of Lactic Acid Bacteria in Wine: A Review. *American Journal of Enology and*

Viticulture. 1985;36(4):302-313.

169. Izuagbe YS, Dohman TP, Sandine WE, Heatherbell DA. Characterization of Leuconostoc oenos Isolated from Oregon Wines. *Applied and environmental microbiology.* Sep 1985;50(3):680-684.

170. Lopez I, Lopez R, Santamaria P, Torres C, Ruiz-Larrea F. Performance of malolactic fermentation by inoculation of selected Lactobacillus plantarum and Oenococcus oeni strains isolated from Rioja red wines. *Vitis.* 2008;47(2):123-129.

171. Versari A, Parpinello GP, Cattaneo M. Leuconostoc oenos and malolactic fermentation in wine: a review. *J Ind Microbiol Biotech.* 1999/12/01 1999;23(6):447-455.

172. Knoll C, Fritsch S, Schnell S, Grossmann M, Rauhut D, du Toit M. Influence of pH and ethanol on malolactic fermentation and volatile aroma compound composition in white wines. *LWT - Food Science and Technology.* 2011;44(10):2077-2086.

173. Bauer R, Dicks, L M T. Control of malolactic fermentation in wine. A review *South African Journal of Enology and Viticulture* 2004;25(2):74-88

174. Mira de Orduña R, Liu SQ, Patchett ML, Pilone GJ. Ethyl carbamate precursor citrulline formation from arginine degradation by malolactic wine lactic acid bacteria. *FEMS Microbiology Letters.* 2000;183(1):31-35.

175. Liu SQ. Malolactic fermentation in wine – beyond deacidification. *Journal of applied microbiology.* 2002;92(4):589-601.

176. Van Vuuren HJJ, Dicks LMT. Leuconostoc Oenos - a Review. *American Journal of Enology and Viticulture.* 1993;44(1):99-112.

177. Leitão MC, Teixeira HC, Barreto Crespo MT, San Romão MV. Biogenic Amines Occurrence in Wine. Amino Acid Decarboxylase and Proteolytic Activities Expression by Oenococcus oeni. *Journal of Agricultural and Food Chemistry.* 2000/07/01 2000;48(7):2780-2784.

178. Volchenk H, Van Vuuren, H. J. J, Viljoen-bloom, M. Malic acid in wine: Origin, function and metabolism during vinification *South African Journal of Enology and Viticulture* 2006;27 (2):113-122

179. Reguant C, Carrete R, Ferrer N, Bordons A. Molecular analysis of Oenococcus oeni population dynamics and the effect of aeration and temperature during alcoholic fermentation on malolactic fermentation. *Int J Food Sci Tech.* Apr 2005;40(4):451-459.

180. van de Guchte M, Serror P, Chervaux C, Smokvina T, Ehrlich SD, Maguin E. Stress responses in lactic acid bacteria. *Anton Leeuw Int J G.* Aug 2002;82(1-4):187-216.

181. Britz TJ, Tracey RP. The Combination Effect of Ph, So2, Ethanol and Temperature on the Growth of Leuconostoc-Oenos. *J Appl Bacteriol.* Jan 1990;68(1):23-31.

182. Sanders JW, Venema G, Kok J. Environmental stress responses in Lactococcus lactis. *FEMS microbiology reviews.* Jul 1999;23(4):483-501.

183. Abee T, Wouters JA. Microbial stress response in minimal processing. *International Journal of Food Microbiology.* Sep 15 1999;50(1-2):65-91.

184. Drlica K. Control of Bacterial-DNA Supercoiling. *Mol Microbiol.* Feb 1992;6(4):425-433.

185. Hutkins RW, Nannen NL. pH Homeostasis in Lactic Acid Bacteria. *Journal of*

Dairy Science. 1993;76(8):2354-2365.

186. Kunkee RE. Malo-Lactic Fermentation. In: Wayne WU, ed. *Advances in Applied Microbiology.* Vol Volume 9: Academic Press; 1968:235-279.

187. Fleet GHUhbgcabivmQC. *Wine Microbiology and Biotechnology.* Taylor & Francis; 1993.

188. Maicas S, González-cabo P, Ferrer S, Pardo I. Production of Oenococcus oeni biomass to induce malolactic fermentation in wine by control of pH and substrate addition. *Biotechnology Letters.* 1999/04/01 1999;21(4):349-353.

189. E GA, Lopez I, Ruiz JI, et al. High tolerance of wild Lactobacillus plantarum and Oenococcus oeni strains to lyophilisation and stress environmental conditions of acid pH and ethanol. *FEMS Microbiology Letters.* 2004;230(1):53-61.

190. Weber FJ, deBont JAM. Adaptation mechanisms of microorganisms to the toxic effects of organic solvents on membranes. *Bba-Rev Biomembranes.* Oct 29 1996;1286(3):225-245.

191. Jones RP. Biological Principles for the Effects of Ethanol. *Enzyme and Microbial Technology.* Mar 1989;11(3):130-153.

192. Chang IS, Kim BH, Shin PK. Use of sulfite and hydrogen peroxide to control bacterial contamination in ethanol fermentation. *Applied and environmental microbiology.* Jan 1997;63(1):1-6.

193. Alexandre H, Costello PJ, Remize F, Guzzo J, Guilloux-Benatier M. Saccharomyces cerevisiae-Oenococcus oeni interactions in wine: current knowledge and perspectives. *Int J Food Microbiol.* Jun 1 2004;93(2):141-154.

194. Comitini F, Ferretti R, Clementi F, Mannazzu I, Ciani M. Interactions between Saccharomyces cerevisiae and malolactic bacteria: preliminary characterization of a yeast proteinaceous compound(s) active against Oenococcus oeni. *Journal of applied microbiology.* 2005;99(1):105-111.

195. Guilloux-Benatier M, Remize F, Gal L, Guzzo J, Alexandre H. Effects of yeast proteolytic activity on Oenococcus oeni and malolactic fermentation. *Fems Microbiology Letters.* Oct 2006;263(2):183-188.

196. Osborne JP, Dube Morneau A, Mira de Orduna R. Degradation of free and sulfur-dioxide-bound acetaldehyde by malolactic lactic acid bacteria in white wine. *Journal of applied microbiology.* Aug 2006;101(2):474-479.

197. Alexandre H, Ansanay-Galeote V, Dequin S, Blondin B. Global gene expression during short-term ethanol stress in Saccharomyces cerevisiae. *Febs Lett.* Jun 1 2001;498(1):98-103.

198. Lonvaud-Funel A, Joyeux A. Antagonism between lactic acid bacteria of wines: inhibition of Leuconostoc oenos by Lactobacillus plantarum and Pediococcus pentosaceus. *Food microbiology.* 1993;10(5):411-419.

199. Yurdug, x000Fc, l S, Bozoglu F. Studies on an inhibitor produced by lactic acid bacteria of wines on the control of malolactic fermentation. *European Food Research and Technology.* 2002;215(1):38-41.

200. Henick-Kling T, Lee TH, Nicholas DJD. Characterization of the lytic activity of bacteriophages of Leuconostoc oenos isolated from wine. *J Appl Bacteriol.* 1986;61(6):525-534.

201. Poblet-Icart M, Bordons A, Lonvaud-Funel A. Lysogeny of Oenococcus oeni (syn. Leuconostoc oenos) and study of their induced bacteriophages. *Current microbiology.* Jun 1998;36(6):365-369.

202. Vollmer W, Joris B, Charlier P, Foster S. Bacterial peptidoglycan (murein) hydrolases. *FEMS microbiology reviews.* Mar 2008;32(2):259-286.

203. Malinowska-Panczyk E, Kolodziejska I., Dunajski E. Effect of high pressure on selected bacteria at subzero temperature. *Polish Journal of Food and Nutrition Sciences* 2008;58(4):419-424.

204. Navarre WW, Schneewind O. Surface proteins of gram-positive bacteria and mechanisms of their targeting to the cell wall envelope. *Microbiology and molecular biology reviews : MMBR.* Mar 1999;63(1):174-229.

205. Samuelson P, Gunneriusson E, Nygren PA, Stahl S. Display of proteins on bacteria. *Journal of biotechnology.* Jun 26 2002;96(2):129-154.

206. Dicks LMT, Dellaglio F, Collins MD. Proposal to Reclassify Leuconostoc-Oenos as Oenococcus-Oeni [Corrig] Gen-Nov, Comb-Nov. *International journal of systematic bacteriology.* Apr 1995;45(2):395-397.

207. Zhang D, Lovitt RW. Strategies for enhanced malolactic fermentation in wine and cider maturation. *Journal of Chemical Technology & Biotechnology.* 2006;81(7):1130-1140.

208. Swiegers JH, Bartowsky EJ, Henschke PA, Pretorius IS. Yeast and bacterial modulation of wine aroma and flavour. *Aust J Grape Wine R.* 2005;11(2):139-173.

209. Morenzoni R, ed *MALOLACTIC FERMENTATION IN WINE.* Selected from nature LALLEMAND; 2005.

210. Hemme D, Foucaud-Scheunemann C. Leuconostoc, characteristics, use in dairy technology and prospects in functional foods. *International Dairy Journal.* 2004;14(6):467-494.

211. von Weymarn N, Hujanen M, Leisola M. Production of D-mannitol by heterofermentative lactic acid bacteria. *Process Biochem.* Jun 2002;37(11):1207-1213.

212. Ritt JF, Guilloux-Benatier M, Guzzo J, Alexandre H, Remize F. Oligopeptide assimilation and transport by Oenococcus oeni. *Journal of applied microbiology.* Feb 2008;104(2):573-580.

213. Fourcassie P, Makagakabindamassard E, Belarbi A, Maujean A. Growth, D-Glucose Utilization and Malolactic Fermentation by Leuconostoc-Oenos Strains in 18 Media Deficient in One Amino-Acid. *J Appl Bacteriol.* Dec 1992;73(6):489-496.

214. Ferreira RB, Piçarra-Pereira MA, Monteiro S, Loureiro VlB, Teixeira AR. The wine proteins. *Trends in Food Science & Technology.* 2001;12(7):230-239.

215. Tonon T, Lonvaud-Funel A. Metabolism of arginine and its positive effect on growth and revival of Oenococcus oeni. *Journal of applied microbiology.* Sep 2000;89(3):526-531.

216. Liu SQ, Pritchard GG, Hardman MJ, Pilone GJ. Arginine catabolism in wine lactic acid bacteria: is it via the arginine deiminase pathway or the arginase-urease pathway? *J Appl Bacteriol.* 1996;81(5):486-492.

217. Mira De Orduna R, Patchett ML, Liu SQ, Pilone GJ. Growth and arginine metabolism of the wine lactic acid bacteria Lactobacillus buchneri and Oenococcus oeni at different pH values and arginine concentrations. *Applied and environmental microbiology.* Apr 2001;67(4):1657-1662.

218. Champagne CP, Gardner N, Doyon G. Production of Leuconostoc-Oenos Biomass under Ph Control. *Applied and environmental microbiology.* Oct 1989;55(10):2488-2492.

219. Firme MP, Leitao MC, Sanromao MV. The Metabolism of Sugar and Malic-Acid by Leuconostoc-Oenos - Effect of Malic-Acid, Ph and Aeration Conditions. *J Appl Bacteriol.* Feb 1994;76(2):173-181.

220. Tracey RP, Vanrooyen TJ. Utilization of Glucose, Fructose and Malic-Acid by Malolactic Bacteria - Effect of Ethanol and Formation of Mannitol and Volatile Acids. *J Appl Bacteriol.* Aug 1988;65(2):113-118.

221. Schumann C, Michlmayr H, Del Hierro AM, et al. Malolactic enzyme from Oenococcus oeni: heterologous expression in Escherichia coli and biochemical characterization. *Bioengineered.* May-Jun 2013;4(3):147-152.

222. Caspritz G, Radler F. Malolactic enzyme of Lactobacillus plantarum. Purification, properties, and distribution among bacteria. *The Journal of biological chemistry.* Apr 25 1983;258(8):4907-4910.

223. Groisillier A, Lonvaud-Funel A. Comparison of partial malolactic enzyme gene sequences for phylogenetic analysis of some lactic acid bacteria species and relationships with the malic enzyme. *International journal of systematic bacteriology.* Oct 1999;49 Pt 4:1417-1428.

224. Kosseva MR. Immobilization of Microbial Cells in Food Fermentation Processes. *Food and Bioprocess Technology.* Aug 2011;4(6):1089-1118.

225. Maicas S. The use of alternative technologies to develop malolactic fermentation in wine. *Applied microbiology and biotechnology.* 2001;56(1-2):35-39.

226. Kosseva M, Beschkov V, Kennedy JF, Lloyd LL. Malolactic fermentation in Chardonnay wine by immobilised Lactobacillus casei cells. *Process Biochem.* Nov 1998;33(8):793-797.

227. Nedovic VA, Durieux A, Van Nedervelde L, et al. Continuous cider fermentation with co-immobilized yeast and Leuconostoc oenos cells. *Enzyme and Microbial Technology.* Jun 2000;26(9-10):834-839.

228. Herrero M, Laca A, Garcia LA, Diaz M. Controlled malolactic fermentation in cider using Oenococcus oeni immobilized in alginate beads and comparison with free cell fermentation. *Enzyme and Microbial Technology.* Jan 2 2001;28(1):35-41.

229. Kosseva MR, Kennedy JF. Encapsulated lactic acid bacteria for control of malolactic fermentation in wine. *Artificial cells, blood substitutes, and immobilization biotechnology.* Feb 2004;32(1):55-65.

230. Crapisi A, Spettoli P, Nuti MP, Zamorani A. Comparative Traits of Lactobacillus-Brevis, Lact Fructivorans and Leuconostoc-Oenos Immobilized Cells for the Control of Malo-Lactic Fermentation in Wine. *J Appl Bacteriol.* Dec 1987;63(6):513-521.

231. Mccord JD, Ryu DDY. Development of Malolactic Fermentation Process Using Immobilized Whole Cells and Enzymes. *American Journal of Enology and Viticulture.* 1985;36(3):214-218.

232. Spettoli P, Nuti MP, Crapisi A, Zamorani A. Technological Improvement of Malolactic Fermentation in Wine by Immobilized Microbial-Cells in a Continuous-Flow Reactor. *Ann Ny Acad Sci.* Jun 15 1987;501:386-389.

233. Maicas S, Pardo I, Ferrer S. The potential of positively-charged cellulose sponge for malolactic fermentation of wine, using Oenococcus oeni. *Enzyme and Microbial Technology.* Mar 8 2001;28(4-5):415-419.

234. Agouridis N, Kopsahelis N, Plessas S, Koutinas AA, Kanellaki M. Oenococcus oeni cells immobilized on delignified cellulosic material for malolactic fermentation of wine. *Bioresource technology.* Dec 2008;99(18):9017-9020.

235. Durieux A, Nicolay X, Simon JP. Continuous malolactic fermentation by Oenococcus oeni entrapped in LentiKats. *Biotechnology Letters.* Nov 2000;22(21):1679-1684.

236. Genisheva Z, Mussatto SI, Oliveira JM, Teixeira JA. Malolactic fermentation of wines with immobilised lactic acid bacteria - influence of concentration, type of support material and storage conditions. *Food chemistry.* Jun 1 2013;138(2-3):1510-1514.

237. Battermann G, Radler F. A Comparative-Study of Malolactic Enzyme and Malic Enzyme of Different Lactic-Acid Bacteria. *Can J Microbiol.* Mar 1991;37(3):211-217.

238. Bele M. Preparation and Flow Cytometry of Uniform Silica-Fluorescent Dye Microspheres. *Journal of Colloid and Interface Science.* 2002;254(2):274-282.

239. Partec. *CyFlow instrument operating manual.* Partec GmbH; 2004.

240. Barrera C, Herrera AP, Bezares N, et al. Effect of poly(ethylene oxide)-silane graft molecular weight on the colloidal properties of iron oxide nanoparticles for biomedical applications. *J Colloid Interface Sci.* Jul 1 2012;377(1):40-50.

241. Kralj S, Makovec D. The chemically directed assembly of nanoparticle clusters from superparamagnetic iron-oxide nanoparticles. *RSC Advances.* 2014;4(25):13167.

242. Cerbelaud M, Videcoq A, Abélard P, Pagnoux C, Rossignol F, Ferrando R. Heteroaggregation between Al2O3 Submicrometer Particles and SiO2 Nanoparticles: Experiment and Simulation. *Langmuir : the ACS journal of surfaces and colloids.* 2008/04/01 2008;24(7):3001-3008.

243. Bio-Adembeads Streptavidin / Plus / Divin / Rec. 2014; http://www.ademtech.com/products.aspx?id_p=23. Accessed November 28, 2014.

244. MagnaBind Beads and Magnets. 2014; http://www.piercenet.com/product/magnabind-magnetic-beads-magnets. Accessed November 28, 2014.

245. Wei XL, Wang WL, Xiao J, Zhang L, Chen HY, Ding J. Hierarchically porous aluminosilicates as the water vapor adsorbents for dehumidification. *Chemical Engineering Journal.* Jul 15 2013;228:1133-1139.

246. Jiang W, Saxena A, Song B, Ward BB, Beveridge TJ, Myneni SC. Elucidation of functional groups on gram-positive and gram-negative bacterial surfaces using infrared spectroscopy. *Langmuir : the ACS journal of surfaces and colloids.* Dec 21 2004;20(26):11433-11442.

247. Davey HM, Kell DB. Flow cytometry and cell sorting of heterogeneous microbial populations: the importance of single-cell analyses. *Microbiological reviews.* Dec 1996;60(4):641-696.

248. Bouix M, Ghorbal S. Rapid enumeration of Oenococcus oeni during malolactic fermentation by flow cytometry. *Journal of applied microbiology.* Apr 2013;114(4):1075-1081.

249. wine Ioova. *International Oenological Codex.* Paris2014.

250. Salma M, Rousseaux S, Sequeira-Le Grand A, Alexandre H. Cytofluorometric detection of wine lactic acid bacteria: application of malolactic fermentation to the monitoring. *Journal of industrial microbiology & biotechnology.* Jan 2013;40(1):63-73.

251. Lopez-Lopez JM, Schmitt A, Moncho-Jorda A, Hidalgo-Alvarez R. Electrostatic heteroaggregation regimes in colloidal suspensions. *Advances in colloid and interface science.* Mar-Jun 2009;147-148:186-204.

252. Viota JL, Raşa M, Sacanna S, Philipse AP. Stability of mixtures of charged silica, silica–alumina, and magnetite colloids. *Journal of Colloid and Interface Science.* 2005;290(2):419-425.

253. Fernández-Barbero A, Vincent B. Charge heteroaggregation between hard and soft particles. *Physical Review E.* 2000;63(1):011509.

254. Gaulding JC, Saxena S, Montanari DE, Lyon LA. Packed Colloidal Phases Mediate the Synthesis of Raspberry-Structured Microgel Heteroaggregates. *Acs Macro Lett.* Apr 2013;2(4):337-340.

255. Rasa M, Philipse AP, Meeldijk JD. Heteroaggregation, repeptization and stability in mixtures of oppositely charged colloids. *J Colloid Interface Sci.* Oct 1 2004;278(1):115-125.

256. Yu WL, Borkovec M. Distinguishing Heteroaggregation from Homoaggregation in Mixed Binary Particle Suspensions by Multiangle Static and Dynamic Light Scattering. *The Journal of Physical Chemistry B.* 2002/12/01 2002;106(51):13106-13110.

257. He YT, Wan J, Tokunaga T. Kinetic stability of hematite nanoparticles: the effect of particle sizes. *Journal of Nanoparticle Research.* 2007;10(2):321-332.

258. Borkovec M, Papastavrou G. Interactions between solid surfaces with adsorbed polyelectrolytes of opposite charge. *Current Opinion in Colloid & Interface Science.* 2008;13(6):429-437.

259. Chen KL, Mylon SE, Elimelech M. Aggregation Kinetics of Alginate-Coated Hematite Nanoparticles in Monovalent and Divalent Electrolytes. *Environmental science & technology.* 2006/03/01 2006;40(5):1516-1523.

260. Chen KL, Mylon SE, Elimelech M. Enhanced Aggregation of Alginate-Coated Iron Oxide (Hematite) Nanoparticles in the Presence of Calcium, Strontium, and Barium Cations. *Langmuir : the ACS journal of surfaces and colloids.* 2007/05/01 2007;23(11):5920-5928.

261. Rollié S, Sundmacher K. Determination of Cluster Composition in Heteroaggregation of Binary Particle Systems by Flow Cytometry. *Langmuir : the ACS journal of surfaces and colloids.* 2008/12/02 2008;24(23):13348-13358.

262. Bradley M, Lazim AM, Eastoe J. Stimulus-Responsive Heteroaggregation of Colloidal Dispersions: Reversible Systems and Composite Materials. *Polymers.* 2011;3(4):1036-1050.

263. Akagi T, Baba M, Akashi M. Preparation of nanoparticles by the self-organization of polymers consisting of hydrophobic and hydrophilic segments: Potential applications. *Polymer.* Nov 2 2007;48(23):6729-6747.

264. Liu XM, He JH. Hierarchically structured superhydrophilic coatings fabricated by self-assembling raspberry-like silica nanospheres. *Journal of Colloid and Interface Science.* Oct 1 2007;314(1):341-345.

265. Bromberg L, Chang EP, Hatton TA, Concheiro A, Magarinos B, Alvarez-Lorenzo C. Bactericidal core-shell paramagnetic nanoparticles functionalized with poly(hexamethylene biguanide). *Langmuir : the ACS journal of surfaces and colloids.* Jan 4 2011;27(1):420-429.

266. Vukomanocić M. *Sonochemical synthesis and characterization of hydroxyapatite/metal-based composite materials for biomedical applications* [Doctoral Dissertation], Jožef Stefan International Postgraduate School; 2012.

267. Kaiser G. Osmosis—a Cell in an Environment That Is Hypotonic. 2007;

http://www.microbelibrary.org/library/biology/3120-osmosis-a-cell-in-an-environment-that-is-hypotonic. Accessed January, 1, 2015.

268. Safarik I, Safarikova M. Magnetically modified microbial cells: A new type of magnetic adsorbents. *China Particuology.* 2007;5(1-2):19-25.

269. Ribéreau-Gayon P, Glories Y, Maujean A, Dubourdieu D. *Handbook of Enology, The Chemistry of Wine: Stabilization and Treatments.* Wiley; 2006.

270. Uskokovic V, Hoover C, Vukomanovic M, Uskokovic DP, Desai TA. Osteogenic and antimicrobial nanoparticulate calcium phosphate and poly-(D,L-lactide-co-glycolide) powders for the treatment of osteomyelitis. *Mat Sci Eng C-Mater.* Aug 1 2013;33(6):3362-3373.

271. Lokina S, Stephen A, Kaviyarasan V, Arulvasu C, Narayanan V. Cytotoxicity and antimicrobial activities of green synthesized silver nanoparticles. *Eur J Med Chem.* Apr 9 2014;76:256-263.

272. Schwegmann H, Feitz AJ, Frimmel FH. Influence of the zeta potential on the sorption and toxicity of iron oxide nanoparticles on S. cerevisiae and E. coli. *J Colloid Interface Sci.* Jul 1 2010;347(1):43-48.

273. Gao X, Yu KM, Tam KY, Tsang SC. Colloidal stable silica encapsulated nano-magnetic composite as a novel bio-catalyst carrier. *Chem Commun (Camb).* Dec 21 2003(24):2998-2999.

274. Delfini C, Cersosimo M, Del Prete V, et al. Resistance screening essay of wine lactic acid bacteria on lysozyme: Efficacy of lysozyme in unclarified grape musts. *Journal of Agricultural and Food Chemistry.* Apr 7 2004;52(7):1861-1866.

275. Vrščaj Vodušek T. *The Influence of variety, vintage and addition of starters in grape must or wine on the course of malolactic fermentation*. Ljubljana: Biotehnical Faculty, Department of Food Science and Technology, Universtity of Ljubljana; 2007.

276. Berlot M, Rehar T, Fefer D, Berovic M. The Influence of Treatment of Saccharomyces cerevisiae Inoculum with a Magnetic Field on Subsequent Grape Must Fermentation. *Chem Biochem Eng Q.* Dec 2013;27(4):423-429.

277. Theodore D, Krieger S, Costello P, Dumont A, Lallemand. Bacterial nutrition - the key to successful malolactic fermentation. *Australian & New Zealand Grapegrower and Winemaker* 2005;495:65-68.

278. ENZYMATIC KITS 2009; http://www.oenolab.com/enzymatic.html. Accessed November 28, 2014.

279. Smith AC, Hussey MA. Gram Stain Protocols. 2005; http://www.microbelibrary.org/component/resource/gram-stain/2886-gram-stain-protocols. Accessed December 29, 2005.

Index of Figures

Index of Tables

Appendix

A1.1 Cell wall and metabolism of LAB

The cell wall of *O. oeni* is essentially composed of a peptidoglycan that is only found in prokaryotes (Figure A1).

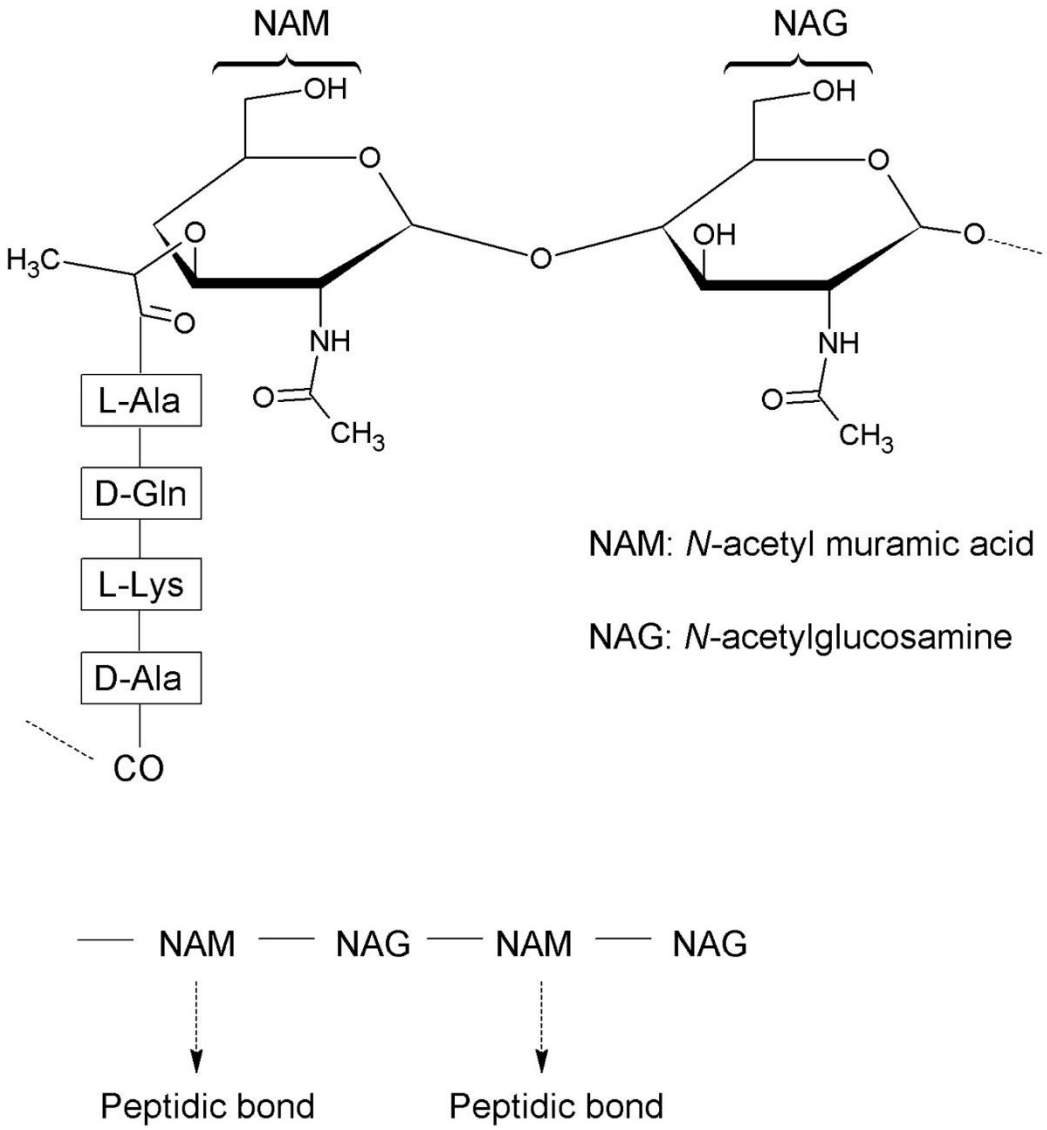

Figure A1: *Polysaccharidic chain of bacterium peptidoglycan [166].*

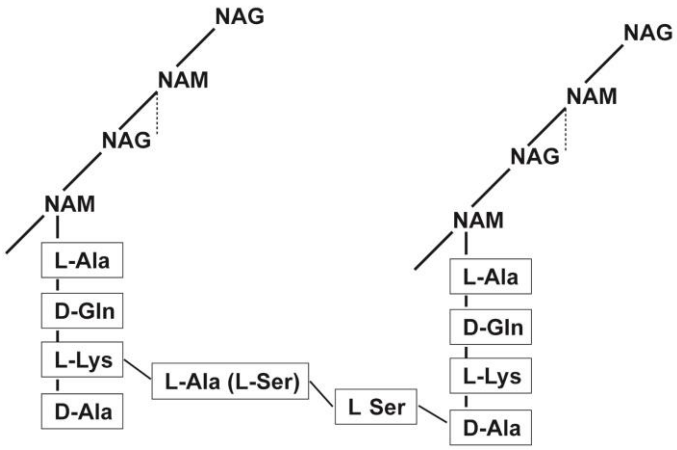

Figure A2: *Structure diagram of the peptidoglycan of O. oeni bacteria [166].*

A1.2 Metabolism of LAB

A1.2.1 Heterofermentative metabolism of hexoses

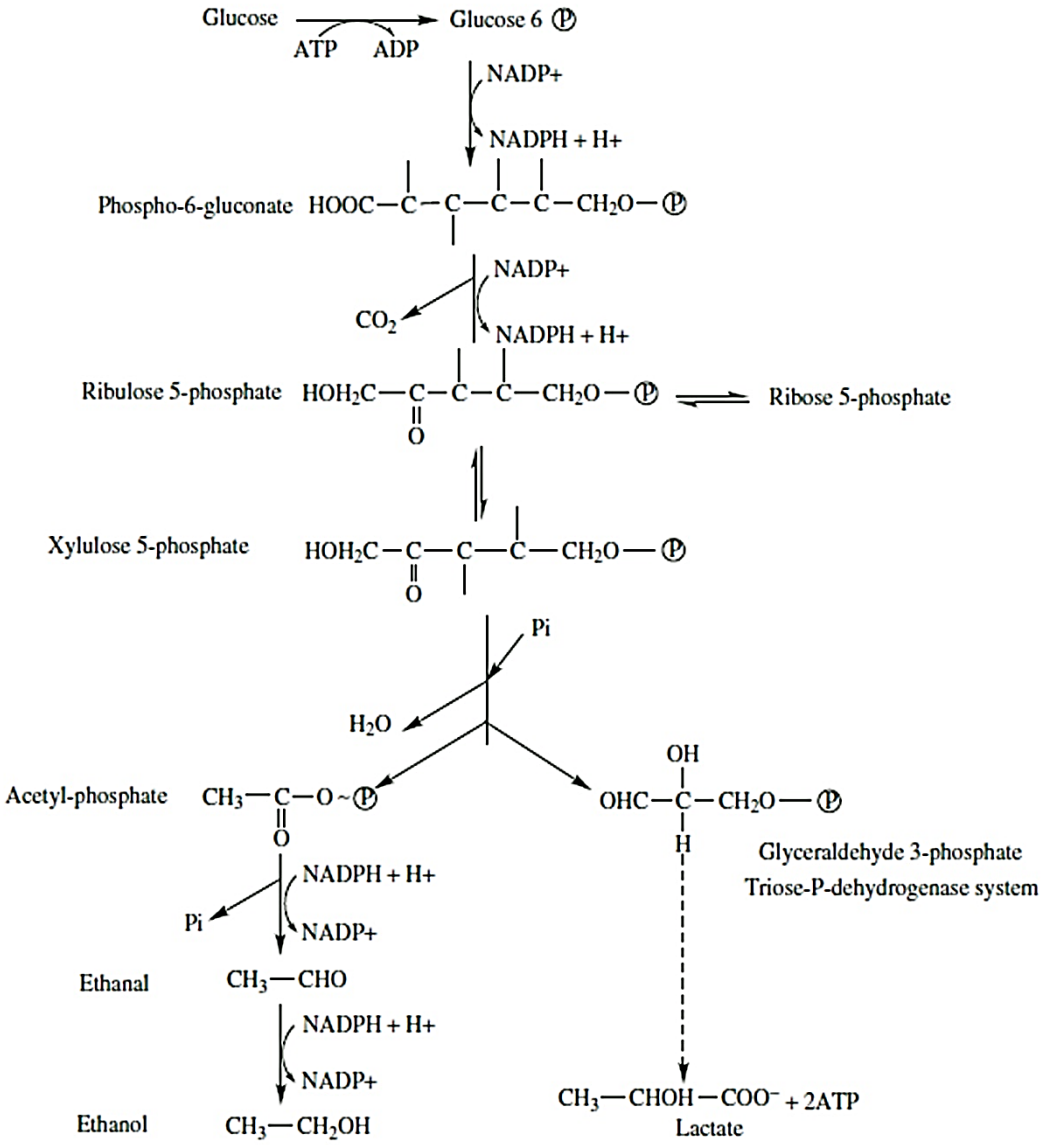

Figure A3: *Metabolic pathway of glucose fermentation by O. oeni (pentose phosphate pathway) [166].*

A1.2.2 Metabolism of amino acids

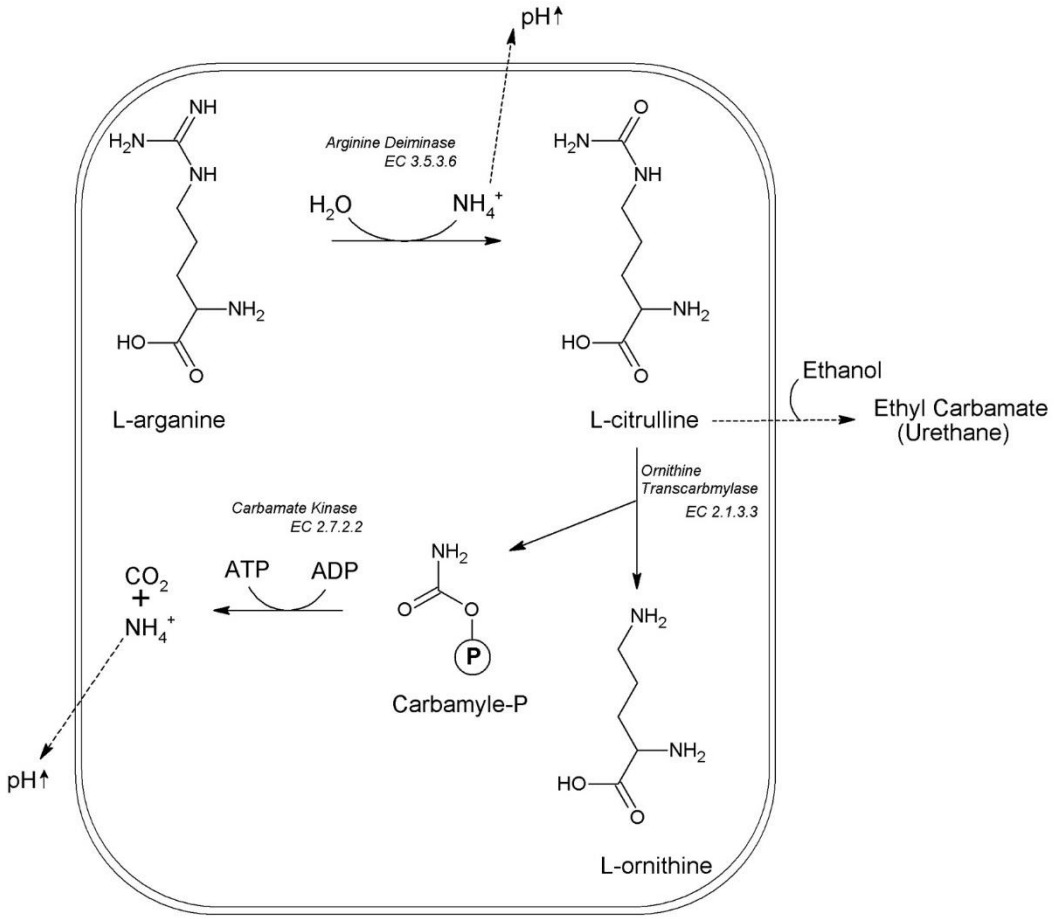

Figure A4: *Arginine degradation mechanism by O. oeni and its enological significance. Modified from [166,217].*

A1.2.3 Metabolism of organic acids of wine

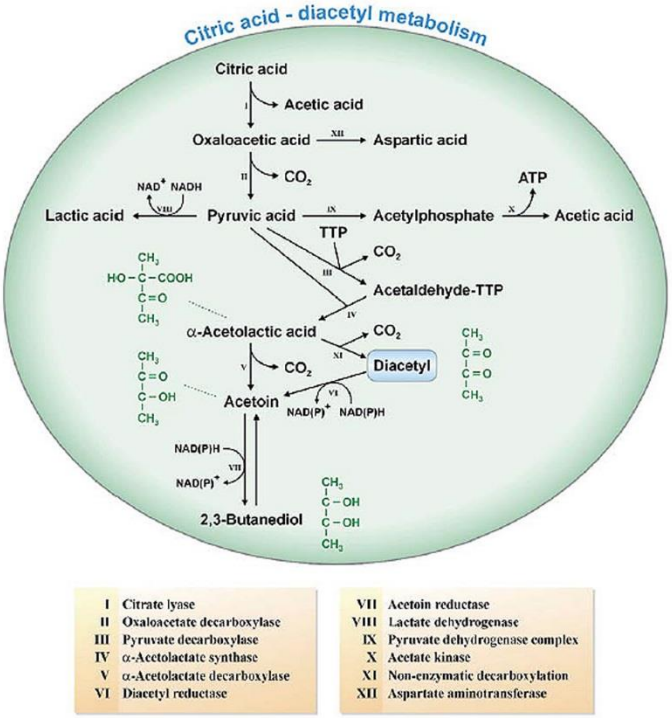

Figure A5: *Metabolic pathway for citric acid degradation and the synthesis of diacetyl by O. oeni [208].*

A1.2.4 Enzymatic decarboxylation of L-malic acid

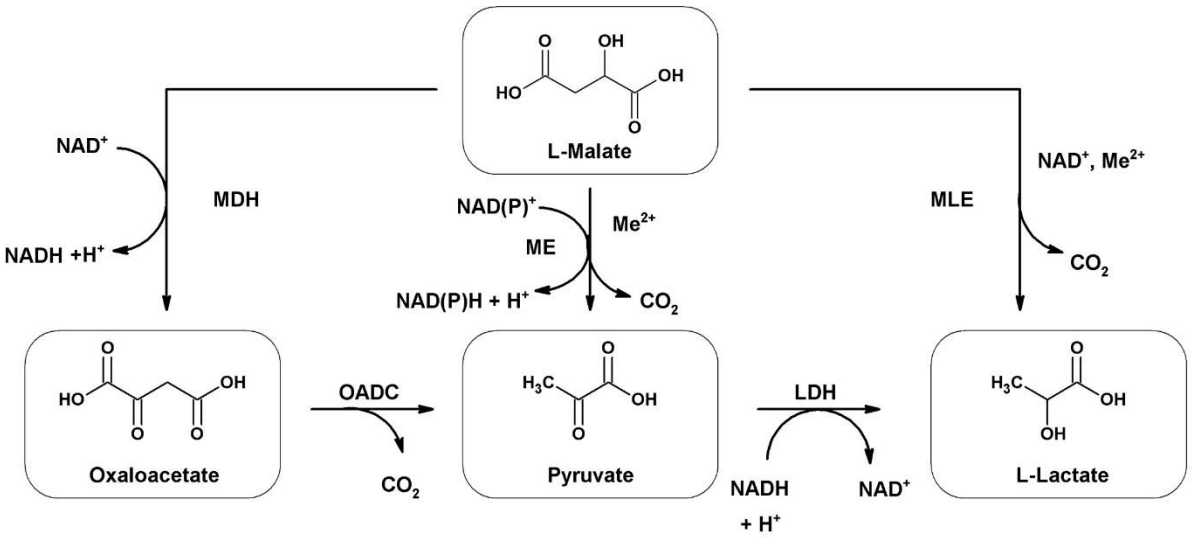

Figure A6: *Possible pathways for the conversion of L-malic acid to L-lactic acid by different enzymes.* MDH, malate dehydrogenase; ME, malic enzyme; MLE, malolactic enzyme; OADC, oxaloacetate decarboxylase; LDH, lactate dehydrogenase [221].

A1.3 Synthesis and functionalization of the nanoparticles

A1.3.1 Materials

Iron (III) sulphate hydrate, iron (II) sulphate heptahydrate (ACS, 99+%), citric acid (99+%), tetraethoxysilane (TEOS, 99.9%), 3-(2-aminoethylamino) propylmethyldimethoxysilane (APMS, 97%), *N*,*N*-dimethylformamide (DMF, 99%), succinic anhydride (SA, 99%) and dimethyl sulfoxide (DMSO, 99,8+%) and potassium chloride (KCl, 99%) were from Alfa Aesar. The 1-ethyl-3-[3-dimethylaminopropyl]carbodiimide hydrochloride (EDC), *N*-hydroxysulfosuccinimide (Sulfo-NHS), carboxy-(polyethylene glycol)n-amine ($CAPEG_n$) with 8 (CAPEG8) or 24 (CAPEG24) ethylene glycol units were purchased from Thermo Scientific. Acetone (AppliChem GmbH), sodium hydroxide (NaOH) (Carlo Erba, ACS), methanol (Merck, ACS), ethanol absolute (Carlo Erba, reagent-USP), ammonium hydroxide (NH_4OH) (aq) (Fluka, p.a., 25%), and hydrochloric acid (HCl) 1 mol/L (p.a., Riedl-de-Haën) were used as received.

A1.3.2 Synthesis of amino-functionalized silica nanoparticles

SNPs were synthesized using a modified Stöber process by Dr. Marjan Bele from the National Institute of Chemistry, Ljubljana Slovenia [238]. For amino functionalization of the SNPs 3-(2-aminoethylamino) propylmethyldimethoxysilane (APMS) (molecule structure presented on Figure A8a) was grafted onto their surfaces, as described elsewhere [74], with some modification. In brief, the APMS (37.5 μL) dissolved in ethanol (100 mL) was added to 100 mL of suspension containing the silica nanoparticles (500 mg). The addition of APMS was 5 μmol, calculated per 1 m^2 of the nanoparticle surface. Then, the pH value of the reaction mixture was set to 11, using NH_4OH, and the reaction mixture was heated to 50 °C and stirred for 5 h (the reaction is presented on Figure A7). The aSNPs were precipitated from a suspension by the addition of 1 mL of saturated NaCl solution and thoroughly washed with 200 mL of methanol and 30 mL of acetone to remove any unbound APMS from the suspension. Finally, the aSNPs were re-dispersed in distilled water.

For the electrostatic heteroagglomeration the pH of the aSNPs aqueous suspension was set to 5.5 with HCl (0.01 mol/L). By decreasing the starting pH value of the aSNPs aqueous suspension from 9.5 to 5.5 small flocculates were observed in the suspension of aSNPs, which could be redispersed by shaking the suspension.

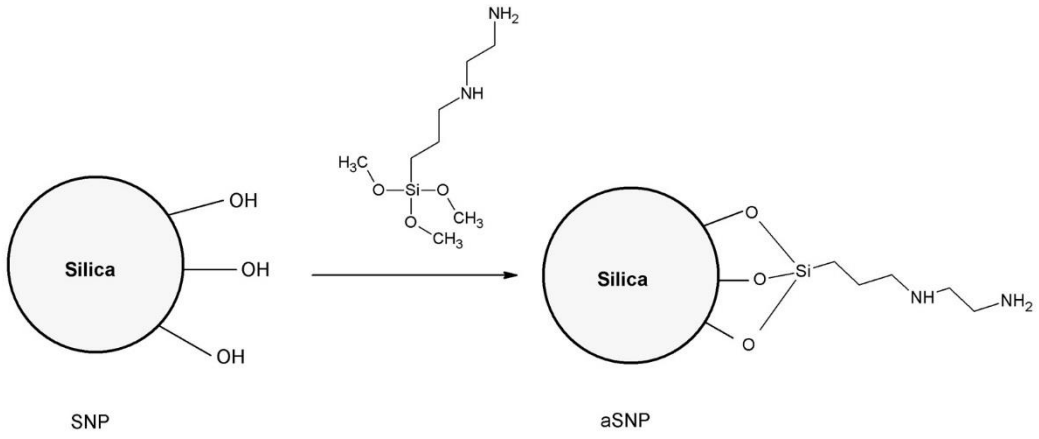

Figure A7: *Functionalization of the SNP with APMS reagent.*

A1.3.3 Synthesis of carboxyl-functionalized silica-coated maghemite nanoparticles

Maghemite (γ-Fe_2O_3) nanoparticles were synthesized using co-precipitation from aqueous solutions and then the stable aqueous suspension of the nanoparticles was prepared using citric acid as the surfactant, as described elsewhere [70]. The nanoparticles in the stable aqueous suspension were coated with a layer of silica using hydrolysis and the polycondensation of TEOS in the presence of an alkaline catalyst NH_4OH, as described in ref. [69]. In the vast majority of cases a silica layer with a fairly constant thickness, approximately 4 nm thick, grew homogeneously on the individual maghemite nanoparticles; however, in a few cases small aggregates containing several nanoparticles were coated. The MNPs were functionalized by grafting pre-synthesized carboxyl-terminated silane molecules onto their surfaces. The pre-synthesized carboxyl-terminated silane molecules were synthesized by reacting the APMS and SA in DMF, as described in ref. [74] (the reaction with the molecular structures is presented in Figure A9). Briefly, the pre-synthesized carboxyl-terminated silane molecules were synthesized by incubating APMS (1.4 mmol) with SA in 2 mL anhydrous DMF and mixing overnight at room temperature. The pre-synthesized carboxyl-terminated silane molecule was prepared using an APMS: SA molar ratio of 1: 2. The pre-synthesized carboxyl-terminated silane molecules were subsequently reacted with the MNPs (the reaction is presented in Figure A8). The pre-synthesized carboxyl-terminated silane molecules (452 μL) were dissolved in 5 mL of ethanol and added to 20 mL of the aqueous suspension containing 100 mg of MNPs. The pH value of the reaction mixture was set to 10 using NH_4OH. The reaction mixture was then heated to 50 °C and stirred for 5 h. After ageing, the cMNPs suspension was thoroughly washed with distilled water to remove any unbound reagents from the suspension.

For electrostatic heteroagglomeration the pH of the cMNPs aqueous suspension was set to 5.5 with HCl (0.01 mol/L). No particle agglomeration was observed by lowering the cMNPs suspension’s pH from 9 to 5.5.

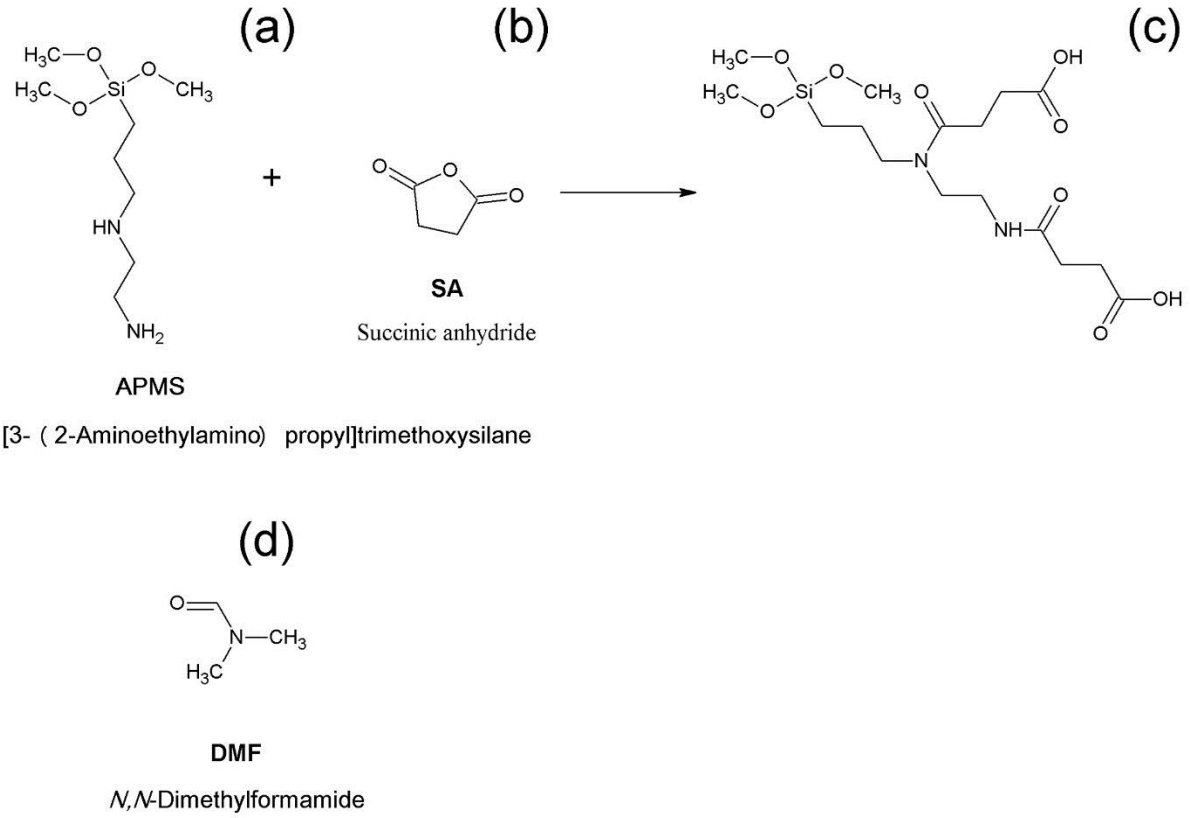

Figure A8: *The synthesis of the pre-synthesized carboxyl-terminated silane molecule (c) by APMS (a) and SA (b) reagents in anhydrous DMF (d).*

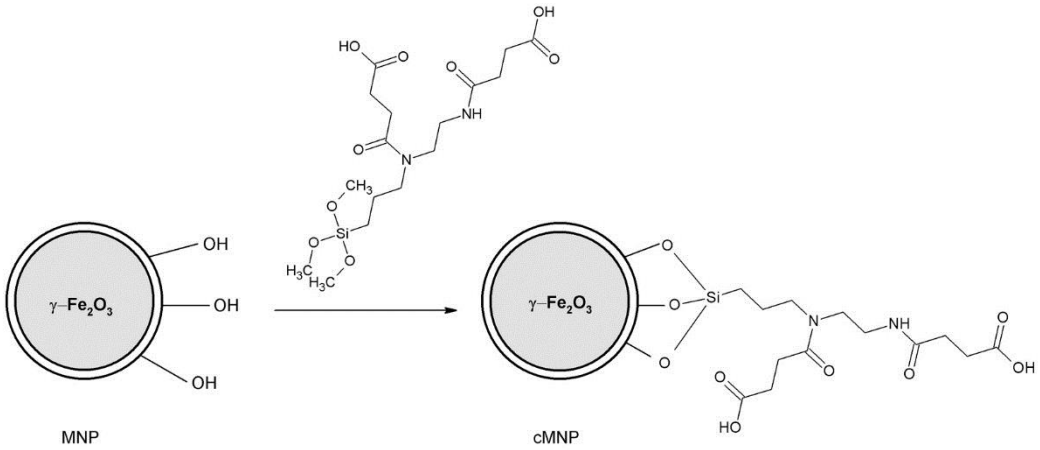

Figure A9: *Functionalization of MNP with the pre-synthesized carboxyl-terminated silane reagent.*

A1.3.4 Amino-functionalization of silica-coated maghemite nanoparticles

The MNPs were amino-functionalized by grafting APMS onto their surfaces. Briefly, the APMS (14.2 µL) dissolved in ethanol (26 mL) was added to 26 mL of suspension

containing the MNPs (130 mg). The addition of APMS was 5 µmol, calculated per 1 m^2 of the nanoparticle surface. Then, the pH value of the reaction mixture was set to 11, using NH_4OH, and the reaction mixture was heated to 50 °C and stirred for 5 h (the functionalization of MNPs with the molecular structures is presented in Figure A10). After ageing, the aMNPs suspension was thoroughly washed with distilled water to remove any unbound reagents from the suspension.

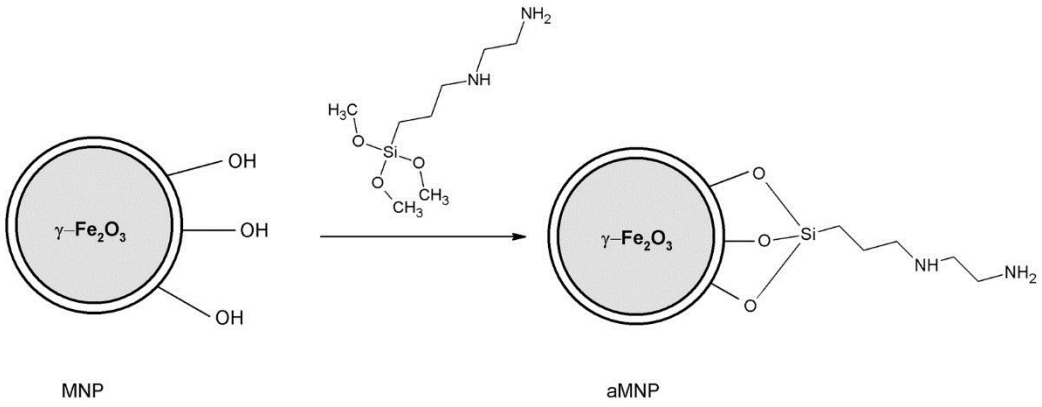

Figure A10: *Functionalization of MNP with APMS reagent.*

A1.3.5 Heterobifunctional crosslinker

Molecular structures with descriptions of $CAPEG_n$ reagents.

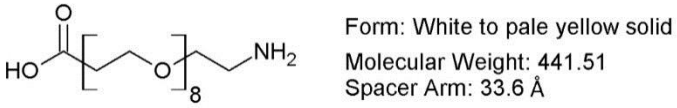

Figure A11: *$CAPEG_n$ with 8 (CAPEG8) ethylene glycol units.*

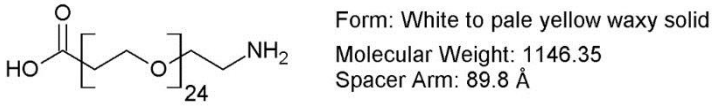

Figure A12: *$CAPEG_n$ with 24 (CAPEG24) ethylene glycol units.*

A1.4 Characterization of starting suspensions

The magnetic properties of the nanoparticles were measured with a vibrating-sample magnetometer (VSM) (Lake Shore 7307 VSM).

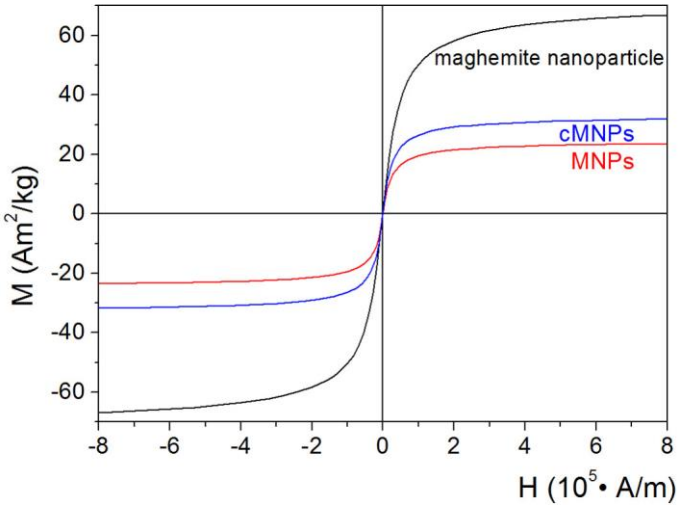

Figure A13: *Room-temperature measurement of magnetization (M) as a function of magnetic field strength (H) for the as-precipitated maghemite nanoparticles (black line), MNPs (red line) and cMNPs (blue line).*

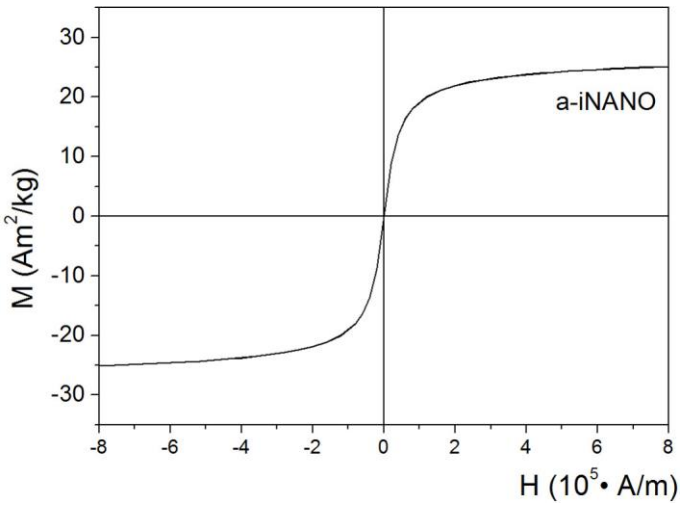

Figure A14: *Room-temperature measurement of the magnetization (M) as a function of magnetic field strength (H) for the a-iNANO.*

The ζ-potential of starting nanoparticles' suspensions was measured as a function of pH with a ZetaProbe Analyzer (Zeta PALS Zeta Potential Analyzer, Brookhaven Instruments Corporation). Figure A15 shows the ζ-potential as a function of pH for the a-iNANO.

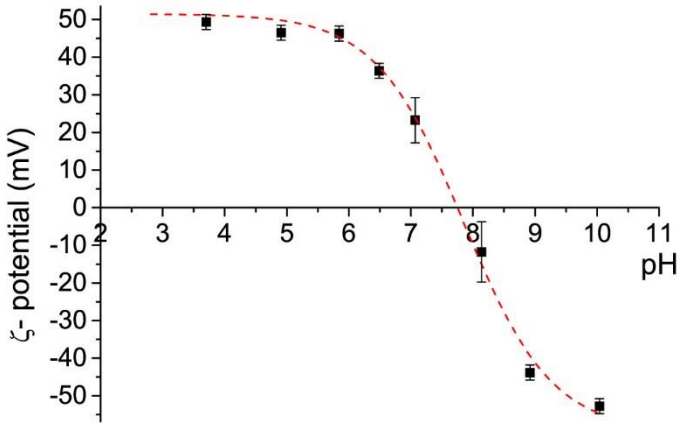

Figure A15: *The changes in the ζ-potential with different pH values for a-iNANO.*

Figure A16 proves that the functionalized nanoparticles in their aqueous suspensions do not agglomerate over time if there is no increase of the ionic strength. The continuous DLS measurements of the aqueous suspensions of the functionalized nanoparticles, cMNPs (0.7 mg/mL, pH 5.5), aMNP (0.2 mg/mL, pH 4) and aSNPs (0.5 mg/mL, pH 5.5), over time showed no increase in the normalized hydrodynamic diameter.

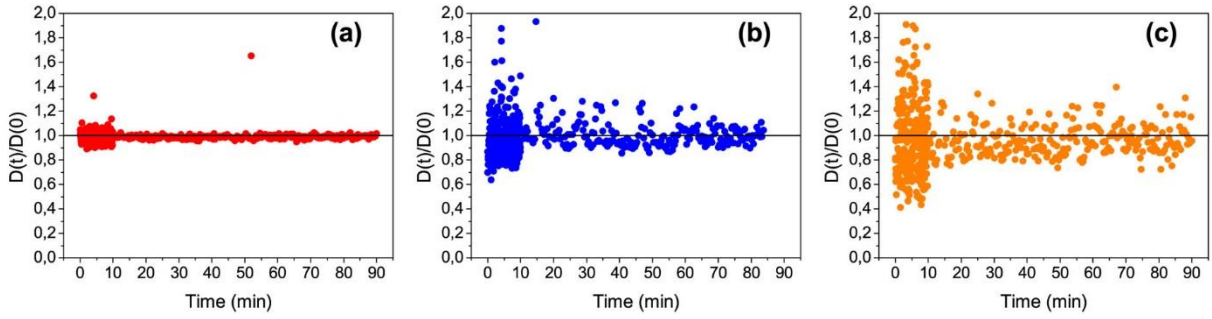

Figure A16: *The continuous DLS measurements of the aqueous suspensions of the functionalized nanoparticles over time.* (a) cMNPs (0.7 mg/mL, pH 5.5), (b) aMNP (0.2 mg/mL, pH 4) and (c) aSNPs (0.5 mg/mL, pH 5.5).

A1.5 Bioactivator composition

- Supervit (Esseco; ammonia phosphate 33%, ammonia sulphate 66%, potassium bicarbonate 5%, vitamine B1 0,2%).

- Opti'malo plus (Danstar Ferment AG; Lot: 81211250530727E04; highly-enriched inactive yeasts with bio-available amino acids and parietal polysaccharides, mineral cofactors and vitamins, as well as cellulose [277].

A1.6 Analysis of organic acids

Princip of enzymatic kit for determination of [278]:

L-lactic acid

$$L-\text{lactate} + NAD^{+} \xrightarrow{LDH} \text{Pyruvate} + NADH + H^{+} \quad \text{(A9)}$$

L-malic acid

$$\text{L}-\text{malate} + \text{NAD}^{+} \xrightarrow{\text{MDH}} \text{Oxaloacetate} + \text{NADH} + \text{H}^{+} \quad \text{(A10)}$$

$$\text{Oxaloacetate} + \text{L}-\text{glutamate} \xrightarrow{\text{GOT}} \text{L}-\text{aspartate} + 2-\text{Oxoglutarate} \quad \text{(A11)}$$

A1.7 Characterization of *O. oeni*

A1.7.1 Gram's method

O. oeni were stained according to Gram's method [279]. Purple coloured *O. oeni* on the Figure A17 proves that the *O. oeni* bacteria are Gram-positive. The same method was used to test the influence of attached aMNPs onto bacteria cell wall. If the attached nanoparticles would damage the cell wall, the bacteria would be red coloured due to the Gram's method. In my case there was no difference between bacteria with or without attached nanoparticles. In both cases the colour was purple that proves that the attached nanoparticles did not damaged the cell wall.

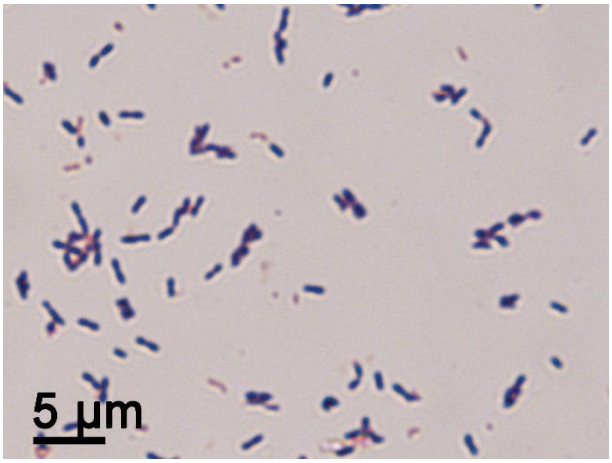

Figure A17: *Stained of O. oeni due to Gram's method.*

A1.8 Flow cytometry method

Before the quantification of *O. oeni* in distilled water, a threshold level determination is required. Distilled water with or without *O. oeni* was analysed and compared by flow cytometry using only the FSC and SSC parameters (logarithmic scale). This allowed setting an electronic threshold on FSC to eliminate instrument noise and background linked to distilled water debris smaller than bacteria (data not shown). Figure A18 and Figure A19 show the flow cytometry analysis of *O. oeni* rehydrated in distilled water without (Figure A18) and with addition of 1:1 % (v/v) absolute ethanol (Figure A19) using LIVE/DEAD Bacterial Viability kit. *O. oeni* population in distilled water is shown on quadrants Q2 on the Figure A18a. The viable bacterial population, i.e., PI-negative cells, demonstrated strong green fluorescence and weak red fluorescence (Figure A18b). Figure A19 presents *O. oeni* in distilled water with addition of ethanol. The population of cells is completely permeabilized, i.e., PI-positive cells, showing weak green fluorescence (Figure A19b) and strong red fluorescence (Figure A19c). The PI-negative cells are

shown on quadrants Q4 on Figure A18d and Figure A19d, whereas PI-positive cells are shown on quadrants Q2 on Figure A18d and Figure A19d.

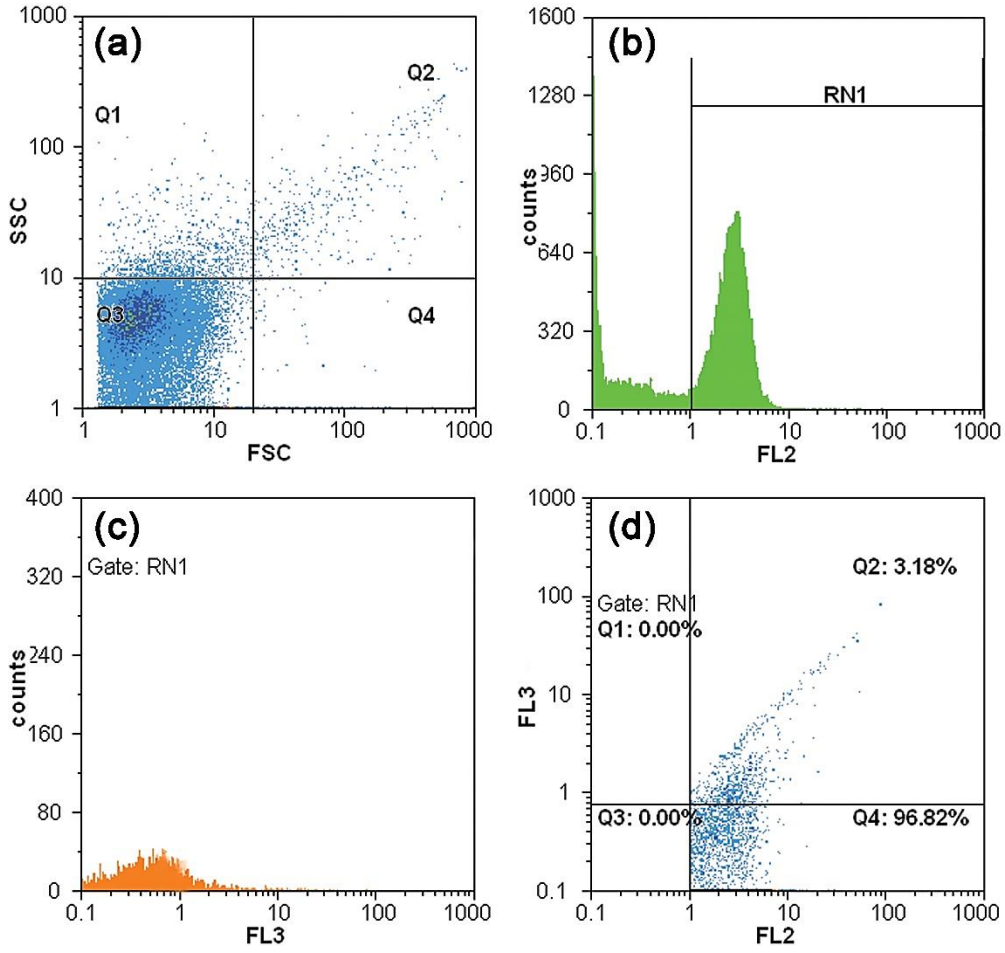

Figure A18: *Flow cytometry analysis of O. oeni (10^6 CFU/mL) in distilled water and stained with LIVE/DEAD Bacterial Viability kit.* (a) dot plot shows FSC and SSC results from flow cytometry analyses for *O. oeni* in distilled water. (b) histogram presenting PI-negative cells demonstrating strong green fluorescence and weak red fluorescence on (c) histogram. Graph (d) shows green fluorescence intensity on the x-axe, and red fluorescence intensity on the y-axe. The percentage of PI-positive cells is presented in quadrants Q2; PI-negative cells is presented in quadrants Q4.

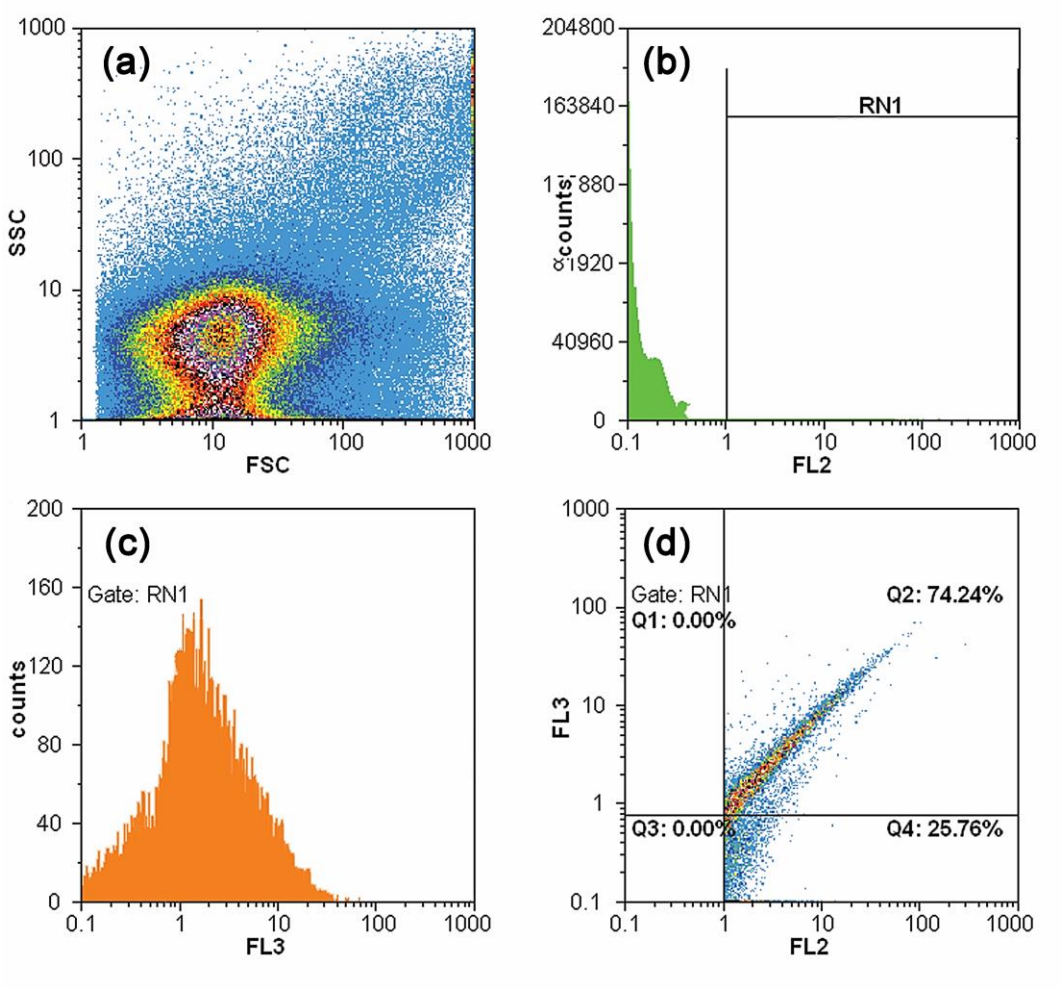

Figure A19: *Flow cytometry analysis of O. oeni (10^6 CFU/mL) in distilled water with addition of ethanol and stained with LIVE/DEAD Bacterial Viability kit.* (a) dot plot shows FSC and SSC results from flow cytometry analyses for *O. oeni* in ethanol. (b) histogram presenting PI-negative cells demonstrating weak green fluorescence and strong red fluorescence on (c) histogram. Graph (d) shows green fluorescence intensity on the x-axe, and red fluorescence intensity on the y-axe. The percentage of PI-positive cells is presented in quadrants Q2; PI-negative cells is presented in quadrants Q4.

Graphs on Figure A20 present *O. oeni* without and with attached nanoparticles. When the nanoparticles are attached onto the bacteria cell wall, the two-dimensional dot plot (Figure A20a) moved in a distinctive curve-shaped manner (Figure A20b).

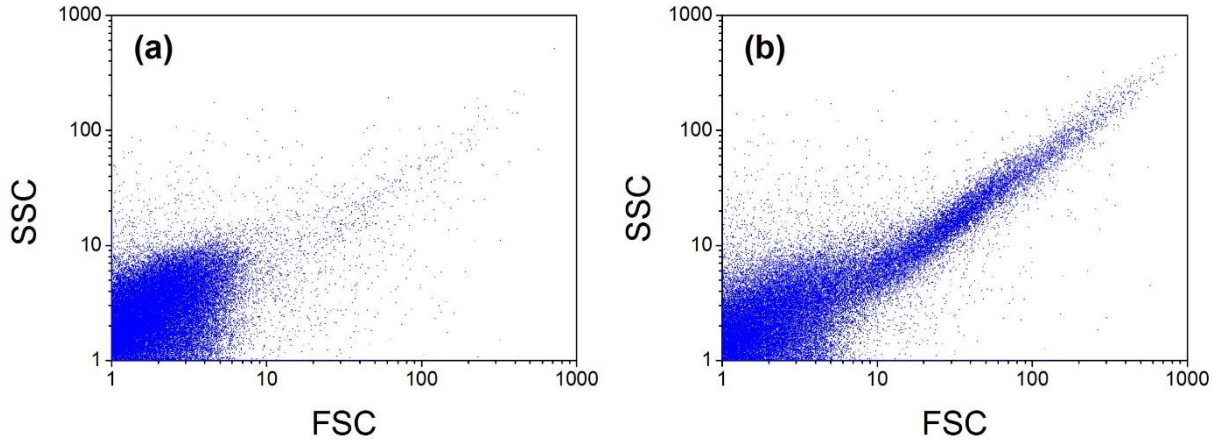

Figure A20: *Dot plots showing FSC and SSC results from flow cytometry analyses of O. oeni (10^6 CFU/mL) (a) without and (b) with attached aMNPs in distilled water and stained with LIVE/DEAD Bacterial Viability kit*.

A1.9 HGMS method

To set up the HGMS method, samples of the suspension, containing MNPs, were taken at different stages of HGMS. To characterize the HGMS process the magnetic properties of the nanoparticles in the suspension were measured using VSM. Measurements of magnetization as a function of magnetic field for batch HGMS samples are presented on the Figure A21. Red line presents the MNPs suspension before HGMS, blue line, the suspension of eluted magnetic nanoparticles from the column after the HGMS and purple line the suspension at the end of washing the column with distilled water. The filtrate had similar response as the suspension at the end of washing the column (data not shown).

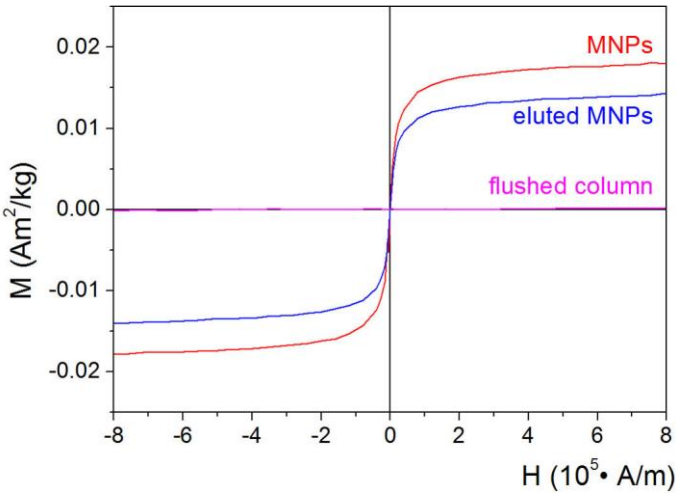

Figure A21: *Room-temperature measurement of the magnetization (M) as a function of magnetic field strength (H) for the MNPs (red line), eluted MNPs (blue line) and flushed column (purple line) suspension.*

The hydrodynamic size distributions of the MNPs in their aqueous suspensions before HGMS (Figure A22a) and eluted MNPs from the column after HGMS (Figure A22b) were measured using DLS (Fritsch, ANALYSETTE 12 DynaSizer). The plots in Figure A22 were generated by statistical method obtained by instrument software nanoQ™ which uses Pade Laplace method to obtain the size distributions from the raw data.

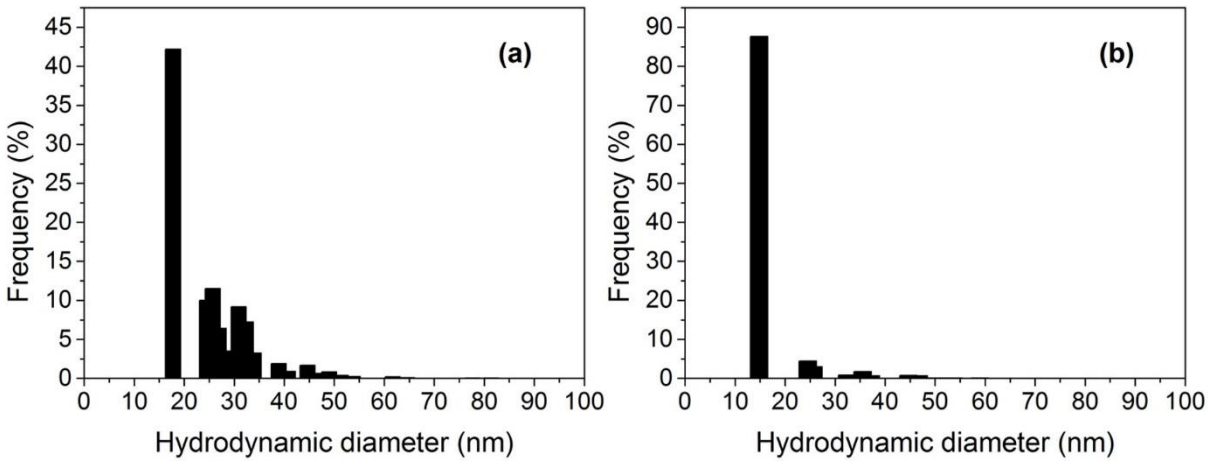

Figure A22: *DLS graphs showing number-weighted size distribution of (a) MNPs before HGMS separation (1 mg/mL, pH 9) and (b) eluted MNPs (0.5 mg/mL, pH 9) from the column after the HGMS.*

Appendix (Bibliography)

Original scientific article

Dušak P, Mertelj A, Kralj S, Makovec D. Controlled heteroaggregation of two types of nanoparticles in an aqueous suspension. Journal of Colloid and Interface Science. 2015;438(0):235-243.

Mesarič T, Baweja L, Drašler B, et al. Effects of surface curvature and surface characteristics of carbon-based nanomaterials on the adsorption and activity of acetylcholinesterase. Carbon. 2013;62(0):222-232.

Published scientific conference contribution

Klemenčič, Danijela, Simončič, Barbara, Tomšič, Brigita, Demšar, Andrej, Kovač, Franci, Aneja, A. P., Žagar, Kristina, Dušak, Peter. Preparation of silver nanoparticles and their antimicrobial activity on cotton fabric. V: 13th Autex Conference, May 22-24, 2013, Dresden, Germany. Conference proceedings. Dresden: Technische Universität Dresden, ITM, 2013, 5 f.

Dušak, Peter, Kralj, Slavko, Makovec, Darko. Synthesis of superparamagnetic clusters as a carrier for wine fining agents. V: 5. študentska konferenca Mednarodne podiplomske šole Jožefa Stefana = 5th Jožef Stefan International Postgraduate School Students Conference, 23. maj 2013, Ljubljana, Slovenija. TRDIN, Nejc (ur.), et al. Zbornik = Proceedings. Ljubljana: Mednarodna podiplomska šola Jožefa Stefana, 2013, str. 257-267.

Published scientific conference contribution abstract

Dušak, Peter, Kralj, Slavko, Makovec, Darko. Controlled agglomeration of nanoparticles in aqueous suspensions. V: SLONANO 2012, 24-26 October 2012, Ljubljana, Slovenia. MIHAILOVIĆ, Dragan (ur.), et al. Book of abstracts. Ljubljana: Institut Jožef Stefan, 2012, str. 52

Dušak, Peter, Mertelj, Alenka, Kralj, Slavko, Makovec, Darko. Heteroagglomeration of two types of nanoparticles in an aqueous suspension. V: SLONANO 2013, 23-25 October 2013, Ljubljana, Slovenia. MIHAILOVIĆ, Dragan (ur.), et al. Book of abstracts. Ljubljana: Jožef Stefan Institute, 2013, str. 44.

Dušak, Peter, Kralj, Slavko, Makovec, Darko. Synthesis of superparamagnetic cluster with controlled heteroagglomeration of nanoparticles in aqueous suspensions. V: 7th Young Researchers' Day, 19 February, 2013, Ljubljana, Slovenia. LISJAK, Darja (ur.), DUŠAK, Peter (ur.), KRALJ, Slavko (ur.). [Program and abstract book]. Ljubljana: Institut Jožef Stefan, 2013, str. 39.

Dušak, Peter, Kralj, Slavko, Mertelj, Alenka, Makovec, Darko. Synthesis of superparamagnetic clusters with controlled heteroagglomeration of the nanoparticles in aqueous suspensions. V: E-MRS 2013 Spring Meeting, May 27-31, Strasbourg, France. Strasbourg: European Materials Research Society, 2013. http://www.emrs-strasbourg.com/index.php?option=com_abstract&task=view&id=216&day=2013-05-

27&year=2013&Itemid=&id_season=9.

Sopotnik, Maja, Mesarič, Tina, Sepčić, Kristina, Drobne, Damjana, Makovec, Darko, Dušak, Peter. Albumin pre-coating of carbon-based nanoparticles reduces their sorbent and inhibitory potential for cholinesterases. V: NanoTox 2014: program & abstracts. [S. l.: s. n., 2014], str. 244.

Dušak, Peter, Mertelj, Alenka, Kralj, Slavko, Makovec, Darko. Heteroagglomeration of two types of nanoparticles in an aqueous suspension. V: 8th Young Researchers' Day, February 18, 2014, Ljubljana. ŽUNIČ, Vojka (ur.), et al. Program and abstract book. Ljubljana: Institut Jožef Stefan, 2014, str. 13.

Treatise, preliminary study, study

Makovec, Darko, Dušak, Peter, Anželak, Bernarda, Kralj, Slavko. Measurement of nanoparticles size using transmission, (IJS delovno poročilo, 11337, confidential). 2013.

Makovec, Darko, Dušak, Peter, Anželak, Bernarda, Kralj, Slavko. Metoda za merjenje velikosti anorganskega jedra nanodelcev, (IJS delovno poročilo, 11339, zaupno). 2013.

7th Young Researchers' Day, 19 February, 2013, Ljubljana, Slovenia, LISJAK, Darja (urednik), DUŠAK, Peter (urednik), KRALJ, Slavko (urednik). [Program and abstract book]. Ljubljana: Institut Jožef Stefan, 2013. 71 str., ilustr.

Makovec, Darko, Dušak, Peter, Belec, Blaž, Anželak, Bernarda, Kralj, Slavko, Rozman Peterka, Tanja. Report on comparative characterization study: measurement of size of an inorganic core of nanoparticles inferumoxytol livi and originator feraheme, (IJS delovno poročilo, 11509, confidential). 2013.

Makovec, Darko, Dušak, Peter, Belec, Blaž, Anželak, Bernarda, Kralj, Slavko, Rozman Peterka, Tanja. Size of an inorganic core of nanoparticles in ferumoxytol drug substance, (IJS delovno poročilo, 11508, confidential). 2013.

Makovec, Darko, Kralj, Slavko, Dušak, Peter, Rozman Peterka, Tanja. Influence of aging on size of an inorganic core of nanoparticles in ferumoxytol livi and originator feraheme, (IJS delovno poročilo, 11547, confidential). 2014.